UNIVERSIDADE DA BEIRA INTERIOR

Engenharia

Sandwich for aeronautical applications: mechanical and electrical characterization

(versão corrigida após defesa de dissertação)

Nuno Neves de Sousa

Dissertação para obtenção do Grau de Mestre em

Engenharia Aeronáutica

(ciclo de estudos integrado)

Orientador: Prof. Doutor Pedro Vieira Gamboa

Orientador: Prof. Doutor Abílio Manuel Pereira da Silva

Co- orientador: Doutor João Pedro Nunes Pereira

Covilhã, outubro de 2018

To my parents, for all their love and effort

Acknowledgments

I am very grateful for all the support I have received from many individuals throughout my time at the Center for Mechanical and Aerospace Science and Technologies (C-MAST, www.aerospace.ubi.pt), it has been a pleasure.

First, I would like to thank my advisor Professor Abílio Silva for his excellent guidance as both an advisor and mentor, for all the disposed time, encouragement, and daily support. I would also like to thank to Professor Pedro V. Gamboa for his guidance and mentorship. Furthermore, I would like to thank Dr. João Pereira for his constant support, guidance and for all the help towards solving unexpected problems along the experimental work. Finally, I would like to thank to João Cardoso, Eng. Paulo Santos, Dr. Marco Silva, and all the other laboratory partners for all the technical support and advisory.

I greatly appreciate the laboratory equipment availability and external services provided by University of Beira Interior (UBI) and the Center for Mechanical and Aerospace Science and Technologies (C-MAST, www.aerospace.ubi.pt), the support from the department of Aerospace Sciences (DCA, www.dca.ubi.pt), and to the department of Electromechanical Engineering (DEM, www.dem.ubi.pt) for the experimental tests. I would also like to thank to the Laboratory of Electronic Microscopy, at the Optic Center of University of Beira Interior, for the availability of the equipment for preparation of samples. Finally, I would like to express my gratitude to the Group of Electroactive Smart Materials from University of Minho, for all the help and efforts to provide the needed technology and software for the electromechanical tests.

Finally, I would like to thank to all my family and friends that stood by my side all these years and enriched my academic life. I would like to express my gratitude to my mother and father for their encouragement, confidence, unwavering support and patience. To my brother and sister for their support and advisement.

This Master Dissertation has been supported by the project Centro-01-0145-FEDER-000017 - EMaDeS - Energy, Materials and Sustainable Development, co-financed by the Portugal 2020 Program (PT 2020), within the Regional Operational Program of the Center (CENTRO 2020) and the European Union through the European Regional Development Fund (ERDF).

Co-financed by:

CENTRO 2020

PORTUGAL 2020

UNIÃO EUROPEIA
Fundo Europeu
de Desenvolvimento Regional

Abstract

Carbon fiber laminates and sandwich structures are widely used due to their extraordinary mechanical performance (high specific strength, specific modulus, resistance to corrosion and resistance to fatigue), in the case of sandwiches, the high performance of the carbon laminates can be increased by the low density of the core. Besides that, carbon fiber is a conductive material, beyond its mechanical advantages, it has the potential to be used as a self-sensing material.

This work aimed to analyze the use of sandwich composite structures in aircraft, to manufacture, and to study the mechanical and electrical properties of a sandwich composed of two carbon fiber faces and a structural foam core.

The experimental work started with a study on the foam core, to access the impact of the adhesive curing temperature in the foam's mechanical behavior. There was an increase on the ductility of the foam, but the flexural strength did not suffer significant changes.

Posteriorly, three-point bending tests were carried out on carbon fiber laminates, with two different geometries, so compressive and tensile failures could be studied. The specimens that failed to compression showed a flexural strength of 1066.21±4.7% MPa, while the ones that failed under a flexural stress of 1238.49±7% MPa.

The sandwich specimens with different adhesive bonds and geometries were tested and the short samples with reinforced bond failed to compression under a flexural stress of 100 MPa ± 5%, while the long samples showed several failure modes under a flexural stress of 86 MPa ± 7%.

An electromechanical analysis was conducted to study the piezoresistive response of the sandwich skins. From this analysis was possible to show that there is indeed a relation between the electrical resistance and the applied strain.

Key-words: Sandwiches, Mechanical behavior; Electromecanical behavior, Multifunctional materials; Self-sensing material.

Resumo

Os laminados de fibra de carbono e as estruturas em *sanduíche* são amplamente utilizadas devido ao seu elevado desempenho mecânico (elevada resistência específica, módulo específico, resistência à corrosão e resistência à fadiga), que no caso das sanduíches, é acrescido da baixa densidade do núcleo. Além disso, a fibra de carbono é um material condutor, portanto para além das vantagens mecânicas, este material tem o potencial de ser utilizado como um material capaz de detetar dano e deformação sem que a necessidade de sensores.

Neste trabalho pretendeu-se analisar o uso de estruturas compósitas em sanduíches em aeronaves, fabricar e estudar as propriedades mecânicas e elétricas de uma *sanduíche* composta por duas faces de fibra de carbono e um núcleo de espuma estrutural.

Na primeira fase do trabalho experimental, foi feito um estudo sobre o núcleo de espuma, com o objetivo de averiguar qual o impacto da temperatura de cura do adesivo. Houve um aumento da ductilidade do material, mas sem impactos significativos ao nível da tensão de cedência.

Posteriormente, foram testados à flexão laminados de fibra de carbono, com duas geometrias de forma a serem obtidos modos de falha à compressão e à tração. Verificou-se que os laminados apresentaram um modo de dano nas fibras à compressão, para uma tensão na ordem dos 1066 MPa ± 5%, enquanto que os laminados cuja ruína ocorreu na face à tração a uma tensão na ordem dos 1238 MPa ± 7%.

As amostras de sanduíches com diferentes composições adesivas e geometrias foram testadas e as de menor dimensão com reforço adesivo cederam à compressão com uma tensão máxima na ordem de 100 MPa ± 5%, enquanto que as de maior dimensão apresentaram diversos modos de falha a uma tensão na ordem dos 86 MPa ± 7%.

Recorrendo a uma análise eletromecânica, foi estudada a resposta piezoresistiva dos laminados constituintes das faces das sanduíches. Desta análise foi possível demonstrar que existe efetivamente uma relação entre a resistência elétrica e a deformação do material.

Palavras chave: CFRP; Sanduiches, Comportamento mecânico; Comportamento eletromecânico, Materiais multifuncionais; Material *self-sensing*.

Table of contents

Acknowledgments V

Abstract VII

Resumo IX

Table of contents XI

List of figures XIII

List of tables XVII

Acronyms XIX

Symbols XXI

1. Introduction 1

1.1 Historical background 1

1.2 Motivation 4

1.3 Objectives 6

1.4 Layout 6

2. State of the Art 7

2.1 Sandwich composite structures 7

2.1.1 History 9

2.1.2 Skins 11

2.1.3 Core 19

2.1.4 Adhesive bonding 21

2.2 Failure in composite structures 25

2.2.1 Failure in FRP 25

2.2.2 Failure in adhesive joints 27

2.2.3 Failure in sandwich structures 28

2.3 Multifunctional materials 31

3. Experimental procedure 35

3.1 Materials and fabrication processes 35

3.2 Experimental setup 41

3.2.1 Archimedes’ principle 41

3.2.2 Definition of test parameters and mechanical tests 43

3.2.3 Piezoresistivity 55

4. Results and discussion 60

4.1 Results 60

4.2 Discussion 69

4.2.1 Foam core 69

4.2.2 CFRP laminates 71

4.2.3 Sandwich specimens 74

4.2.4 Electromechanical tests 79

5. Conclusion 83

5.1 Overview 83

5.2 Future work 84

6. References 87

List of figures

Figure 1.1- Classification scheme of composites based on reinforcement (adapted from [1]) ..2

Figure 1.2- Historical timeline indicating the approximate year when the main types of materials were first used in aviation (adapted from[4])..3

Figure 1.3- Amount of composite material used in aircraft (adapted from [4])....................3

Figure 1.4- Illustration of the composites solutions applied on Boeing 787 (adapted from [3]).4

Figure 1.5- Literature survey on MFM, MFS, MFC and Smart Materials from 1995 to 2017 (data collected from Scopus, August 2018)...5

Figure 2.1-Constituents of a sandwich structure (adapted from [11]) 8

Figure 2.2- Homogeneous core materials (adapted from [6]) 8

Figure 2.3- Structured core materials (adapted from [6]) 8

Figure 2.4- A380 composite sandwich structures applications (adapted from [6]) 9

Figure 2.5- Tensile modulus versus tensile strength for commercially available pitch and PAN based carbon fibers [25] 12

Figure 2.6- Diagram of PAN and Pitch carbon production processes (adapted from [27])...... 13

Figure 2.7- Laminate construction in a [0/90/θ/-θ] symmetric laminate.[2] 15

Figure 2.8- Amount of composite used per passenger to manufacture aircraft from 1974 to 2015 (adapted from [28]) 15

Figure 2.9- Chemical representation of one epoxide group (three member rings of one oxygen atom and two carbon atoms) [27] 18

Figure 2.10- Sandwich beam (adapted from [27]) 19

Figure 2.11- a- AIREX® C70 foam core [30], b- Aramid (Nomex®) honeycomb cores [31]....... 20

Figure 2.12- Schematics of (a)- three sandwich panels with truss core configuration [34] and (b)-five different cell designs [35] 21

Figure 2.13- Comet aircraft [38] 22

Figure 2.14- Representation of failure mechanism in a CFRP composite (adapted from [2]) .. 26

Figure 2.15- Typical modes of failure in FRP adhesive joints [59] 27

Figure 2.16- Sandwich compressive failures, a-Face compressive failure, b- Face wrinkling failure or local buckling (adapted from [64]) 29

Figure 2.17- Core shear failure, a-Real core shear failure, b-Graphic representation of core shear failure and forces that contribute to this failure (adapted from [29]) 29

Figure 2.18- Debonding of the core facing interface 30

Figure 2.19- a- Indentation failure and b- face compression failure in the same specimen ... 30

Figure 2.20- Several failure modes in the same specimen, a-Core shear failure, b-Debonding of the compression face core interface, c- Facing compression failure, d- Indentation failure, e- Partial debonding on the tensile face core interface 30

Figure 3.1- Prepreg transverse cutting 36

Figure 3.2- Heating (a) and setting (b) the first CFRP layer 37

Figure 3.3- Vacuum bag with CFRP 12-layer unidirectional board before the curing prosses . 37

Figure 3.4- CFRP cutting sketch 38

Figure 3.5- Sandwich long samples cutting sketch 39

Figure 3.6- (a)- Sandwich short specimen 15mm x 70mm (b)-Sandwich long specimen 21mmx190mm 40

Figure 3.7- Sandwich specimens with wire integration 40

Figure 3.8- a- Oertling VA204 configuration for dry weight and saturated weight measure, b- Oertling VA204 configuration for suspended weight measures 42

Figure 3.9- Flexural tests experimental setup 43

Figure 3.10- Flexural test arrangements in a three-point bending and b- four-point bending modes 44

Figure 3.11- Example of a strain versus stress of a fiber, matrix and a composite made by these two materials [1] 45

Figure 3.12- Schematic stress-strain diagram showing non-linear elastic behavior and how secant and tangent moduli are determined [1] 46

Figure 3.13- Illustration of stress-strain behavior for brittle and ductile materials [1]........ 47

Figure 3.14- Representation of a sandwich specimen 48

Figure 3.15- Sandwich short specimens' measures 49

Figure 3.16- Sandwich long specimens' measures 49

Figure 3.17- Representation of a CFRP laminate sample 52

Figure 3.18- CFRP long specimen and three-point bending test measures 53

Figure 3.19- Foam samples subjected to different heat treatments, a-sample 1,2 and 3, b-sample 4, 5 and 6, c- sample 7, 8 and 9 54

Figure 3.20- Foam specimen for flexural three-point bending test 55

Figure 3.21- Experimental setup for the electromechanical bending tests 59

Figure 4.1-Foam samples flexural tests, a-Load versus displacement and b- stress versus strain experimental curves of the foam samples 60

Figure 4.2- CFRP short laminates experimental curves, a Load versus Displacement and b Stress versus Strain curves 62

Figure 4.3- Sandwich short beams face bending stress versus strain (a) and core shear stress versus strain (b) charts 63

Figure 4.4-CFRP long beams (a) load versus displacement and (b) stress versus displacement charts 64

Figure 4.5- Sandwich long beams experimental curves, a- face bending stress versus strain and (b) core shear stress versus strain curves 65

Figure 4.6- Sandwich long beam 700N cyclic loading tests (a) with no relaxation time (b) with 5 seconds of relaxation time 66

Figure 4.7- Electromechanical tests performed in CFRP laminates. 67

Figure 4.8- CFRP electromechanical rupture tests 68

Figure 4.9- Sandwich electromechanical tests 68

Figure 4.10- Foams specimens' maximum strain 70

Figure 4.11- Foam three-point bending test (a)- crack view from below (b)- front crack view71

Figure 4.12- CFRP_S failure mode, (a)-top view, (b)- magnification of side view (x4) 71

Figure 4.13- CFRP long samples failure mode, (a)-compression side view, (b)- side view, (c)- tensile side view 72

Figure 4.14- Sandwich short samples Load versus Displacement mean curve with respective error and tangent of the elastic phase 74

Figure 4.15-Fracture surface of sandwich short samples, a- magnification of x2, b- magnification of 4x........ 75

Figure 4.16- Sandwich long samples failure modes 76

Figure 4.17- Visual appearance of an adhesive joint, a-Low magnification of the adhesive failed joint and (b)- High magnification of the adhesive failed joint 77

Figure 4.18-Cyclic mechanical tests. a- CFRP_EM face bending stress versus strain and b- S_EM stress versus strain 79

Figure 4.19- Piezoresistive effect for each cycle of the CFRP samples (a) and sandwich samples (b) 80

Figure 4.20- CFRP electromechanical rupture tests and corresponding piezoresistive effects along the bending tests 81

List of tables

Table 2.1- Thermoset and thermoplastic resins mechanical and physical proprieties [9]...... 17

Table 2.2- Typical adhesives mechanical proprieties values.. 23

Table 2.3- Effects of various surface pretreatments methods on the surface tension, surface roughness, surface chemistry and bond strengths of the polymer composite [44] 24

Table 3.1- - Mechanical proprieties of the cured HS 160 RM prepreg [73] 36

Table 3.2- Curing cycles for adhesive film [76] 38

Table 3.3- Gauge factor of different materials 58

Table 4.1- Flexural proprieties of the tested foam samples 61

Table 4.2- Flexural proprieties of the CFRP small samples 62

Table 4.3- Flexural proprieties of the sandwich short samples 63

Table 4.4- Flexural proprieties of the CFRP long samples... 64

Table 4.5- Flexural proprieties of the sandwich long beams 65

Table 4.6- Temperature exposition of the foam samples 69

Table 4.7- Experimental flexural proprieties CFRP_S AND CFRP_L and Y. Ma et. Al. [90] results 73

Table 4.8- Experimental flexural strength of different studies and the sandwich samples 78

Table 5.1- Experimental flexural proprieties of the tested specimens 83

Acronyms

ASTM- American Society for Testing Materials

CFRP- Carbon Fiber Reinforced Polymer

CIT- Composite Materials Italy

EASA- European Aviation Safety Agency

FRP- Fiber Reinforced Plastic

GF- Gauge Factor

ISO- International organization for Standardization

MFC- Multifunctional Composites

MFM- Multifunctional Materials

MFMS- Multifunctional Material Systems

MFS- Multifunctional Structures

NDE- Nondestructive Evaluations

NDI- Nondestructive Inspections

PTFE- Polytetrafluoroethylene

PVC- Polyvinyl chloride

SHM- Structural Health Monitoring

USFPL – United States Forest Products Laboratory

Symbols

A-Cross section area

b- Width of the beam

c- Core thickness

D- Midspan deflection

D_w- Dry weight

d- Thickness of the beam

E- Modulus

E_s- Flexural modulus of the skin material

I- Electrical current

K- Bending stifness

L- Span length

l- Specimen length

m- Mass

p_p- Weight of the metal beam used to submerge the foam samples

P- Load

p- Apparent porosity

R- Electrical resistance

R_0- Initial electrical resistance

r- Rate of crosshead motion

S- Suspended weight

S_f- Suspended weight of the foam

SD- Standard deviation

t- Skin thickness

V- Volume

V_e- Exterior volume

V_f- Fiber volume fraction

W- Saturated weight

Z- Rate of straining of the outer fiber

σ- Flexural stress

σ_t- Transverse stress

σ_l- Longitudinal stress

σ_{cl}^*- Flexural strength

τ- Core shear stress

ε- Strain

ε_{ym}- Strain at maximum load

ε_f^*- Maximum strain supported before rupture

π_l- Longitudinal piezoresistive coefficient

π_t- Transverse piezoresistive coefficient

ρ_r- Bulk resistivity

σ_0- Electrical conductance in the longitudinal direction

σ_m- Electrical conductance of the matrix

σ_f -Electrical conductance of the fiber

μ- Specific mass

1. Introduction

The goal of this chapter is to provide general information necessary to understand the relevance and timeliness of this work contextualized by an aeronautical engineering perspective.

In the first subchapter, “Historical background”, is presented a brief history of materials’ evolution from prehistory until the modern times. Along this presentation, is given special attention to composite’s importance in modern aviation.

The second subchapter, “Motivation”, it’s given an introduction on multifunctional materials and their advantages in modern aviation.

Along the third subchapter (Objectives), are defined the objectives for this Master dissertation.

Finally, in the fourth subchapter, is presented the structural layout of this work, as well as brief resumes of each chapter.

1.1 Historical background

Materials are essential for the modern society and are widely spread in our daily routine, transportation, housing, clothes, communication and sports are concrete examples. Theoretically, they influence almost every single activity developed by the human beings in the current century, if we had not developed the ability to transform and manipulate raw materials as we did, our society would not be as we know.

Historically, the evolution of the human species is deeply tied to the development of materials, it was so relevant that some periods of the human civilization were named after the discoveries in this area: stone age, bronze age and iron age [1]. The earliest humans had access to only a very limited number of materials, those that occurred naturally: like stone, wood, clay, leather, etc. Despite the evolution has been remarkable over the millennia since the stone age, it was not until relatively recent times that scientists came to understand the relationships between the structural elements of materials and their properties. This knowledge was acquired approximately 100 years ago, it has led the materials science to a whole new level. The discoveries during this period were fundamental, later allowed the technological revolution and were the propeller of the modern society.

Materials have been grouped into three basic configurations: metals, ceramics, and polymers. These groups were made based on chemical makeup and atomic structure, most of materials fall into one distinct group or another, although there are some exceptions. In addition, there are composites, they are defined as a combination of two or more chemically different materials with a distinct interface between them [2], which together present better proprieties than those materials alone. One of these materials forms a continuous phase and is called the matrix. The other major constituent is reinforcement, in form of fibers or particles, they are in general, added to the matrix to improve or alter the matrix properties. Composites can be classified based on reinforcement nature (Figure 1.1):

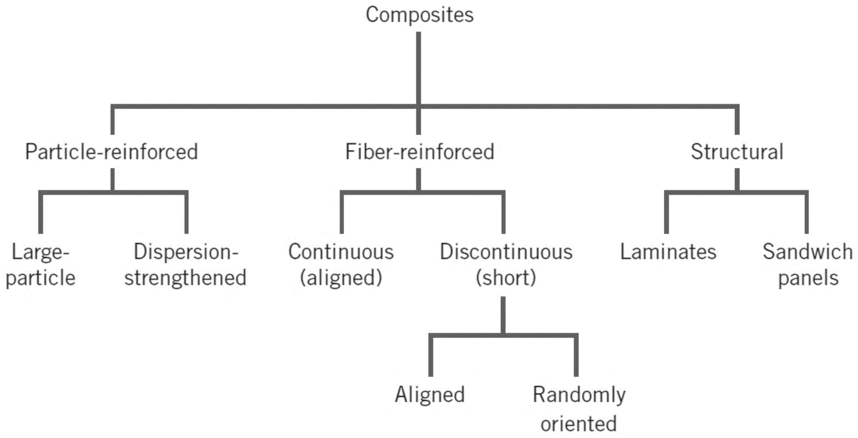
Composites
Particle-reinforced
Fiber-reinforced
Structural
Large-particle
Dispersion-strengthened
Continuous (aligned)
Discontinuous (short)
Laminates
Sandwich panels
Aligned
Randomly oriented

Figure 1.1- Classification scheme of composites based on reinforcement (adapted from [1])

Composites are present in aviation since the first airplane was built by the Wright brothers in 1903, at this time in the form of wood. This was the material with the highest specific strength known back then, neverless it still has some major roles in the structure of some small aircraft today. As it turns out, even in 1903, the weight of structures was already an important criterion when deciding the structural material for an airplane, although the technology has evolved a lot, this principle has not changed. In the aeronautical and space industry, the need for lowest possible structural weight led to the development of high performance composites using carbon fibers and epoxy resins. The advantages of composite materials as compared to metal, become obvious when comparing specific strength and stiffness of high-performance fibers with conventional aircraft materials like aluminum, titanium, and steel [3]. Composites have been in the aviation industry for almost 80 years, in Figure 1.2 is a timeline indicating the approximated year when these materials were introduced in aviation structures.

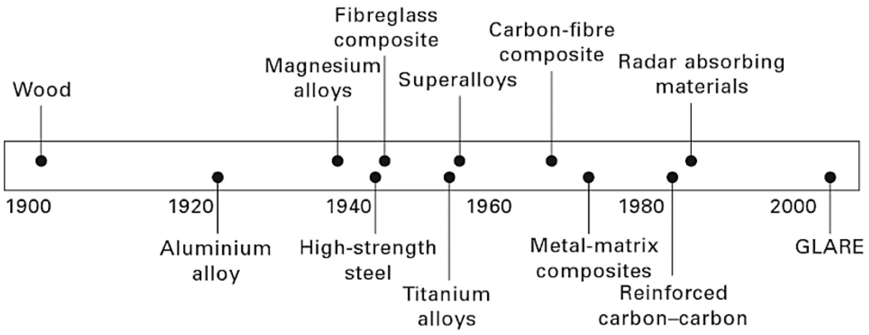
Fibreglass composite
Carbon-fibre composite
Magnesium alloys
Superalloys
Radar absorbing materials
Wood
1900
1920
1940
1960
1980
2000
Aluminium alloy
High-strength steel
Titanium alloys
Metal-matrix composites
Reinforced carbon–carbon
GLARE

Figure 1.2- Historical timeline indicating the approximate year when the main types of materials were first used in aviation (adapted from[4])

Although in 1940 glass fiber started to be implemented in aviation, these applications were used as tertiary components like interior parts, sidewalls, bag racks, and galleys. The implementation of composites occurred gradually over time due to the aviation high safety standards. It was not until the late 1960s that airworthiness authorities gave permission to manufactures to introduce composites into secondary aircraft structures, like spoilers, rudders, ailerons and flaps. The most critical implementation of composite materials was with primary structures like stabilizers, wings and fuselage barrels, it has occurred gradually since the 1980s [3]. The development of these structures was fundamental to the aviation industry, airplanes became much more efficient than they were in the last century and the economic benefits were enormous. Composites provide a substantial weight reduction, allow a significant parts reduction, such as the substitutions of rivets joints for adhesive bonds and don't suffer galvanic corrosion. So, the use of these structures can extend the periods between checks and decreases significantly the parts substitution due to ambient exposure. These facts led the manufactures into a race of composites implementation, this evolution can be seen in Figure 1.3.

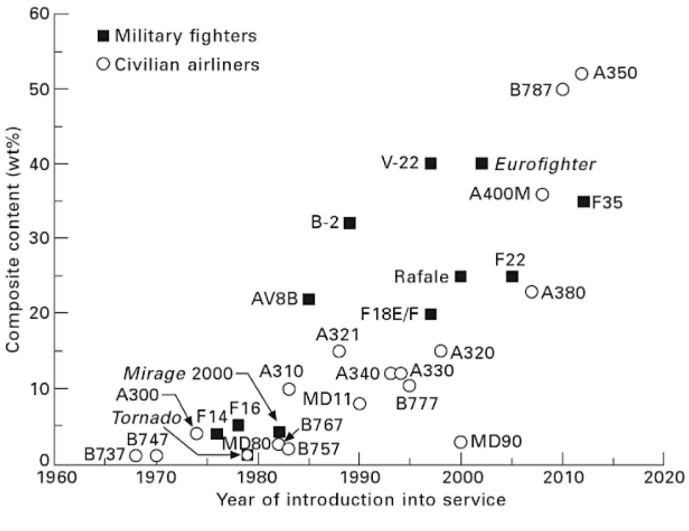

Figure 1.3- Amount of composite material used in aircraft (adapted from [4])

The growth of composite application in aviation has increased from around 5% of the total structural weight of the aircraft, in 1985, to the astonishing 53% of the total structural weight of the recently commercialized Airbus A350. This represents not only an enormous increase in aircraft efficiently, but it is an huge economic advantage for the companies. Boeing 787 is another notable example of efficient composite application in aviation (Figure 1.4), it received the type certificate by the European Aviation Safety Agency (EASA) in September 2011 [5].

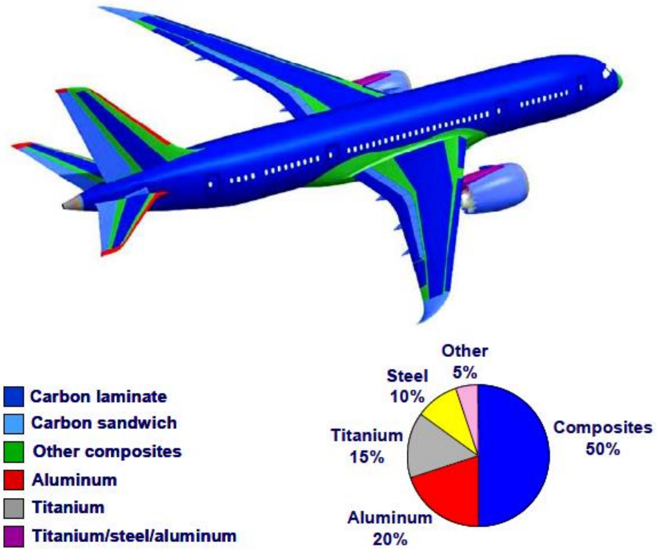

Figure 1.4- Illustration of the composites solutions applied on Boeing 787 (adapted from [3])

One interesting type of composites that was invented much before the composites concept was accepted are the sandwich structures. These structures have been implemented in many areas such as aeronautical, aerospace, nautical, automobiles, wind energy systems, bridge construction and much more. The many advantages of sandwich constructions, the development of newer materials, and the need for high performance, low-weight structures ensure that sandwich construction will continue to be on demand [6].

1.2 Motivation

During the last two decades, a new class of material has emerged, which is characterized by performing two or more functions. Traditionally this doesn't happen, materials are either chosen for their mechanical proprieties, conducting proprieties, others for their chemical or physical proprieties and so on, but it is not unusual for a material to have more than one role in its application. This class of materials is called by different terms in the scientific community. "Smart materials" might be the most known term to designate this class, but it is a term quite lose and can induce some miss understandings. Following the nomenclature adopted by Ferreira et al.[7], throughout this work this class of materials will be called multifunctional material systems (MFMS), where multifunctional materials (MFM), multifunctional composites (MFC) and multifunctional structures (MFS) are integrated. MFMS have the potential to decrease drastically the number of parts, which reduce the need for joining operations, consequently allows a mass and volume reduction. Moreover, some types of MFMS have self-healing/sensing/regulating capabilities, this increases the autonomy, thus decreases the need for human control, therefore maintenance costs will decrease with the development of this technology. The scientific community is aware of this matter, in the last decades the number of publications about MFM, MFC and MFS has been growing and gaining relevance (Figure 1.5).

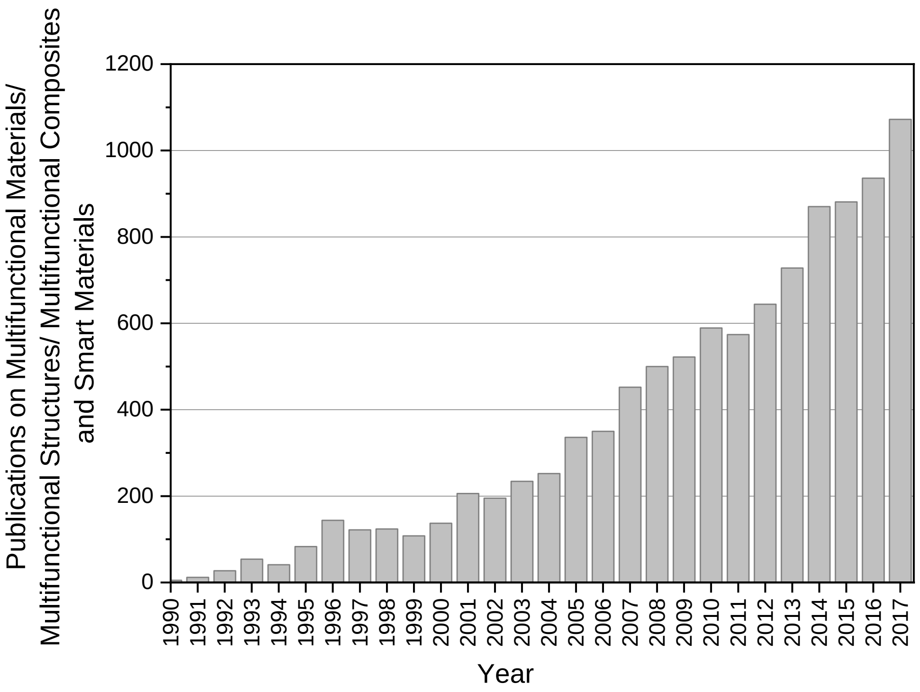

Figure 1.5- Literature survey on MFM, MFS, MFC and Smart Materials from 1995 to 2017 (data collected from Scopus, August 2018)

Real-time monitoring systems have the potential to reduce nondestructive evaluations that are integrated in periodic inspections. This periodic inspections significantly increase the operating expense and vehicle processing time, the need to disassemble and reassemble structural components can lead to damage or degradation of the structure or auxiliary systems [8].

This work has the ambition to produce a reliable MFC, more specifically in a sandwich structure with sensing capabilities, with carbon fiber reinforced polymer (CFRP) skins and a foam core. This system should be capable of measuring deformation throughout the variation of electrical resistance of the CFRP skins. As it was explained previously, aviation industry is one of the major investors in MFM and during this work, will be developed, constructed and tested a self-sensing sandwich structure with possible applications in the aviation.

1.3 Objectives

The present work has the following objectives:

1. Project and manufacture unidirectional carbon fiber sandwich with foam core
2. Characterize the mechanical proprieties of the sandwich material
3. Characterize the electromechanical proprieties of the material
4. Study the self-sensing capabilities of the sandwich structure through the two-probe method
5. Manufacture an effective multifunctional carbon fiber sandwich with possible applications in the aeronautical industry

1.4 Layout

This work is divided into five chapters.

In the present chapter, the study is contextualized in order to provide to the reader with general information needed to understand the relevance and timeliness of this work contextualized by an aeronautical engineering perspective. The objectives are defined along this chapter too.

In the second chapter is presented some of the work that has been developed in the area of sandwich composite structures and multifunctional materials. In this chapter the different constituents of sandwich structures are presented, it's given special relevance no failure modes in sandwich structures.

The third chapter is dedicated to the experimental setup. Along this chapter, every experimental procedure is explained as well as the manufacturing process and the materials used in this work.

In the fourth chapter the results are presented, as well as the respective analysis and discussion. The results are chronologically organized while the discussion is subdivided by the different tested materials.

In the fifth chapter is given an overview of the conclusions taken along this study and suggestion for future work. The suggestions are based on some results that aroused new possibilities of work.

2. State of the Art

The present chapter has the objective to make a detailed review of the literature in the area of sandwich composite structure (e.g. description, classification, historical application, materials and failure analysis) and multifunctional materials.

The first section, “2.1 Sandwich composite structures”, starts with a brief introduction on this matter, followed by a section dedicated to the history of sandwich composite structures (2.1.1). After this section comes the section dedicated to the skins of the sandwich structures (2.1.2) followed by the section dedicated to the core of this material (2.1.3). The fourth section (2.1.4) is dedicated to adhesive bonding.

The second sub-chapter, “2.2 Failure in Composite Structures”, is dedicated to the failure modes of sandwich materials and the different structures that coare integrated in a sandwich structure.

The third sub-chapter, “2.3 Multifunctional materials” is entirely dedicated to showing the evolution of this kind of structures and the importance it has to the aviation industry.

2.1 Sandwich composite structures

A sandwich structure results from the assembly, by bonding or welding, of two thin facings or skins on a lighter core that is used to keep the two skins separated [9]. The skins are the external thin facings material which is characterized by its high stiffness, while the core is a lighter but thicker material, less stiff and it separates the two facing skins. The assembly of the facings with the core is mostly done by adhesive bonding, despite in some cases it can be done by welding. The quality of the bound is fundamental for the performance and life duration of the piece [9]. A typical sandwich structure has a mechanical behavior similar to an I-beam, where the skins carry the “lion” share of bending and in-plane loads, while the core sustains transverse shear, redistributes concentrated normal forces to the skins and maintains the integrity of the structure [10], while maintaining low a density and high specific strength. The constituents previously described are represented in Figure 2.1:

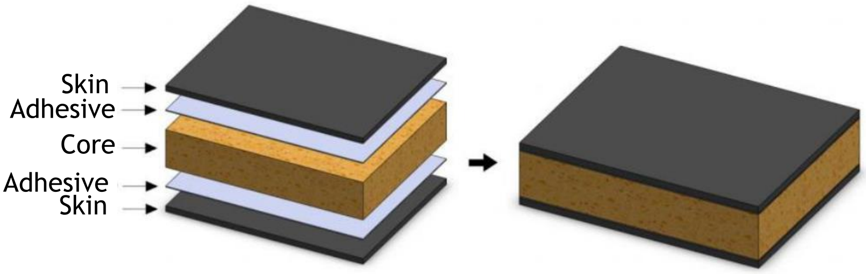
Skin
Adhesive
Core
Adhesive
Skin

Figure 2.1-Constituents of a sandwich structure (adapted from [11])

Sandwich materials are usually classified by its core nature and geometry:

- Homogeneous core materials:

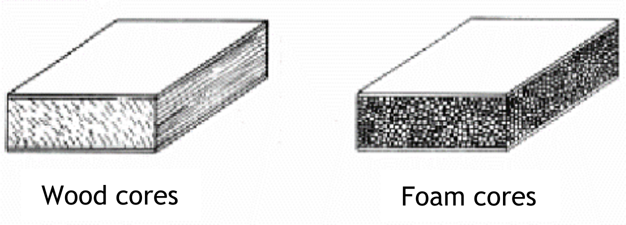
Wood cores
Foam cores

Figure 2.2- Homogeneous core materials (adapted from [6])

- Structured core materials:

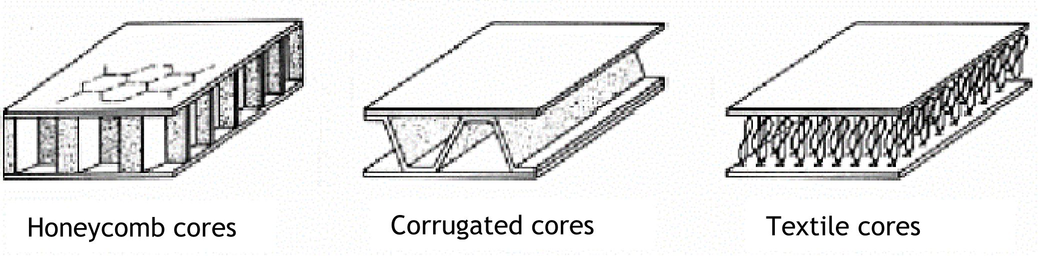
Honeycomb cores
Corrugated cores
Textile cores

Figure 2.3- Structured core materials (adapted from [6])

The use of sandwich structures continues to increase rapidly for applications ranging from satellites, aircraft, ships, automobiles, rail cars, wind energy systems, bridge construction, etc. This kind of materials are being developed to satisfy the increasing demand for high performance, low-weight structures and have become essential for a wide range of engineering fields.

Sandwich composite structures are nowadays one of the major structural constituents of the recently commercialized airplanes. Airbus started to implement composite sandwich structures in the A310, in 1983, with the construction of the rudder in a composite honeycomb sandwich [6]. Since this first implementation, sandwich composite structures have extended its applications to an extended range of components, from primary structures like leading and trailing edge panels on the wings, to tertiary components like floor panels in the passenger compartment. Airbus A380, commercialized in 2005, is an example of composite sandwich structures applications in recent aviation (Figure 2.4):

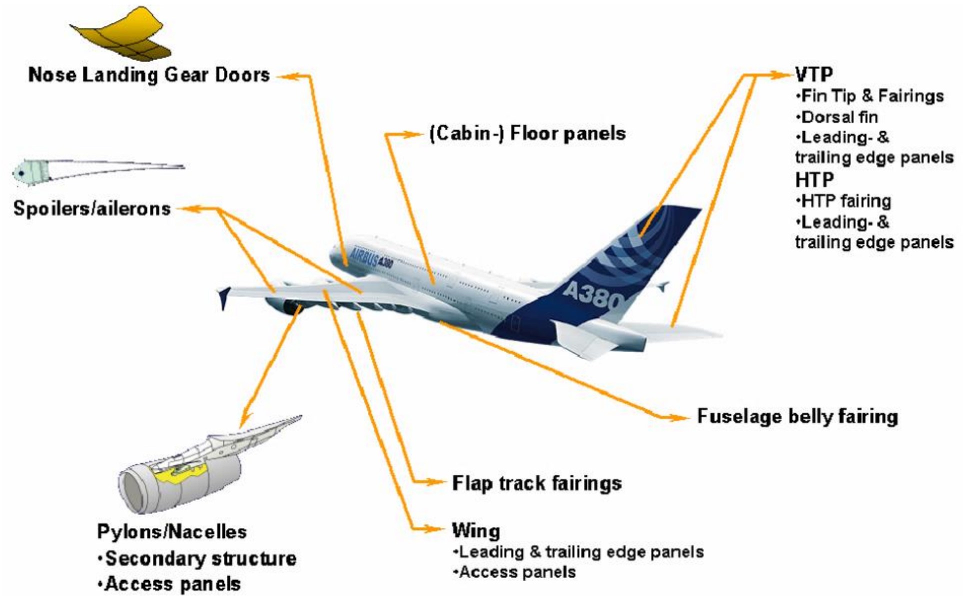
Nose Landing Gear Doors
(Cabin-) Floor panels
VTP
•Fin Tip & Fairings
•Dorsal fin
•Leading- & trailing edge panels
HTP
•HTP fairing
•Leading- & trailing edge panels
Spoilers/ailerons
A380
Fuselage belly fairing
Flap track fairings
Pylons/Nacelles
•Secondary structure
•Access panels
Wing
•Leading & trailing edge panels
•Access panels

Figure 2.4- A380 composite sandwich structures applications (adapted from [6])

Composite sandwich structures cover an extensive range of application in aviation, external structures must stand a wide range of temperatures, sometimes are the first line of thermal isolation of an airplane, they must face simultaneously high aerodynamic loads, must be able to absolve possible impacts during flight and dissipate its energy without cracking. External structures must be prepared to protect the airplane against lighting strikes and at the same time ensure the electromagnetic transmissibility for the avionics systems. On the other hand, floor panels aren't exposed to the adverse conditions of the external components, but must handle with transverse, discrete loads, such as high heels loads, must resist to a wide range of corrosive fluids, which can be spilled by the passenger, and can act as the barrier between pressurized and the unpressurized areas of the aircraft.

2.1.1 History

The concept of sandwich structure goes back to 1849 when Fairbairn projected a sandwich structure composed by iron compression sheets riveted to both sides of a wood core, for the

Britannia Tubular Bridge in North Wales [6]. E. Bishop [6] was the first to implement sandwich principle to powered aircraft, he implemented sandwich concept in the fuselage of the Comet racer, the Albatross and to the wing and fuselage of the Mosquito. This was the first successful airplane with sandwich materials applied to primary structures such as the hull and the wings. It used a balsawood core with facings made of birch plywood, this sandwich concept had some drawbacks due to the use of those bio-degradable materials and their susceptibility to fungi degradation [6].

It wasn't until the World War II that inorganic sandwich composite structures had a substantial role in aeronautical industries, with the construction of the Vultee BT-15 fuselage, using fiberglass-reinforced polyester as the face material using both a glass-fiber honeycomb and balsa core [6].

In 1944, sandwich structures started to develop the interest of the scientific community with the first publication by Marguerre [12], in Germany, dealing with sandwich panels subjected to in-plate compressive loads. In 1948, Libove and Batdorf [13] published a small deflection theory for sandwich plates, and in 1949, Flugge [14] published on sandwich structures optimization. All these works were especially important since these were the first publications on sandwich materials. During this decade, one of the most important companies for sandwich structures development was born, Hexcel Corporation, founded by two World War II veterans. Hexcel is one of todays major producer of honeycomb core materials, with over 50% of market share [15]. In 1951, Bijlaard [16] made important developments in sandwich optimization of a given core depth and face thickness. During the 50s, U.S Forest Products Laboratory (USFPL), which was attached to the University of Wisconsin, made numerous publications of methods of analysis of wood sandwich structures, some of those are still valuable today. In 1956, Gerard [17] wrote one chapter of his book, "Minimum Weight Analysis of Compression Structures", about sandwich structures optimization. During the next year, 1957, Kaechele [18,19] published two USFPL reports on the minimum weight design of sandwich panels and on design procedures and data for sandwich panel tests. In 1966, Plantema [20], from Netherlands, published the first book totally focused on sandwich structures. Three years later, in 1969, H.G. Allen [21] in England, launched another book on sandwich structures, these two books remained as the "bibles" of sandwich structures until the mid-1990s.

The aerospace industry was aware of the potential of sandwich structures and applied this technology to the heat shield of the Apollo capsule. It was a successful project and in 1969 this capsule was able to sustain the stress and heat of the acceleration during the launch and re-entry phase.

During the 70s, a tremendous activity began in Sweden regarding the use of composite sandwich construction for naval ship hulls. Karl-Axel Olsson, from the Royal Institute of Technology, in Stockholm, was a pioneer in the development of sandwich structures. He led the effort among the Swedish Royal Navy and the Swedish shipbuilders to switch from the usual steel hulls to fiberglass composite sandwich structures. Olsson made analysis, small and full-scale tests to prove the effectiveness of composite sandwich hulls and in the end, he was able to show that properly designed composite sandwich hull could be structurally identical or better than steel hulls. As a result, since the 80s, all Royal Navy ship hulls have been made by sandwich constructions [22].

Later in 1996, Noor, Burton and Bert [23], provided an extensive review on sandwich composite structures and computational models applied back then, discussing over than 800 references and provided another 559 references as a supplemental bibliography.

In 1986 the Beech Starship was introduced, the first all sandwich aircraft, its entire structure used Nomex honeycomb with graphite and Kevlar. Although it wasn't a successful aircraft for various reasons, the starship was a pioneer in the use of sandwich composite structures.

Since 1989 to date, have been twelve International Conferences on Sandwich Constructions. The first was hosted by Karl-Axel Olsson, in Stockholm and since then eleven more took place in different continents proving the importance of this type of composites. The last one took place in Lausanne, Switzerland, from 19 to 22 August 2018.

In 1990 Bitzer, from Hexcel Corporation, stated that every two, or more, jet engine aircraft in the western world utilized some honeycomb core sandwich. He stated that the Boeing 707, commercialized since 1957, had only 8% of wetted area made by sandwich structure while the newer Boeing 757/767 (released in 1982) had 46% of wetted area made by honeycomb sandwich material [24].

2.1.2 Skins

The skins of the sandwich structure are the external faces which are built of stiff and strong materials and are much thinner than the light and relatively compliant core. The choice of the sandwich materials depends on the structural application, lifetime loading, availability and cost. Graphite-epoxy and carbon-epoxy multilayered skins are typically used in aerospace applications, while glass-epoxy or glass-vinyl ester are used in the facings of civil and marine structures [10]. The material chosen for the skins of the sandwich structure developed in this work was a carbon fiber reinforced polymer (CFRP). Thus, these materials are introduced and described in detail along the following sub-sections.

2.1.2.1 Carbon Fibers and CFRPs

Fibers occupy the largest volume fraction in a fiber reinforced polymer (FRP) and share the major portion of the load acting on this composite structure. So, proper selection of the fiber type, fiber volume fraction, fiber length, and fiber orientation must be done carefully, since the final proprieties of the composite are dependent from these factors [2].

Based on diameter and character, fibers are grouped into three different classifications: whiskers, fibers, and wires[1]. Whiskers are very thin single crystals that have extremely large length-to-diameter ratios, this type of fibers have a high degree of crystalline perfection and are virtually flaw free. Although whiskers possess these exceptional proprieties, they aren't used as much as expected because this kind of fibers are extremely expensive, besides that, they are difficult to incorporate uniformly into a matrix. On the other hand, fibers are either polycrystalline or amorphous and have diameters much smaller than their length. This kind of materials are the most commonly used as reinforcement, they are either polymers or ceramics and offer great mechanical proprieties. These fibrous materials are cheaper than whiskers and their implementation in the matrix is easier. Wires, or fine wires, have diameters relatively larger than fibers and are usually made by metallic materials [1].

Carbon fibers are commercially available with a large variety of tensile modulus and tensile strengths, generally, low-modulus fibers have a lower density, lower cost, higher tensile and compressive strengths, and higher tensile strains-to-failure than high modulus fibers (Figure 2.5).

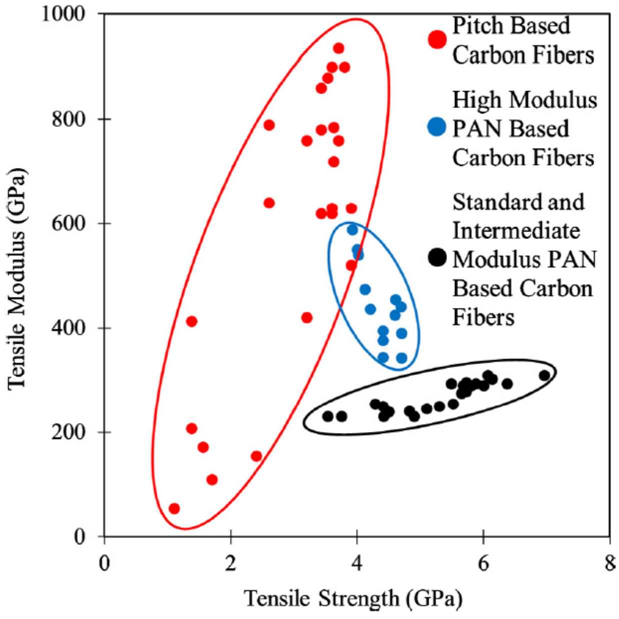

Figure 2.5- Tensile modulus versus tensile strength for commercially available pitch and PAN based carbon fibers [25]

Carbon fibers are manufactured from two types of precursors (starting materials), namely, textile precursors and pitch precursors. The most common textile precursor is polyacrylonitrile (PAN), while Pitch, is a product of petroleum refining or coal coking, it has a higher production cost than PAN [26]. The manufacturing process for each type of precursor is represented in Figure 2.6. It shows the major steps of the two types of carbon fiber production, the carbonization and graphitization processes are identical for both types of precursors. Pitch carbon demands a primary heat treatment, followed by a melt spinning to produce pitch filaments, this is succeeded by a stabilization process. These processes are not needed to transform polyacrylonitrile (PAN) in polyacrylonitrile filaments, this precursor just needs a spinning and stretching process followed by a heat stabilization to produce filaments [27].

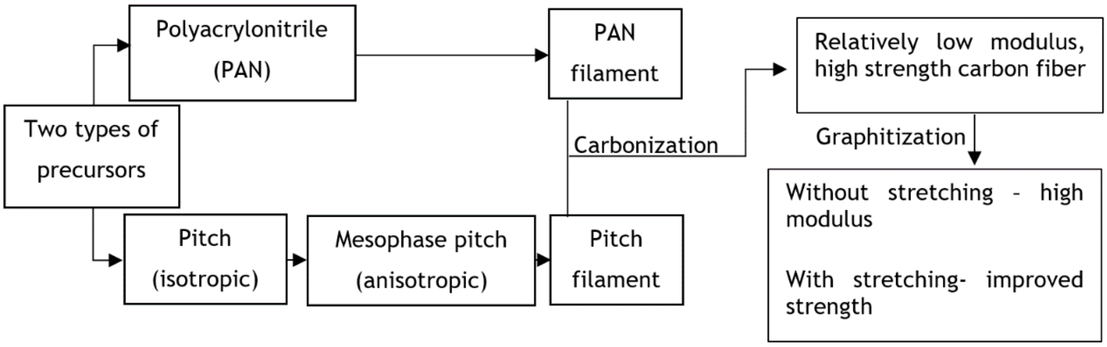
Polyacrylonitrile (PAN)
PAN filament
Relatively low modulus, high strength carbon fiber
Two types of precursors
Carbonization
Graphitization
Without stretching - high modulus
With stretching- improved strength
Pitch (isotropic)
Mesophase pitch (anisotropic)
Pitch filament

Figure 2.6- Diagram of PAN and Pitch carbon production processes (adapted from [27])

PAN filaments are produced from a treatment that consists in a wet spinning and stretching of polyacrylonitrile, followed by a heat stabilization in an oxygenated environment (room concentrations), at a temperature between 200°C and 300°C for 2h. After this cycle, the PAN filaments are ready for the carbonization process.

Pitch carbon needs two different processes to be ready for carbonization: first, it suffers a heat treatment between 300°C and 500°C, which refines and reforms pitch from an isotropic to anisotropic material, it is called mesophase pitch. After this, the mesophase pitch suffers a melt-spinning and extraction process followed by a heat stabilization at temperatures between 200°C and 300°C.

To produce carbon fibers, the filaments must suffer a carbonization treatment: the filaments are heated and stretched in an inert atmosphere, at temperatures that can go from 1000°C to 2000°C, depending on the modulus and strength it must have, for approximately 30 min.

To produce high strength and high modulus carbon fibers, after carbonization the carbon fibers are exposed to a graphitization treatment, which is a thermal treatment above 2000°C with stretching to improve strength.

CFRPs are composites with polymeric matrix and reinforced by carbon fibers. Carbon fibers are known by their low density and high modulus and stiffness, normally the goal of this composites is to maximize strength and/or stiffness on a weight basis. These characteristics are expressed in terms of specific strength (strength-weight ratio), and specific modulus (modulus-weight ratio). These ratios are obtained by dividing the absolute values with the specific weight[1] of the respective material.

Many structural composites, especially for aerospace and aeronautical applications, have laminated structures consisting of multiple layers of long continuous fibers embedded in a matrix. Fiber type, fiber orientation, and fiber architecture may be varied from layer to layer. Each layer, called a lamina or a ply, is typically 0.125 mm thick [2]. These layers can either be cut from prepreg, which is a long sheet of continuous fibers pre-impregnated with a polymer matrix (see section 2.1.2.2), or cut from a carbon sheet and then mixed with the matrix. They are then stacked in the desired fashion and consolidated at elevated temperatures and pressures. A prepreg or a carbon sheet may contain either unidirectional or bidirectional fibers in either a thermoset or a thermoplastic resin. In the unidirectional laminate, the fiber orientation is the same in all plies, for example […0°/0°/0°…]. In this case, the laminate will be anisotropic, i.e. the mechanical characteristics depend on the direction the load is applied and will present the best mechanical response when the load is applied in the same direction of the fibers orientation. The fiber orientation angle can be different in various laminae of a laminated composite. The order in which the laminae with different fiber orientations are stacked is called the stacking sequence, it is engineered to obtain the desired stiffness and/or strength for the laminate. Different stacking sequences produce various kinds of laminates, such as angle-ply laminates […-θ/+θ/-θ/+θ…], cross-ply laminates […0/90/0/90…], symmetric laminates and quasi-isotropic laminates.

---

[1] Specific weight is defined as weight per unit volume and is obtained by multiplying density with the acceleration due to gravity [2].

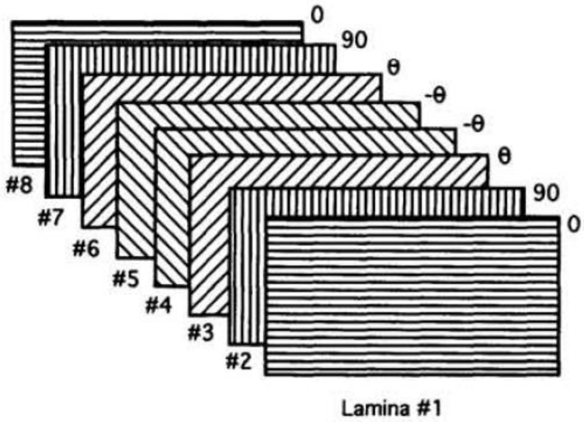

Figure 2.7- Laminate construction in a [0/90/θ/-θ] symmetric laminate.[2]

In Figure 2.7, is a presented a symmetric laminate, where the fiber orientation is symmetrical about the midplane of laminate. For example, [0/+45/-45/-45/+45/0] is a symmetric laminate and can be written as $[0/\pm45]_s$. Symmetric laminates do not exhibit extension-bending coupling, which means that a plane force on the laminate does not produce a bending or twisting curvature, and a bending or twisting moment does not produce any in-plane extension or shear at the midplane of the laminate. Quasi-isotropic laminates are made of three or more laminae, with specific fiber orientation angles to produce an isotropic elastic modulus, Poisson's ratio, and shear modulus in the plane of the laminate. Fiber orientation such as [0/+60/-60], [0/+45/-45/90] and $[0/+45/-45/90]_s$ are examples of widely used symmetric quasi-isotropic laminates. As an example of quasi-isotropic behavior, consider a unidirectional laminate and a quasi-isotropic laminate, both containing T-300 carbon fibers in an epoxy matrix. For the unidirectional laminate, the elastic modulus in the longitudinal and transverse direction are 132.4 and 10.8 GPa, respectively. On the other hand, for the quasi-isotropic laminate, the modulus is 52.3 GPa irrespective of the direction of the measurement.[2]

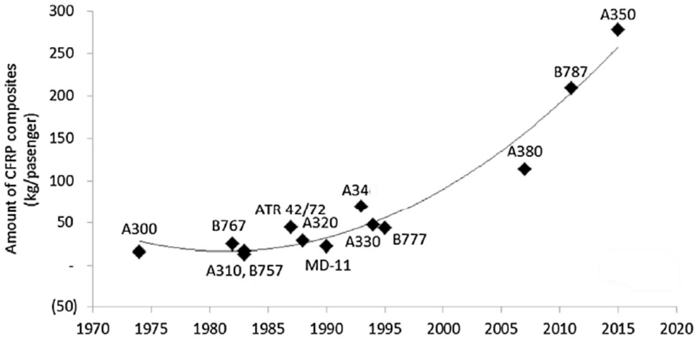

Figure 2.8- Amount of composite used per passenger to manufacture aircraft from 1974 to 2015 (adapted from [28])

The possibility of combining different fiber orientation in different layers make this kind of materials extremely versatile and offer an enormous design flexibility. By manipulating fiber orientation in different layers, the mechanical, thermal and electrical characteristics can be tailored and suited to the design requirements of the structure under consideration. This versatility is one of the principal reasons these laminated structures are slowly replacing most commonly used metal alloys in aeronautical and automotive industries (Figure 2.8) [28].

2.1.2.2 Matrix

Despite existing many types of matrix, such as ceramic, carbon or metal matrix, in this introduction will be given special relevance to thermoset polymeric matrix, specifically, epoxy matrix.

A polymer is defined as a long-chain molecule containing one or more repeating units of atoms, joined together by strong covalent bonds. A polymeric material (commonly called as plastic) is a collection of many polymer molecules of similar chemical structure. In the solid state, usually at room temperature, these molecules are frozen in space, either in random orientation as amorphous polymers, or in a mixture of random orientations and orderly oriented as semicrystalline polymers. Polymers are divided into two categories: thermoplastics and thermosets [2,27].

In thermoplastic polymers, individual molecules are not chemically joined together, they are either bonded by intermolecular forces or secondary bonds, such as Van der Waals bonds and hydrogen bonds. With the application of heat, these secondary bonds can be temporarily broken, which allows molecules to move freely relative to each other or, if pressure is applied, they can flow to a new configuration. When the polymer cools down, it freezes, and secondary bonds are restored, which results in a thermoplastic polymer with a different form.

On the other hand, thermoset resins, once cured, cannot be remelted or reformed. This kind of polymers form three-dimensional molecular chains, is called cross-linking. Due to these bonds, the molecules are not flexible and cannot be remelted and reshaped as in thermoplastic polymers. The higher the number of cross-linking bonds, the more rigid and thermally stable the material will be.

When projecting a high-performance composite, the most desirable proprieties of a matrix are [27]:

1. High tensile modulus, which influences the compressive strength of the composite
2. High tensile strength, which controls the interplay cracking in a composite laminate
3. High fracture toughness, which controls ply delamination and cracks growth

In Table 2.1 are categorized some thermoset and thermoplastic resins and some physical proprieties.

Table 2.1- Thermoset and thermoplastic resins mechanical and physical proprieties [9]

Matrix		Tensile Modulus, *[GPa]*	Tensile Strength, *[MPa]*	Density, *[g/cm^3]*
Thermoset	Epoxy	2.5-5	50-110	1.2-1.4
	Phenolic	2.7-4,1	35-60	1.2-1.4
	Polyester	1.6-4.1	35-95	1.1-1.4
	Polycarbonate	2.4	60	1.2
	Silicone	2.2	35	1.1
	Urethane	0.7-7	30	1.1
	Polyimide	4-19	70	1.4
Thermoplastic	Nylon	1.3-3.5	55-90	1.1
	Polyether ether ketone (PEEK)	3.5-4.4	100	1.3-1.35
	Polyphenylene sulfite (PPS)	3.4	80	1.3-1.4
	Polyester	2.1-2.8	55-60	1.3-1.4
	Polycarbonate	2.1-3.5	55-70	1.2
	Acetal	3,5	70	1,4
	Polyethylene	0.7-1.4	20-35	0.9-1.0

Depending on the application field, other considerations should be taken, such as a good dimensional stability at elevated temperatures, resistance to moister or solvents, resistance to UV radiation, conducting proprieties, etc. Looking at the desirable proprieties for a matrix, thermoplastic polymers offer better mechanical proprieties than thermoset polymers. Thermoplastic polymers have higher impact strength, strain-to-failure and fracture resistance, which offer excellent damage tolerance to the composite. Despite thermoplastic distinct advantages, they have not been used as much as thermoset polymers in composites, mainly because of their lower thermal stability and lower creep resistance.

Epoxy matrix has been the most used polymer in high performance composites, mainly because of their versatility: epoxy resins have many starting materials, curing agents and modifiers. During the cure, this polymer does not release volatile matter, exhibits low shrinkage (during the cure) and offers excellent resistance to chemicals and solvents.

Starting materials for epoxy matrix are low-molecular weight organic liquid resins, containing a number of epoxide groups, which are three-member rings of one oxygen atom and two carbon atoms (Figure 2.9) [27]:

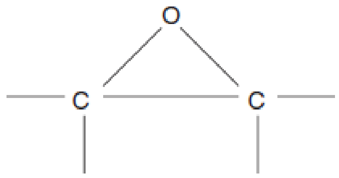

Figure 2.9- Chemical representation of one epoxide group (three member rings of one oxygen atom and two carbon atoms) [27]

A common starting material is diglycidyl ether of bisphenol A (DGE BA), which both contain two epoxide groups. It's usual to add diluents to the starting liquid to reduce the viscosity, in some types cases flexibilizers are added to improve the impact strength of the cured matrix [27][2]. By changing the formulation, properties of epoxies can be changed, the cure rate can be modified, the processing temperature requirement can be changed, the cycle time can be modified, the drape and tack can be varied, the toughness can be changed, the temperature resistance can be improved, etc. To start the polymerization (curing) reaction, which is the solidification reaction, small amounts of a curing agent, such as amines, anhydrides, phenols, carboxylic acids and alcohols, are added just before incorporating fibers into the liquid mix [2]. Cure rates can be controlled through proper selection of hardeners and/or catalysts, each hardener provides different cure characteristics and different properties to the final product. The higher the cure rate, the lower the process cycle time and thus higher production volume rates. Epoxy-based composites provide good performance at room and elevated temperatures. Epoxies can operate well up to temperatures of 90 to 120°C, and epoxies based on novolac and cycloaliphatics can perform well up to 250°C [27]. For high-temperature and high-performance epoxies, the cost increases, but they offer good chemical and corrosion resistance.

A lot of composites with epoxy matrix are commercialized in a semi-solid state, as pre-impregnated (Prepreg) fibers, this is accomplished by slowing the cure reaction, i.e. lowering the reaction temperature before all the molecules are cross-linked, this resin stage is called the B-stage form. The b-staged resin can be transformed into a hard, insoluble mass by completing the cure, for this reason normally prepreg rollers must be stored at low temperatures and have a limited shelf life. This material provides consistent properties as well as consistent fiber/resin mix and complete wet-out, they also eliminate the need for weighing and mixing resin and catalyst.

2.1.3 Core

The core of a sandwich beam is the material placed between the two faces of the structure (Figure 2.10). The core is composed of a lightweight material, less stiff than the faces but stiffer enough to resist the structure deformation. This structure separates the two faces and by this mean guarantee a parallel position between them, avoids slipping, supports shear and bending stresses, transfers applied forces from one face to the opposite face and can act as a thermal and acoustic isolator depending on the material.

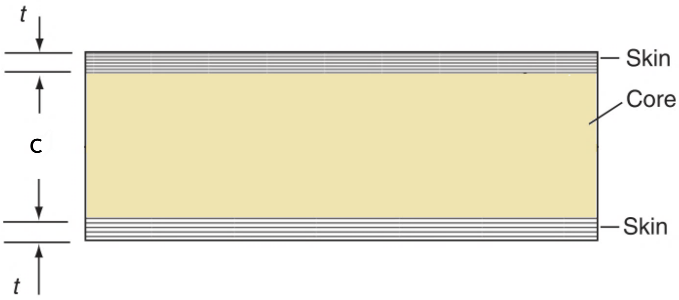

Figure 2.10- Sandwich beam (adapted from [27])

Actually, the most effective method of reducing the weight of a beam or a panel without sacrificing its bending stiffness is to use a sandwich construction (Figure 2.10). The bending stiffness of a sandwich beam is given by equation 1 [6]:

$$K = E_s \frac{bt^3}{6} + 2bE_s t \left(\frac{c+t}{2}\right)^2 + E_c \frac{bd^3}{12} \tag{1}$$

Where:

E_s is the modulus of the skin material

E_c is the modulus of the core material

b is the beam with

t is the skin thickness

c is the core thickness

Equation 1 shows that the bending stiffness of a sandwich beam can be increased significantly by increasing the value of c, that is, by using a thicker core, since core materials have low density, this increase will not add much weight. This is one of the great advantages of using sandwich constructions, but it should be noted that the core material also has a low shear modulus. Thus, unless the ratio of span to skin thickness of the sandwich beam is high, its deflection will be increased owing to the transverse shear effect [27].

Core geometry can either be homogeneous (i.e. wood or foam cores) or structured cores (i.e. honeycomb or corrugated cores). There is a wide variety of foam core available on the market, based on different chemistry and processing technics with different proposes: either structural or isolating, besides many isolating foams can act as a structural reinforcement, since every material that carries a load can be claimed to be a structural core material [29]. One successful material applied to this type of structure is polyvinyl chloride (PVC) foam (Figure 2.11-a) since it has impressive mechanical performance to a very low weight. PVC foam has almost become a trade name even though it is a combination of almost equal parts of polyurea and PVC. Balsa is another popular material inserted in the family of homogeneous cores, comes from balsa wood and its produced by cutting it in thin laminas from timber and glue them together with the balsa cells oriented in the same direction. A concern with balsa is the risk of moisture uptake as with all wood materials, which makes it susceptible to rot if not properly installed or maintained [29].

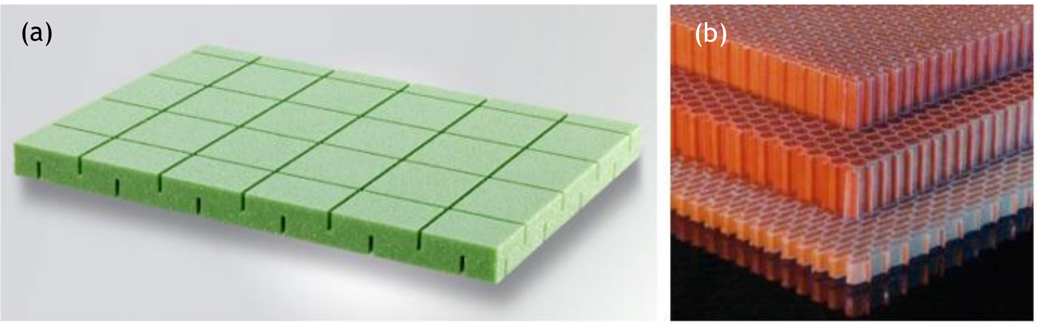

Figure 2.11- a- AIREX® C70 foam core [30], b- Aramid (Nomex®) honeycomb cores [31]

Honeycomb material is a core geometry, normally it comes in hexagonal shape and the most popular materials are aluminum, aramid (Nomex®), polycarbonate and polypropylene [32]. These type of materials provide predictable crash behavior and are used for the design of crash-resistant parts [32], namely aircraft fairings and floor panels in the passenger compartment [6]. Honeycomb materials have been applicated to communication rooms because of their radiations shielding characteristics, the repetitive cellular structure acts as a myriad of waveguides, attenuating signals across a wide frequency range [33].

Recently, new geometries and concept cores have been developed (Figure 2.12), namely truss-cores which takes the excellent mechanical proprieties of carbon fiber nanotubes to the cores of sandwich structures and innovative cell designs capable of better performances than honeycomb cells.

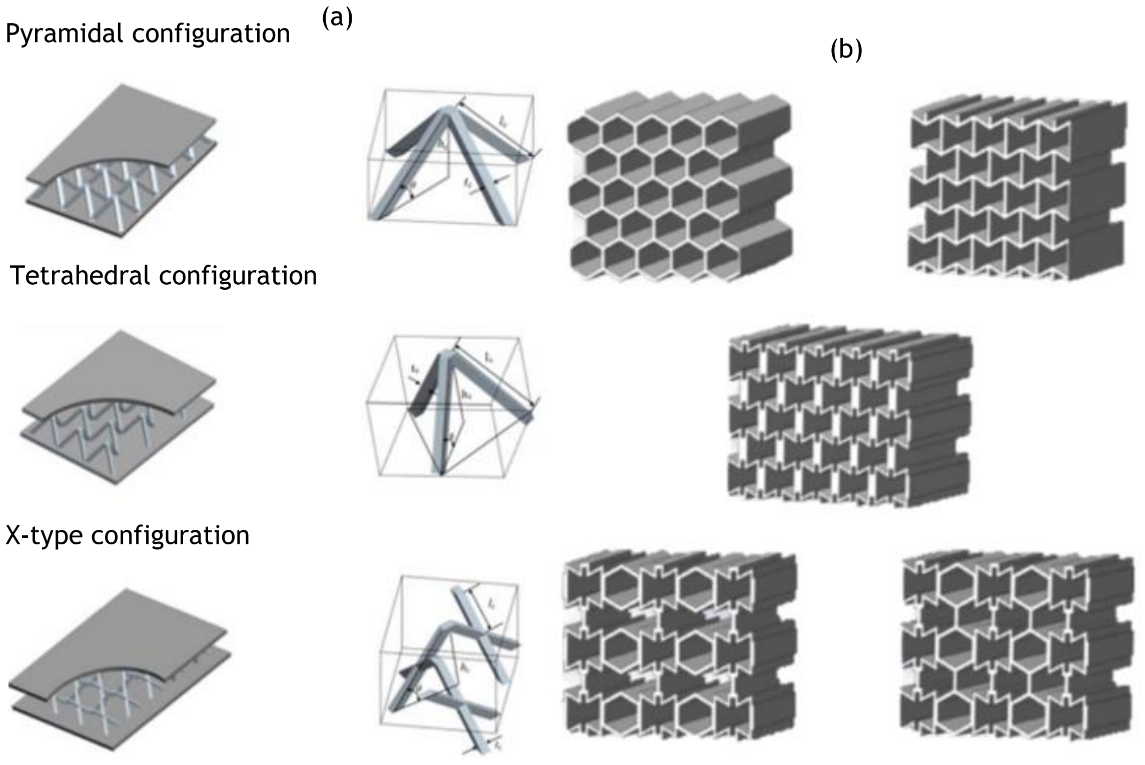

Figure 2.12- Schematics of (a)- three sandwich panels with truss core configuration [34] and (b)-five different cell designs [35]

A series of truss core configurations (Figure 2.12- (b)) under different range of temperature was investigated by Yuan et.al. [34] as well as a comparative study was performed by Ingrole et.al. [35], where they demonstrate the advantages of a hybrid structure combining regular honeycomb and auxetic-strut (Figure 2.12- (b)) structure over honeycomb cells. Many others innovative studies are reviewed by Birman and Kardomateas in [10].

2.1.4 Adhesive bonding

Adhesive bonding is a joining process, between two materials, in which an adhesive is placed between the adherent surfaces, solidifies to produce an adhesive bound [36]. This kind of process offers a great alternative to the conventional used mechanical fasteners such as rivets and screws. Adhesive bounding offers lower structural weight, lower fabrication cost, improved damage tolerance and offer much more versatility and design flexibility when compared to the common fastener methods. Adhesive bonding is especially useful when applied to fiber reinforced composites since it avoids the fiber discontinuities imposed by the fastener methods. The bound is continuous and homogeneous throughout the bounding surfaces so no stress concentrations are created and the structural integrity is increased [36].

The first adhesive bonding with structural applications comes back to 1941, where De Bruyne and Newall developed an adhesive based on phenol-formaldehyde which was marketed under the trade name Redux®, this adhesive was developed for the aviation industry to aid construction of propeller blades. Redux® bonds proved to be so successful that were used in the iconic British civil aircraft Comet (Figure 2.13) and later in the Nimrod [37].

Figure 2.13- Comet aircraft [38]

Since the first applications adhesives have been extensively investigated and developed with the objective of replacing the fastener methods. Adhesives used in structural applications have grown to an extensive family of different chemical products, with different characteristics for different applications. So, before an adhesive can be specified for a specific application, a study in the market should be directed to determine the best adhesives for the application, then tests should be conducted to determine and evaluate the different adhesion parameters. M D Banea and L F M da Silva [36] give a summary of the different types of adhesives that exist in the market and some of their characteristics :

- Epoxy- High strength and temperature resistance, relatively low cure temperatures, easy to use, low cost
- Cyanoacrylates- Fast bonding capability to plastic and rubber but poor resistance to moisture and high temperature
- Anaerobics- Designed for fastening and sealing applications in which a tight seal must be formed without light, heat or oxygen, suitable for bonding cylindrical shapes
- Acrylics- Versatile adhesives with capabilities of fast curing and tolerate dirtier and less prepared surfaces
- Polyurethanes- Good flexibility at low temperatures and resistant to fatigue, offers good impact resistance, and durability
- Silicones- Excellent sealant for low stress applications, high degree of flexibility and very high temperature resistance, capability to seal or bond materials of various natures, long cure times, and low strength

- Phenolics- Good strength retention for short periods of time, limited resistance to thermal shocks
- Polyimides- Good thermal stability, dependent on a number of factors, difficult processability

Typical adhesives tensile modulus are listed in Table 2.2

Table 2.2- Typical adhesives mechanical proprieties values

Adhesive	Type	Tensile Modulus E [GPa]
EA451 U150 [39]	**Epoxy film (unsupported)**	**6.2±2%**
Redux 326 film [40]	Modified bismaleimide (sup- ported)	6.06
Hysol EA 9359.3 [40]	Two-part, modified epoxy paste	2.15
Supreme 10HT [40]	One-part, modified epoxy paste	3.45

The quality of an adhesive bond is dependent on many factors, such as the external and environmental factors like solvents exposition, humidity, UV radiation, exposition to big temperature amplitudes, etc., those can influence the durability of the bond if the adhesive is not correctly chosen, threated or isolated [41]. Another fundamental factor is the fabrication quality, the curing methods must be strictly followed as described by the manufacturer, the manufacturing environment should be as clean as possible to avoid contamination, exposition to deteriorating agents, the adherent surfaces must be cleaned and pretreated. In fact, surface pretreatment and preparation is, perhaps, the most important process step governing the quality of an adhesive bond [42]. To improve bond strength and durability, surface preparation is a necessary pretreatment prior to adhesive bonding. Structural adhesives form chemical bonds between the adherent surfaces atoms and the adhesive compounds, it creates mainly covalent bounds but, in some cases, ionic and static attractive bounds may also be present [43]. Surface pretreatments increase the bond efficiently mainly by increasing the surface tension, increasing the surface roughness and by changing the surface chemistry. The most used surface pretreatments are abrasion/solvent cleaning, grit blasting, peel-ply, tear-ply, acid etching, corona discharge treatment, plasma treatment, and laser treatment, often more than one of these treatments are used on the same surface [36], in Table 2.3 is shown the different operating modes of the various pretreatments listed before.

Table 2.3- Effects of various surface pretreatments methods on the surface tension, surface roughness, surface chemistry and bond strengths of the polymer composite [44]

Treatment type	Material	Nature of treatment	Surface tension	Surface roughness	Surface chemistry	Bound strength	Ref.
Abrasion and solvent wipe	Thermoset and thermoplastic	Remove mold release		✓		Increased for thermosets	[37,38]
Grit blasting	Thermoset and thermoplastic	Remove mold release		✓		Increased for thermosets	[39,40,46]
Acid etch	Thermoset and thermoplastic	Etch*	✓		✓	Slight Increase	[41,42,46]
Pill ply	Thermoset	Remove mold release		✓		Increase	[46]
Tear ply	Thermoset	Remove mold release		✓		Increase	[51]
Corona discharge	Thermoplastic	Oxidising	✓		✓	Double	[48]
Plasma treatment	Thermoplastic	Ablation and/or oxidation*	✓	✓	✓	Increase	[42-45]
Flame treatment	Thermoplastic	Oxidising*	✓			Increase	[38,45]
Laser treatment	Thermoset and thermoplastic	Abolation and/or oxidation		✓	✓	Increase	[46]

*Depends on polymer matrix material

In the case of bonding CFRP to an epoxy adhesive, it is recommended to use a peel-ply, on the adherent surface, to increase the surface roughness and to isolate from the humidity and other detrimental agents, that will weaken the bond between the polymeric matrix and the adhesive. When the peel ply is released from the CFRP, its fundamental to abrade the surface until the first layers of resin is removed but with precaution to do not expose the fiber, since the epoxy adhesive will bond much better to epoxy matrix rather than the fiber [36]. In fact, most adhesive bound failures can be attributed to poor processes during fabrication, with lack of quality surface treatment being the most significant deficiency [53].

2.2 Failure in composite structures

The present subchapter explains the different failure mechanisms of sandwich structures.

It is divided into three subsections: Failure in CFRP and fiber/matrix interface, failure in adhesive interface and failure in sandwich structures.

2.2.1 Failure in FRP

In practice, fibers can exhibit some limitations as to how these layers should be stacked and what fibers orientations are desirable. For example, unless a symmetric laminate is selected there will be curvatures caused by in-plane loads such as uniaxial tension and pure shear. There are other limitations due to the development of interlaminar stresses, which can cause delamination or separation between the layers. Interlaminar stresses are due to the mismatch of Poisson's ratio and shear extension coupling between adjacent layers, that's the reason why the proper selection of fiber orientation in adjacent layers is fundamental to prevent delamination and prevent da failure of the composite.

Since composites are a set of two or more materials, the damage occurs from different mechanisms of the simple materials like metal alloys, damage either occurs from matrix cracking, delamination, fiber breakage, and fiber waviness [2]. According to P.K. Mallick [2], damage in laminated structures can be classified into two categories: process-induced damage and service induced damage. Process-induced damage is a consequence of defects originated by problems during the fabrication process, porosity, fiber waviness, surface scratches, delamination/dents and debonding are examples of process-induced damages. On the other hand, service-induced damage, is a consequence of the mechanical and chemical conditions the composite is subjected during its service period. Abrasion, surface oxidation and swelling are examples of service-induced damage which is caused by the aggressive environments the material is exposed during its in-service phase. Matrix cracking/delamination, fiber breakage, penetration, hole elongation, sublaminate buckling and lamina crushing are examples of service-induced damage originated by mechanical overloads during the in-service period [2].

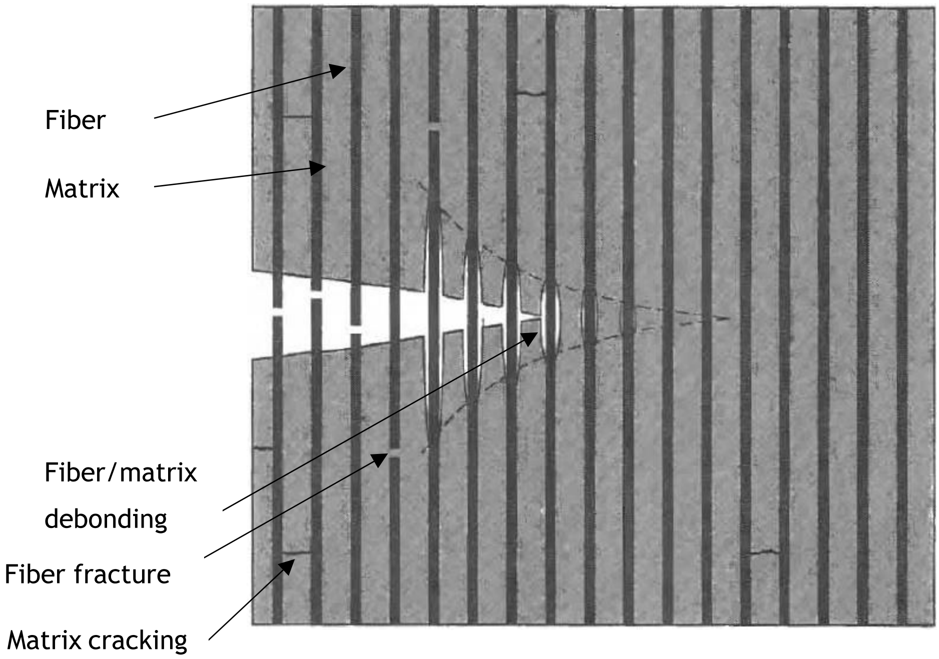

Figure 2.14- Representation of failure mechanism in a CFRP composite (adapted from [2])

In Figure 2.14, is represented a set of failure modes.

Matrix cracking is one of the most common forms of damage that occurs in CFRPs, since this type of failure is hard to be diagnosed, the current design approach is to eliminate or reduce the frequency of matrix cracking by focusing research on the ability to predict and model the initiation and growth of matrix cracks [2].In 1985, A. Wang [54] proved that laminates internal and external geometries, like ply fiber orientation, ply thickness and ply stacking sequence have a strong influence in the formation of matrix cracks. Thus, it is fundamental to understand the mechanisms which provoke this kind of failure and to focus the research on the prediction and prevention. Despite the research on the development of numerical algorithms to predict the formation of matrix cracks, today still is very hard to develop an accurate and computationally efficient numerical procedure to predict damage since its extremely difficult to relate the material microstructural changes to the response of the material [55].

Fiber/matrix interfacial debonding is a consequence of cracks propagation, it induces shear stress at the fiber/matrix interface which can result in interfacial deboning. The debonding will occur in the zone ahead of the crack tip if the interfacial shear strength (τ) isn't high enough, on the other hand if τ is too high, matrix and fibers will fracture without significant interfacial debonding, resulting in low toughness and catastrophic failure.

Delamination is the separation of different plies stacked together due to applied in-plane loads. This type of failure tends to initiate at the free edges, like a free edge of a plate, the free edge of a boundary, like a hole… Due to different Poisson's ratios between plies, each lamina will experience different deformations when acting independently, but when bonded together they must have the same deformation. This simultaneous deformation is achieved through the interlaminar stresses, which have been reviewed by Pagano and Soni [56] and Herakovich [57]. Delamination is usually difficult to detect by visual inspection and sometimes are invisible, this can cause low reliability for primary structures [58]. This is one of the most known failure modes, the physics of delamination is to a certain degree understood [55]. Akira Todoroki et al.[58] have studied the effects of delamination on the electric resistance of CFRPs.

2.2.2 Failure in adhesive joints

Failure modes adhesives bonds are determined by the quality of the bond at each interface, specimen geometry, and loading type [36]. According to ASTM D5573 “Standard Practice for Classifying Failure Modes in Fiber-Reinforced-Plastic (FRP) Joints” [59], there are seven typical characterized modes of failure in FRP adhesive joints (Figure 2.15):

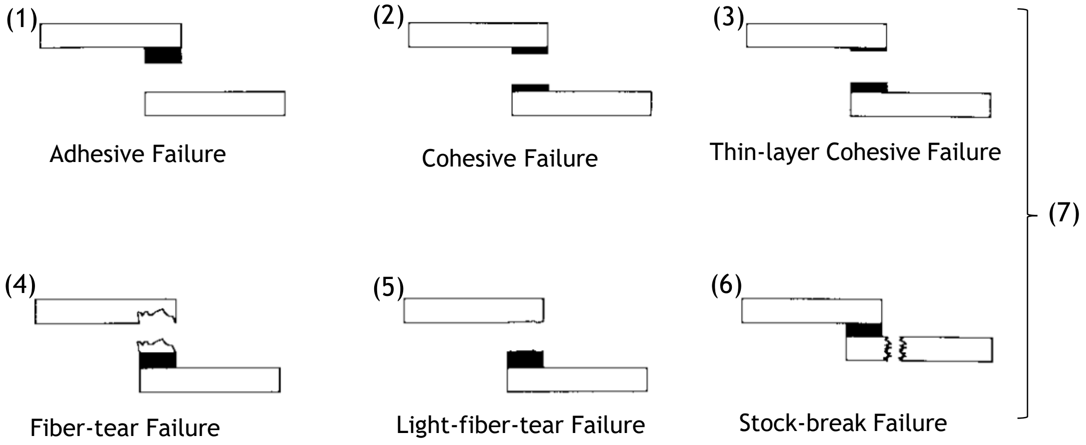

Figure 2.15- Typical modes of failure in FRP adhesive joints [59]

(1)- Adhesive failure corresponds to a rupture of the adhesively bonded joint, such that the separation appears to be at the adhesive-adherend interface.

(2)-Cohesive failure is the rupture of an adhesively bonded joint, such that the separation is within the adhesive.

(3)-Thin layer cohesive failure is similar to cohesive failure, except that the failure is very close to the adhesive-substrate interface, characterized by a light dusting of adhesive on one substrate surface and a thick layer of adhesive left on the other.

(4)- Fiber-tear failure occurs exclusively within the FRP matrix, characterized by the appearance of reinforcing fibers on both ruptured surfaces.

(5)- Light-fiber-tear failure occurring within the FRP substrate, near the surface, characterized by a thin layer of the FRP resin matrix visible on the adhesive, with few or no fibers transferred from the substrate to the adhesive.

(6)-Stock-break failure corresponds to the break of the FRP substrate outside the adhesively bonded-joint region, often occurring near it.

(7)-Mixed failure is any combination of two or more of the six classes of failure mode defined in (1),(2),(3),(4),(5) and (6).

Each failure mode classification is based solely on a visual observation of the failure surface without the aid of a microscope or other means to magnify the surface [59]. Despite many studies for failure predictions for composites bonded joints were performed during the last decades, failure prediction of these joints is still difficult because the failure strength and modes are different according to various bonding methods and parameters [36].

2.2.3 Failure in sandwich structures

When a sandwich structure is exposed to any type of stress, its behavior depends on mechanical proprieties of the constituents (facings, adhesive), core, geometric dimensions and type of loading [60]-63]. Sandwich beams under general bending, shear and in-plane loading can display several types of failure, many times more than one at the same time. It is not easy to predict sandwich failure modes because of the nonlinear and inelastic behavior of the several parts and the complex interaction between different failure modes [62]. As it was explained earlier, the construction quality of the beam is one of the most important factors for the sandwich performance under high stress levels. Possible failure modes include compressive and tensile failure of the faces, core shear failure, face wrinkling failure due to compression, debonding in the core-facing interface, local indentation and global buckling [61].

Facing compressive failure (Figure 2.16-a) occurs when the axial compressive stress on the face exceeds the compressive strength of the facing material [62]. It is highly unprobeable to a structure fail due to core compressive failure because of its low stiffness and high ultimate strain, nevertheless, it could happen when combined with other failure modes that can gather the conditions for this kind of failure. Face wrinkling failure due to compression (Figure 2.16-b) occurs when small wrinkles appear in the compressed due to stress concentrations, these wrinkles are local elasto-plastic deformations, this failure mode can be called local buckling[2] too [63].

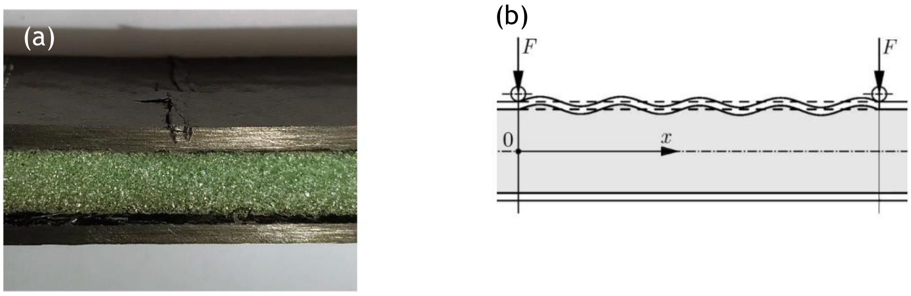

Figure 2.16- Sandwich compressive failures, a-Face compressive failure, b- Face wrinkling failure or local buckling (adapted from [64])

Tensile failure occurs in the tensile face, when the deformation induces flexural stress higher than the flexural strength of the tensile face. In a three-point bending test, this failure starts on the tensile side of the tensile face, directly above the point of load application, where the tensile stress is maximum and propagates in direction of the structure compressed face.

Core shear failure (Figure 2.17) is induced by the shear stress in the core. The shearing force is taken mainly by the core, resulting in high core strains due to the low shear modulus of the core. Along the elastic region, the core is under nearly uniform shear stress, but when the material enters in the plastic region, the core begins to yield, and the shear strain becomes highly nonuniform peaking at the center[62]. If any shear stress peak exceeds the material shear strength, a core shear failure is eminent at that point.

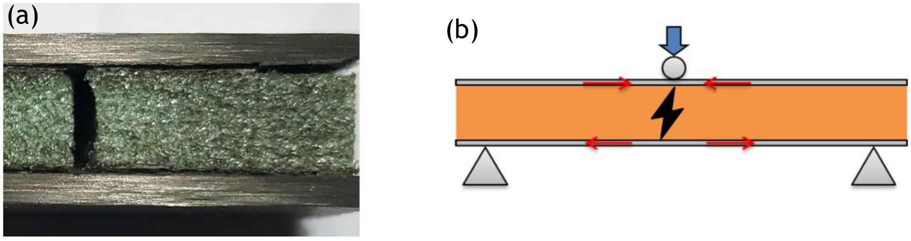

Figure 2.17- Core shear failure, a-Real core shear failure, b-Graphic representation of core shear failure and forces that contribute to this failure (adapted from [29])

Debonding in the core-facing interface (Figure 2.18)Figure 3.10, is a failure induced by shear stress between the core and the faces. Contrarily to the core shear failure, where the core fails to sustain the shear forces, in this case, is the adhesive that fails to stand the shear loads.

---

[2] Deformable state where the straight configuration of the beam becomes unstable.

Adhesive failure, cohesive failure and thin layer cohesive failure are the adhesive failures that are associated with the debonding of the core-facing interface.

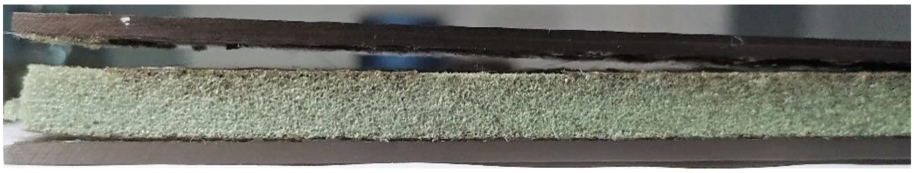

Figure 2.18- Debonding of the core facing interface

Indentation failure (Figure 2.19- a) is a predominant failure mode in cases where the applied load is distributed over a small area [65]. Indentation failure occurs when the core yields to the significant local deformation of the loaded facing, which causes high local stress concentrations, when this interfacial stress reaches the yield strength of the sandwich core, indentation failure occurs [63, 66].

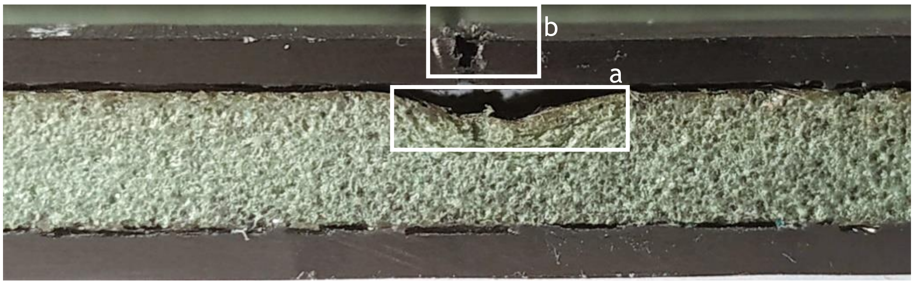

Figure 2.19- a- Indentation failure and b- face compression failure in the same specimen

Global buckling of a sandwich beam is a geometric instability where the structure under compressive stress reaches a buckling state, when the response of the material to the compressive stress becomes unstable[63]. Normally a structure does not fail to buckle but can fail due to buckle, since when a structure reaches this unstable state can deform much easier than in normal conditions and other types of failures may occur.

It is important to notice that it is common to have several failure modes together, the interaction of failure modes may occur, the first failure will weak the structure which can lead to another failure mode. Figure 2.20 is an example of the interaction between failures.

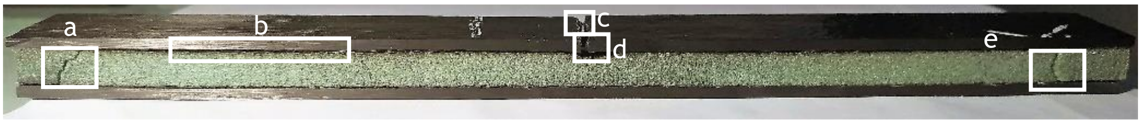

Figure 2.20- Several failure modes in the same specimen, a-Core shear failure, b-Debonding of the compression face core interface, c- Facing compression failure, d- Indentation failure, e-Partial debonding on the tensile face core interface

Taking Figure 2.20 as an example, the first failures modes were in both tips of the specimen, a partial debonding of the tensile face core interface (e), followed by core shear failure (a). After the specimen continued to deform and showing signs of larger strain on the compressed face this led to the debonding of the compression facing-core interface, as the specimens continued to deform the core started to show indentation signs (d), a consequence of the lack of support of the shear forces that led to high stress concentrations directly below the load application point, finally the top face failed to compression (c) in the point of load application.

2.3 Multifunctional materials

A challenging issue presented in the aircraft community is how to maximize the performance of materials and structures, as to strengthen their integrity and reliability, and meantime lower production, operation and maintenance cost. As a response to these demands, the level of interest in multifunctional materials has increased during the last two decades.

A multifunctional material is by definition a composite [66], it is characterized for performing more than one function in its application. The attributes of a MFS may include the abilities of self-diagnose, repair, recover, report and learn [67]. In the process of designing and building this type of structures, in most cases is necessary to embed sensors, processors and actuators to get the multifunctionality desired. According to Ferreira et al. [7], multifunctional material systems are divided into three types:

1. Multifunctional structure (MFS)- which is composed of distinct materials, each with different functions, mounted, coated or laminated onto another.
2. Multifunctional composite (MFC)- is a material composed of distinct materials, embedded onto another, simultaneously taking more than one function.
3. Multifunctional material (MFM)- which is a single material that combines different functions at a molecular level. Hybrid multifunctional materials are integrated into this category.

During this work will be given special relevance to stimulus responsive materials for structural health monitoring (SHM).

The G-11 SHM committee for Structural Health Monitoring and Management, Aerospace Industry Steering Committee [68], defined SHM as “the process of acquiring and analyzing data from onboard sensors to evaluate the health of a structure”. SHM facilitates the detection and characterization of damage to a structure or component that may result in its ability to fully and safely perform its function. The ultimate goal of this technology is to identify damage at the earliest stages, so corrective actions can be performed to minimize downtime, operational costs, maintenance costs, and at the same time reduce the risk of catastrophic failure, injury and loss of life. This technology has experienced some great progress during the last twenty years, mostly due to the increasing development of MFM and MFS. Applications have expanded from aerospace, civil and mechanical structures, to essentially all other types of critical structures, including those in the nuclear, marine and wind turbine industries [69]. SHM when fully developed, should be able to decrease drastically the need for nondestructive inspections (NDI) and nondestructive evaluation (NDE), such as visual inspections, ultrasonic inspections, eddy current, acoustic emissions, X-ray inspections, radiography inspections and thermography inspections. These methods often require partial disassembly or removal of aircraft components, which demands down-time depending on the type of check (A, B, C, and D), downtime can go from eight hours interval (A checks) to two months (D checks) [70]. These checks are either scheduled or taken if some structural degradation is suspected, which limits the inspections to schedule intervals and leaves a time gap where small failures can occur without notice. These inspections are always taken for prevention, so they are scheduled with a large margin of safety which represents heavy expenses for the companies. SHM technologies have the potential to reduce these NDI and allow the continual examination, even while the vehicle is in service.

Sensing and actuation are two closely related non-structural functions, and in many cases, the same material or device can perform both functions. These materials respond to a specific stimulus by altering some of their physical and/or chemical proprieties. In this work, it will be given special relevance to structural CFRPs with mechano-responsive capabilities. There is a wide range of stimulus witch materials can be sensitive [7]:

- Mechano-responsive- responds to stress changes either by producing a voltage when the material is stressed (piezoelectric) or by sensing the differences in the materials' electrical resistance when stressed (piezoresistive).
- Thermo-responsive- responds to temperature variation of the material, either by changing color (thermochromic), converting temperature changes in differences into a voltage (thermoelectric) and even shape memory alloys, polymers and ceramics are integrated into this category.
- Electro-responsive- responds to electrical current or voltage, either by changing color (electrochromic), by producing strains under the influence of an external electric field (dielectric elastomers), by exhibiting changes in shape when an electric stimulus is applied (electro-active polymers), piezoelectric, piezoresistive and thermos electric materials are included in this category too.
- Magneto-responsive- responds to magnetic stimulus, either by changing shape when a magnetic charge is applied (Magnetorheological fluids), or by changing the materials'

magnetization under stress or changing shape if subjected to a magnetic field (magnetostrictive)

- Chemo-responsive- responds to pH changes, smart gels are examples of a polymer which can react to this kind of stimulus.
- Photo-responsive- responds to light changes, either by changing color (photochromic) or changing shape under light exposure (photomechanical).

Most damage detection approaches require the use of multiple sensors located near the damaged locations, so it is fundamental to predict the possible places where the structure may fail. It is always important to take practical considerations, such as cost, weight, and limit the implementation of these sensors to the specific locations where structural damage is more likely to occur.

Many solutions for damage detection have been investigated, as an example, implementing fiber optic sensors can be accomplished by implementing fiber Bragg gratings and use variations in the refractive index of the fiber to determine changes in strain or temperature at each Bragg rating location [8]. Piezoelectric sensors have been widely investigated and offer an easy implementation and reliable results [57].

One of the many particularities of CFRP composites is their electrical conductivity, since their main constituent is carbon, when fiber networks are stretched, compressed or break within the structure, its electrical resistance is expected to change, this propriety is called piezoresistivity, a strain gage is a known example of the use of piezoresistivity as a strain sensor [71]. This conductivity makes CFRP a self-sensing material and this method does not cause a reduction on static strength or fatigue strength [58], so using this principle is possible to monitor and measure applied strain without the implementation of additional sensors which offers excellent economic advantages, when compared to expensive sensors sometimes with difficult implementation. Carbon fiber was first used as strain sensor in 1969, by P. C. Conor and C. N. Owston [72] by stretching different fibers at a controlled rate and simultaneously measuring the variation in electrical conductivity. Although this principle has many advantages, it was not until recent years that electrical conductivity caught the attention of the scientific community, because when CFRP is plied in multidirectional orientations has very high anisotropic electrical resistance, which for many years was a barrier to the development of this technology [71]. In unidirectional carbon fibers the electrical conductance in the longitudinal direction (σ_0) is easily calculated by multiplying the fiber volume fraction (V_f) by the electrical conductance of the fiber (σ_f), equation 2. If the matrix volume fraction and matrix conductance (σ_m) are not considered since the matrix acts as an isolator and its conductance is redundant, equation 3 [58]:

$$\sigma_0 = \sigma_f V_f + \sigma_m (1 - V_f) \tag{2}$$

$$\sigma_0 = \sigma_f V_f \tag{3}$$

The volume fraction of the fibers can be estimated by taking images from the cross-section of the laminate, then the volume fraction can be calculated by dividing the number of fibers by the volume of the cross section photographed. Depending on the degree of compaction of the fibers, the composite produces non-zero electrical conductance in the transverse direction. This propriety is accentuated in prepreg CFRPs because during production the laminates are pressed with rollers against each other augmenting the degree of compaction and consequently the contact between fibers from different plies. In multidirectional fibers, this conductance can be hard to estimate [71]. Depending on the stacking sequence, the material must be electrically characterized in every direction in order to achieve a good estimation of this propriety. After this initial characterization, it is possible to detect future damage, such as delamination or matrix cracks: delamination decreases the contact between piles while a matrix crack growth breaks the fiber-contact-network between plies, which can lead to delamination, so in both phenomena the composite will experience a decrease in electrical conductance which can be detected if this propriety is monitored.

3. Experimental procedure

In this third subchapter is presented all the information and procedures used to prepare the experimental work and guarantee valid results.

In the first subchapter, “3.1 Materials and fabrication prosses”, are presented the materials used in the experimental processes, and is explained in detail all the processes used to produce the different specimens.

The second subchapter, “3.2 Experimental setup”, is shown every equipment used to test and collect the necessary data for this study. Moreover, are explained the principles and calculations used to define the test parameters for the different specimens and tests that took part in this work.

3.1 Materials and fabrication processes

With the objective of characterizing mechanically and electrically the sandwich beams, a set of specimens was projected. The beams were composed of two facing skins of unidirectional CFRP, made of twelve layers of prepreg HS 160 RM [73], supplied by CIT- Composite Materials Italy, and an AIREX® C70 [74]foam core. The adhesive film used to stick the facing skins to the foam core was a structural epoxy adhesive film, EA451 U150 [39], designed for co-cure and secondary bonding of composite substrates, also for bonding honeycomb and foam core sandwich panels.

First, two unidirectional carbon fiber laminates were fabricated from the HS 160 RM prepreg roll. This roll was stored at -18°C, to minimize the curing reactions of the epoxy matrix pre-impregnated in the carbon fiber reinforcement, the mechanical proprieties gave by the manufacturer are listed in Table 3.1.

Table 3.1- - Mechanical proprieties of the cured HS 160 RM prepreg [73]

	Value Actual 54% F.V.	Value Normalized 60% F.V.	Standard
Tensile modulus, *GPa*	123	136	ASTM D3030-00
Tensile strength, *MPa*	2294	2549	
Poisson's ratio	0.34	-	
Flexural modulus, *GPa*	134	149	ASTM D790-03
Flexural strength, *MPa*	1857	2063	
Interlaminar shear strength, *MPa*	81.5	-	ASTM D5528-01
Interlaminar fracture toughness, J/m^2	800	-	

The pre-impregnated resin was an epoxy matrix [75], it can be cured under a wide range of temperatures, but the manufacturer recommends a curing process under 125°C for 60 minutes. This temperature corresponds to the temperature from which the viscosity of the resin grows exponentially, therefore, under these conditions the impregnation of the resin into the reinforcement is maximized [39].

The curing prosses was made under the conditions recommended by the manufacturer. An autoclave with a maximum working area of 30x30 *cm* was programmed to perform cycles of 60 minutes, with a temperature of 125°*C*, pressure of 5*bar* and the samples were isolated by a high temperature nylon Stretchlon 700 bag to remove the air bubbles that could be infiltrated between layers.

The first step was to cut twelve squares of CFRP measuring 30*cm* x 30*cm* from the roll, the instruments used to perform this process was a box cutter and a ruler to guarantee a straight cut, Figure 3.1.

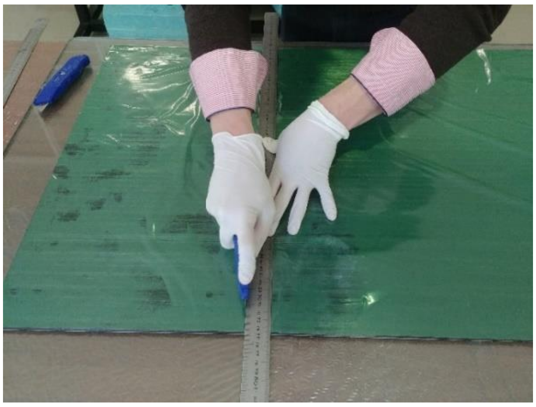

Figure 3.1- Prepreg transverse cutting

The carbon fiber is a very rigid material and offers great resistance when the cutting force is applied perpendicular to the direction of the fibers, so it is important to say that the box cutter must be propriety sharp to perform a smooth and efficient cut. Contrarily to the transverse cut, the longitudinal cut (direction of the fibers) was easier, when cutting in this direction, the blade just had to separate parallel fibers and penetrate the pre-impregnated resin.

The next step was to glue the twelve laminas previously cut, so a heat gun was used to improve and uniformize the sticking process between the laminas (Figure 3.2- (a)) and then pressed for two minutes to promote the elimination of air bubbles that might have formed during this process. The first layer, placed between the metal mold and the CFRP plate, is a Teflon Release 234 TFP which minimizes the adhesion between the prepreg resin and the mold. The next layer, the white tissue under the laminas in Figure 3.2, is a pill ply, which is a removable layer that has the propose of protecting the surface of the CFRP board after its cure.

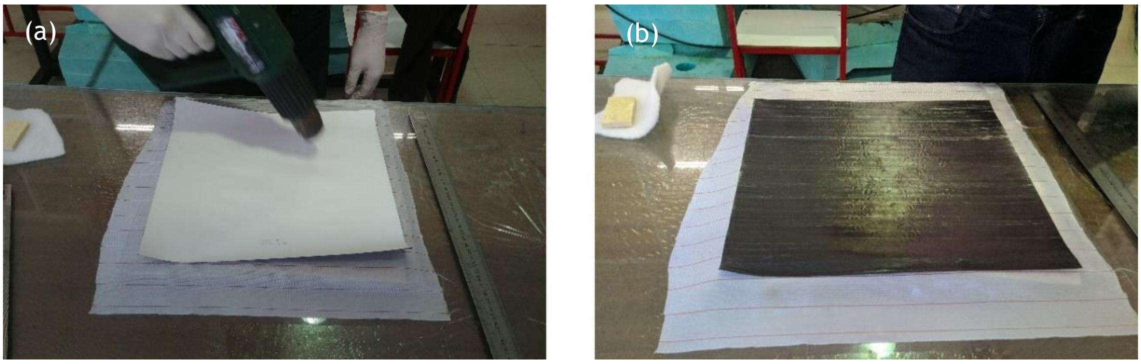

Figure 3.2- Heating (a) and setting (b) the first CFRP layer

The twelve layers were stacked following the procedure described above. When the laminas were all stacked, they were placed into a high temperature nylon Stretchlon 700 bag, along with an absorbent fabric (nylon, wltraweave) then it was placed in the autoclave for sixty minutes (Figure 3.3).

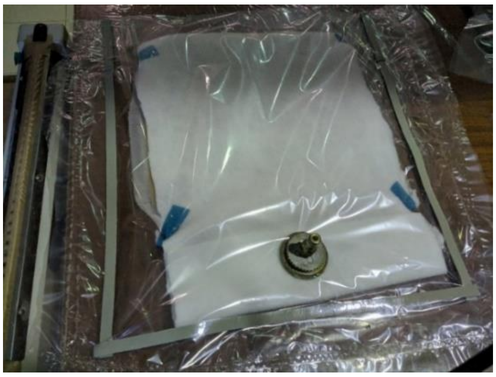

Figure 3.3- Vacuum bag with CFRP 12-layer unidirectional board before the curing prosses

The process previously described was used to produce all the CFRP used in this work.

Two of the CFRP boards were cut in a water jet machine (Pronum, WaterJet 3015) following the sketch represented in Figure 3.4- CFRP cutting

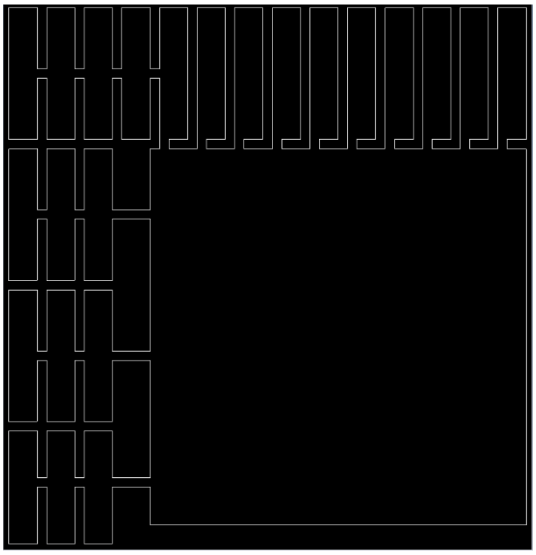

Figure 3.4- CFRP cutting sketch

From the initial 300mm x 300mm CFRP plates, a total of twenty-three CFRP samples were cut from each board: twenty samples measuring 15mm x 70mm, another three samples measuring 15mmx60mm and a square board measuring 200mm x 200mm destined for the production of longer samples.

The adhesive used to bound the carbon fiber facings to the foam core was an epoxy adhesive film, EA451 U150 [76], supplied by Composites Materials Italy, this adhesive has a wide range of curing temperatures, going from 90°C to 180°C, see Table 3.2.

Table 3.2- Curing cycles for adhesive film [76]

Temperature [C°]	Time [h]
90	7
100	4
125	1
135	2
180	2

The curing temperature of the adhesive used in this work was 90°C, since the foam manufacturer recommends a maximum operating temperature of 80°C. The implications of this temperature exposition were tested and analyzed.

Two types of bonding were selected to be tested, simple adhesive bonding with two layers of adhesive on each side of the foam core, and a reinforced bounding with two layers of adhesive reinforced with a glass fiber veil. Ten samples were produced, five reinforced and five unreinforced. The autoclave used as a hoven, so it was set at atmospheric pressure. Since it is difficult to see the reinforcement after the curing process, the samples were previously marked and categorized.

Longer samples were also produced from the square measuring 200mm x 200mm in Figure 3.4 right lower corner. First, a sandwich panel was produced with the exact measures of this square, with a bounding reinforced by glass fiber veil. After the adhesive curing process, the samples were cut with a grinding wheel because the water jet machine does not perform precise cutting in soft materials such as the foam core. Eight samples were projected from the sandwich board measuring 190mm x 21mm ±1mm (Figure 3.5).

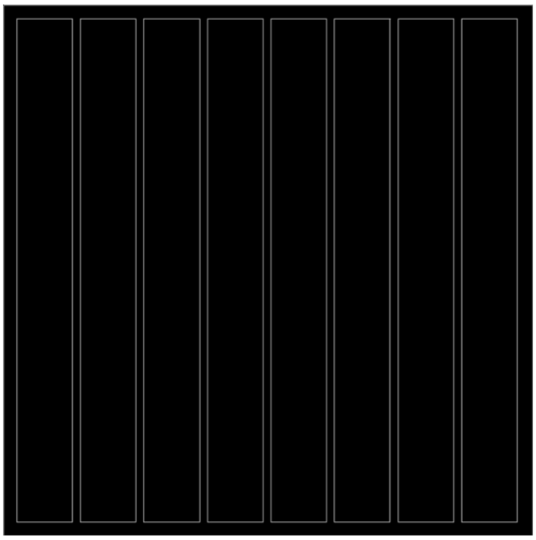

Figure 3.5- Sandwich long samples cutting sketch

In Figure 3.6 is presented the final aspect of the smaller specimens (a) and the final look of the bigger samples (b).

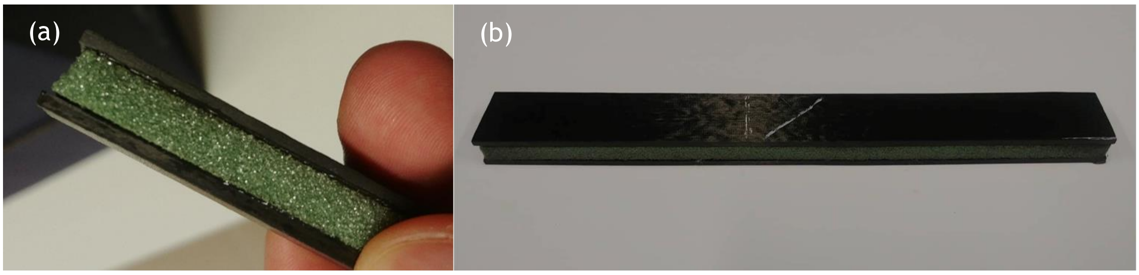

Figure 3.6- (a)- Sandwich short specimen 15mm x 70mm (b)-Sandwich long specimen 21mmx190mm

It’s notable the darker foam core in the specimen (b) due to the different cutting method. Sample (b) was cut directly from a sandwich board by a grinding wheel, the foam sides were exposed to carbon dust produced by this cutting method. The foam core was not affected by the temperature of the grinding weal.

Finally, sandwich and CFRP samples were prepared for the electrical characterization and testing (Figure 3.7).

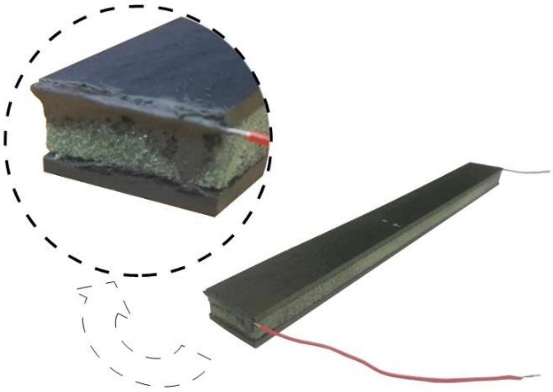

Figure 3.7- Sandwich specimens with wire integration

To prepare the specimens for the electrical characterization and the mechanical testing with simultaneous electrical measures, two copper cables were glued to one of the specimen’s facings. An EM-Tec C39 conductive carbon paste [77] was used to attach the copper wire to the facings tips. This method is called the two probe method [71], it has the objective to maximize the contact area between the facing fibers and the wire, by this mean guarantee that the electrons will be uniformly distributed by the fibers and the electrical resistance minimized. Since carbon fiber is a good electrical conductor and the fibers are all oriented in the longitudinal direction, it is expected that the facings will offer high conductance between the two tips of the facing.

3.2 Experimental setup

3.2.1 Archimedes' principle

Archimedes' principle, or physical law of buoyancy, states that any body completely or partially submerged in a fluid at rest is acted upon by an upward force, the magnitude of which is equal to the weight of the fluid displaced by the body. The specific mass is given by equation 4:

$$\mu = m/V \tag{4}$$

Where,

μ is the specific mass, kg/m^3

m is the mass, kg

V is the volume, m^3

Following the standard ASTM C20-00 [78], it's possible to determine the density and the apparent porosity (open porous) of the specimens.

The density of the CFRP and the foam core was determined separately.

So, following the procedure described in the standard, the carbon and the foam specimens were dried in the oven for two hours and the dry weight (D_w) was measured in the Oertling VA204 (Figure 3.8-a). After this first step, the specimens were submersed in distilled water for 24 hours, which is called the saturation process. The saturated weight (W) was measured in the same balance configuration. Finally, the suspended weight (S) was measured as it is described in the standard (Figure 3.8- b). Since the foam is lighter than water an alternative method was adopted to measure the suspended weight. First, a metal weight was weighed (p_p) under the same conditions totally submerged. Then, the foam specimens were weighed with metal weight above them (S), so the two materials were at rest totally submerged and the suspended weight of the foam (S_f) is given by equation 5:

$$S_f = S - p_p \tag{5}$$

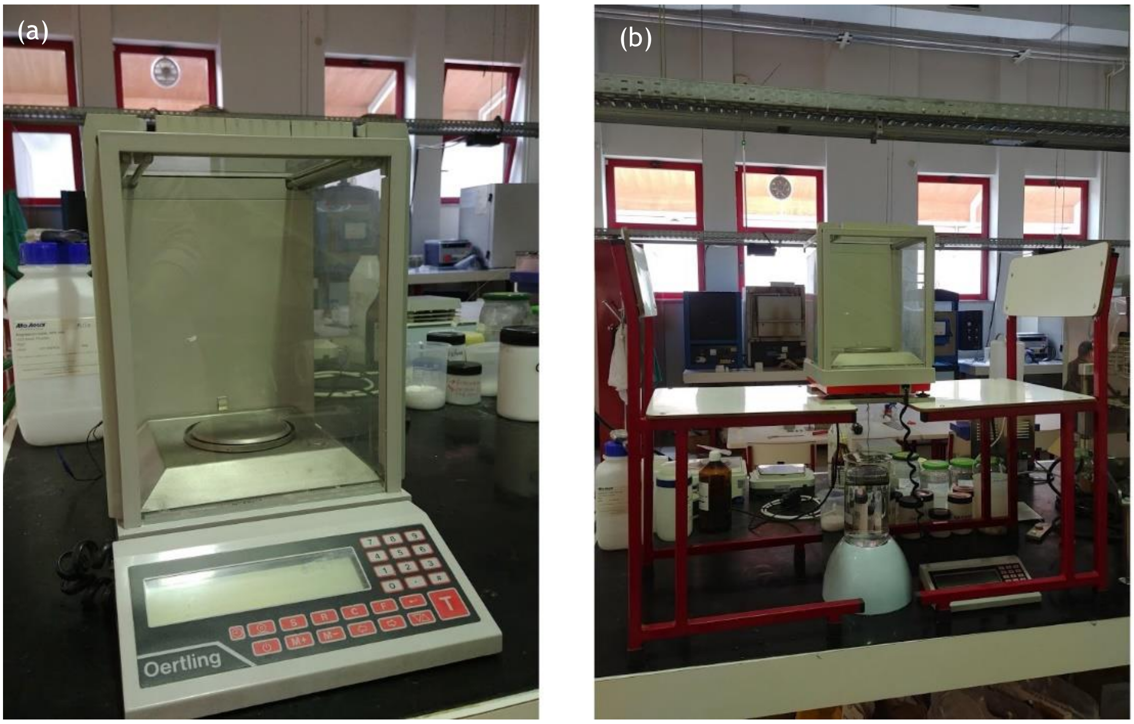

Figure 3.8- a- Oertling VA204 configuration for dry weight and saturated weight measure, b- Oertling VA204 configuration for suspended weight measures

To calculate the density of the materials its necessary to calculate the exterior volume (V_e), in *cm^3*, which is achieved by subtracting the suspended weight (S) from the saturated weight (W), equation 6. It is assumed that the density of the water is 1g/cm^3.

$$V_e = W - S \tag{6}$$

The density (ρ, g/cm^3), is calculated by dividing the dry weight (D) by the respective exterior volume (V_e) of the material, equation 7:

$$\rho = D_w/V_e \tag{7}$$

From this data is possible to calculate the apparent porosity (p, %), equation 8:

$$p = \frac{W - D_w}{V} * 100 \tag{8}$$

This method allows to achieve precise values of the density of the CFRP laminates and especially for the foam core, which has elevated porosity and the bulk density would not be a correct approximation.

3.2.2 Definition of test parameters and mechanical tests

Based on similar works, developed by Morada et al. [79], Crupi et al. [80] and Linul et al. [81], the sandwich three-point bending tests were conducted in the universal testing machine *Shimadzu AGS-X*, with a 10 kN loading cell (Figure 3.9). The software used to acquire the bending tests data was Trapezium X Version 1.4.0. The sandwich flexural tests followed the ASTM C393 standard test method for flexural properties of sandwich constructions [82].

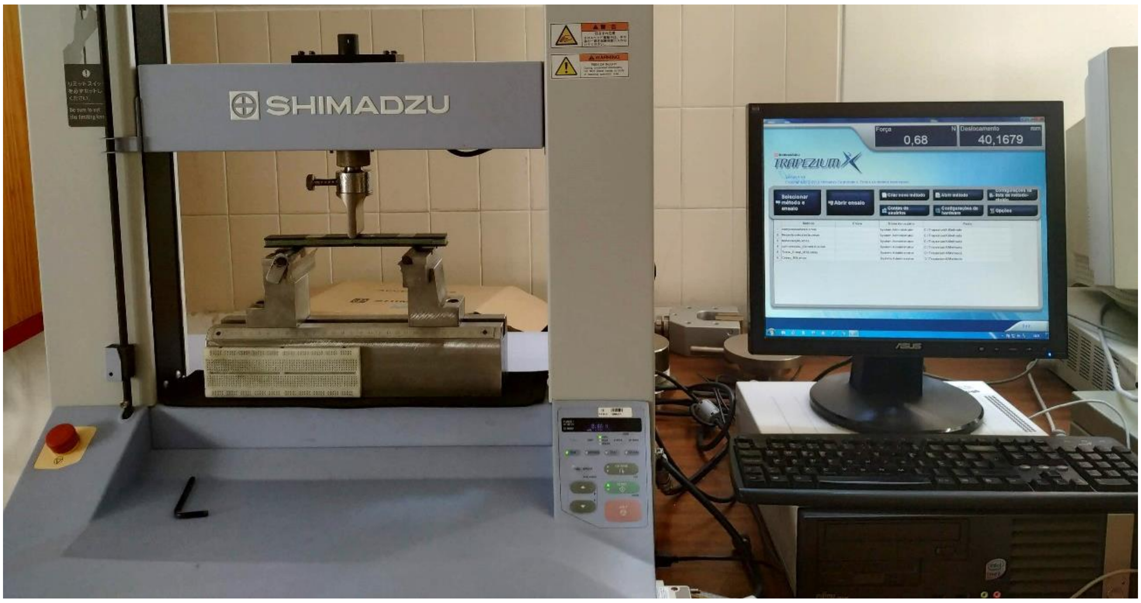

Figure 3.9- Flexural tests experimental setup

The carbon skins were also tested in the same machine, following the ASTM D790 standard test methods for flexural proprieties of unreinforced and reinforced plastics and electrical isolating materials [83].

The foam core flexural proprieties were measured to understand the impact of the curing process in this material.

3.2.2.1 Structural considerations

The mechanical properties of materials are ascertained by performing careful designed laboratory experiments that replicate as nearly as possible the service conditions. It is imperative that there is some consistency in the way tests are conducted, this consistency is accomplished by using standardized testing techniques developed by organizations such as American Society for Testing Materials (ASTM) or International organization for Standardization (ISO). There is a wide range of mechanical tests designed to measure different mechanical proprieties.

Flexural proprieties, such as flexural strength and modulus, are determined by ASTM test method D790 [83]. In this test, a composite beam specimen of rectangular cross section is loaded in either a three-point bending mode (Figure 3.10- a) or a four-point bending mode (Figure 3.10- b).

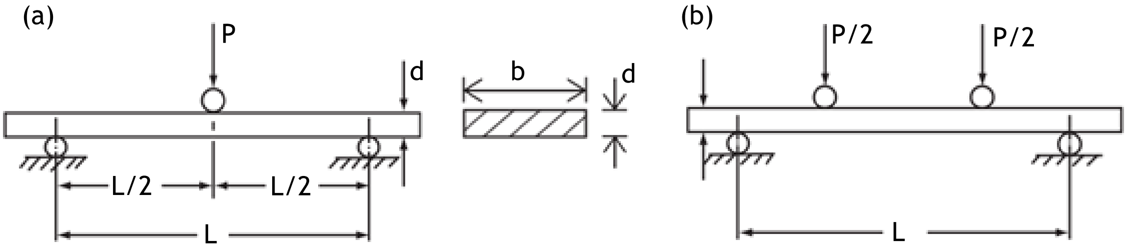

Figure 3.10- Flexural test arrangements in a three-point bending and b- four-point bending modes

Where:

P is the load applied to the beam, [N]

L is the support span, [mm]

b is the width of beam tested, [mm]

d is the thickness of beam tested, [mm]

The output of such flexural test is recorded (using an excel file) as load or force (P) versus midspan deflection (D). To eliminate the geometrical factors, load (P) and deflection (D) are normalized to the respective parameters of stress (σ), equation 9, and strain (ε), equation 10.

$$\sigma = \frac{3PL}{2bd^2} \tag{9}$$

Where σ is the stress in the outer fibers at the midpoint, [MPa*]*

$$\varepsilon = \frac{6Dd}{L^2} \tag{10}$$

Where ε is the strain in the outer surface [mm/mm].

Strain is usually expressed as a percentage which is the strain value multiplied by 100. In Figure 3.11 is an example of a strain versus stress test of a fiber, a matrix and the composite made by these two materials. Typically, FRP experimental stress versus strain graphics have a similar appearance as shown in Figure 3.11 by the continuous green line:

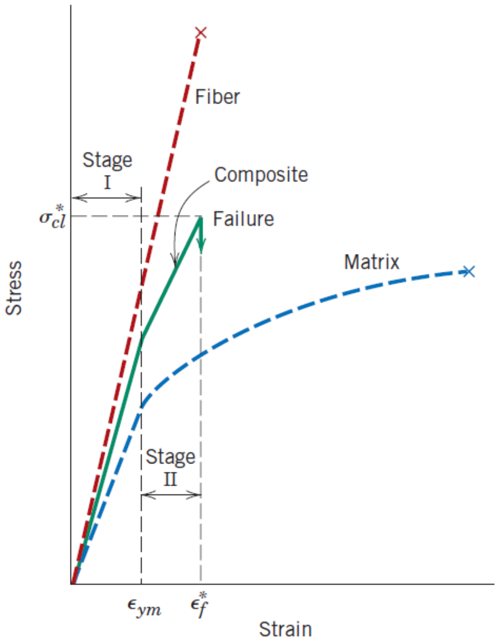

Figure 3.11- Example of a strain versus stress of a fiber, matrix and a composite made by these two materials [1]

In Figure 3.11, Stage I and Stage II represent the elastic and plastic deformation, respectively, of the composite tested. Flexural strength of the composite (σ_{cl}^*) corresponds to the maximum stress that can be sustained by a structure. In the strain axis, ε_{ym} and ε_f^*, are the maximum elastic strain and the maximum strain supported by this composite, respectively.

Most materials, when elastically deformed, stress and strain are proportional to each other throughout equation 11 (Hooke's law):

$$\sigma = E \times \varepsilon \tag{11}$$

In the Hooke's law, the constant of proportionality *E* (*GPa*) is the modulus of elasticity, Young's modulus or simply modulus. The greater the modulus, the stiffer the material, or the smaller the elastic strain that results from the application of a given stress. In most polymers, this elastic portion of the stress-strain curve is not linear. So, in these cases, it is not possible to determine a modulus of elasticity as described above. For this nonlinear behavior, either tangent or secant modulus is used (Figure 3.12).

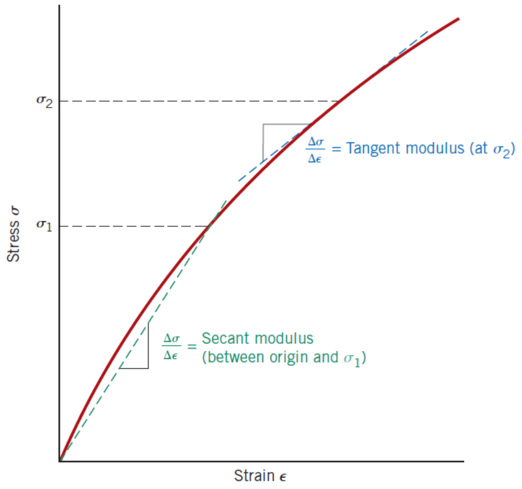

Figure 3.12- Schematic stress-strain diagram showing non-linear elastic behavior and how secant and tangent moduli are determined [1]

In order to the engineer make the proper selection of the material, he has to anticipate, plan for possible failure and, in the event that failure does occur, to accesses its cause and then take the necessary measures against future incidents. So, it is fundamental for an engineer to understand the mechanisms of failure of the material and take the necessary measures to guarantee that, if failure indeed does occur, it does not occur in a catastrophic way and no lives are put at risk.

Mechanical failure occurs from fracture, which is the separation of a body into two or more pieces in response to an imposed stress that is constant or slowly changing with time, and at temperatures that are low relative to the melting temperature of the material. In engineering, there are two modes of possible fracture: ductile and brittle [1]. In a ductile fracture, there is plastic deformation before the fracture, in this type of failure, the material absorbs part of the energy while is permanently deformed. While in a brittle fracture, no apparent plastic deformation takes place before fracture typically involves little energy absorption and occurs at high speeds.

Ductility is a measure of the degree of plastic deformation that has been sustained at fracture [1]. Ductility is expressed as a percentage of plastic strain at fracture which is obtained by multiplying the maximum strain before fracture by 100.

These two types of fracture differ in the ability of the material to experience plastic deformation, or in other words, the ability to absorb energy in form of permanent deformation before the fracture. So, ductile materials exhibit substantial plastic deformation or high energy absorption before failure, while brittle materials exhibit none or almost no plastic deformation and are not able to dissipate energy in form of permanent deformation before fracture [1]. In Figure 3.13 it is possible to see that the brittle material has almost none plastic deformation, in the other hand, the ductile material shows not only elastic deformation but a big region of plastic deformation before failure.

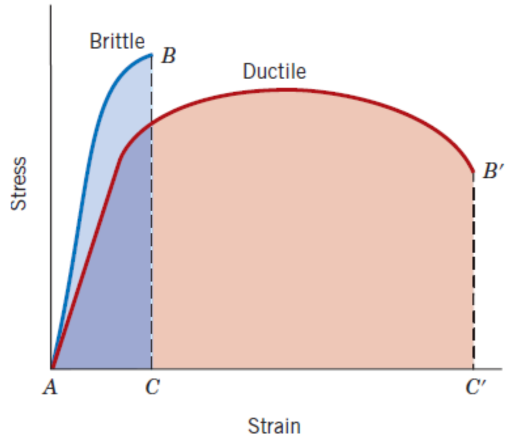

Figure 3.13- Illustration of stress-strain behavior for brittle and ductile materials [1]

Every fracture process involves two steps, the crack formation and the crack propagation. In response an imposed stress, the crack propagation mechanism is what characterizes the type of fracture. Ductile fractures are characterized by extensive plastic deformation in the vicinity of an advancing crack, contrarily, brittle fracture cracks may spread extremely rapidly with almost no plastic deformation in the surroundings of the crack.

Sandwich structures have a unique behavior regarding failure since it normally fails not from the facing martial itself but from adhesion failure or core failure because the faces are much stiffer than the core.

3.2.2.2 Sandwich

According to ASTM C393 Standard Test Method for Flexural Properties of Sandwich Constructions [82], the test specimens shall follow the description: “The test specimen shall be rectangular in cross-section. The depth of the specimen shall be equal to the thickness of the sandwich construction (d), and the width (b) shall be not less than twice the total thickness, not less than three times the dimension of a core cell (c), nor greater than one half the span length (L). The specimen length (l) shall be equal to the span length plus 50 mm or plus one half the sandwich thickness whichever is the greater” [82], see Figure 3.14 and Figure 3.15.

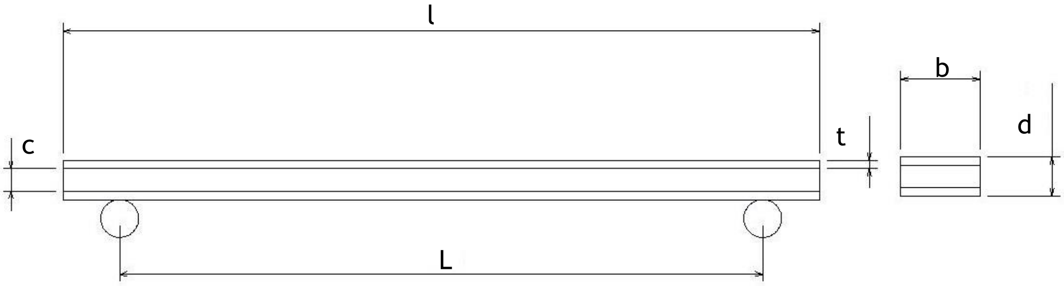

Figure 3.14- Representation of a sandwich specimen

Figure 3.14 is represented a sandwich specimen and the different letters correspond to each measure according to ASTM C393 [82] and ASTM D790 [83]. Where:

l is the length of the specimen, [mm]

L is the support span length, [mm]

c is the core thickness, [mm]

t is the faces thickness, [mm]

d is the total thickness of the beam, [mm]

b is the specimen width, [mm]

Analytically, the restrictions imposed by the standard are:

$$l \gg b \tag{12}$$

$$c + 2t = d \tag{13}$$

$$b \geq 2d \tag{14}$$

$$b \geq 3c \tag{15}$$

$$b \leq l/2 \tag{16}$$

$$l = L + 50 \ \cup \ l = L + d/2 \tag{17}$$

According to the measures of the set of specimens, using the core thickness as $c = 6\,mm$ and the faces thickness as $t = 2.2\,mm$ the sandwich total thickness is $d = 10.4\,mm$. The restriction imposed by the standard is: $b \geq 20.8\,mm$.

The support span for the sandwich short specimens was defined as $L = 60mm$ with a total length of $l = 70mm$.

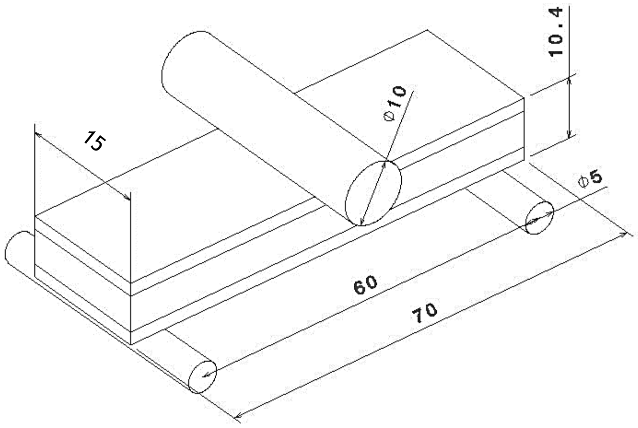

Figure 3.15- Sandwich short specimens' measures

ASTM C393 just imposed restrictions regarding the width of the specimen, so ASTM D790 Standard Test Method for Flexural Properties of Unreinforced and Reinforced Plastics and Electrical Insulation Materials [83] was followed as well to project sandwich long specimens. This standard imposes the following geometric restrictions:

$$l \geq 16d \tag{18}$$

$$b \leq l/4 \tag{19}$$

Based on both standards and in the CFRP three-point bending tests results the final measures of the sandwich long specimens' measures are represented in Figure 3.16:

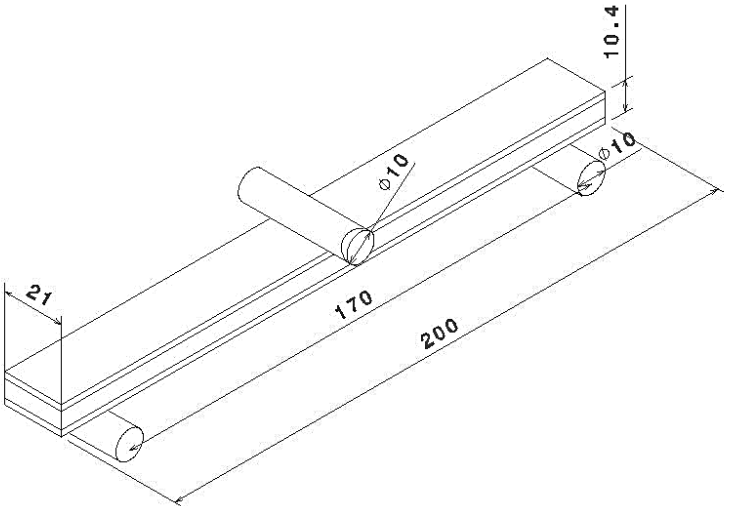

Figure 3.16- Sandwich long specimens' measures

The rate of the crosshead motion is defined in ASTM D790 by equation 20:

$$r = ZL^2/6d \tag{20}$$

Where:

r is the rate of crosshead motion, [mm/min]

Z is the rate of straining of the outer fiber, [mm/mm/min]. Z shall be equal to 0.01.

Thus, the rate of crosshead motion is:

$$r = \frac{0.01 * 170^2}{6 * 10.4} = 4.63 \approx 4.5\, mm/min \tag{21}$$

The cross-head motion was set to 4.5 mm/min.

The tests provide the data necessary to calculate the core shear stress (equation 22) and the facing bending stress (equation 23):

$$\tau = \frac{P}{(d+c)b} \tag{22}$$

Where τ is the core shear stress in [MPa].

$$\sigma = \frac{PL}{2t(d+c)b} \tag{23}$$

Where σ is the facing bending stress in [MPa].

The flexural strain ε, which is the nominal fractional change in the length of an element of the outer surface of the test specimen at midspan [83], may be calculated for any deflection using equation24:

$$\varepsilon = 6Dd/L^2 \tag{24}$$

Where:

ε is the flexural strain [mm/mm]

D is the deflection of the center of the beam, [mm] The modulus of elasticity in de bending, E, is the ratio, within the elastic limit, of stress to corresponding strain. The modulus was calculated by the chord method [83], where two discrete points are chosen at the stress strain curve on the elastic section and the slope is calculated by equation 25:

$$E = (\sigma_2 - \sigma_1)/(\varepsilon_2 - \varepsilon_1) \tag{25}$$

Where σ_1.and σ_2 are the flexural stresses, calculated from equation 23 and measured at the predefined points on the stress strain curve. ε_1 and ε_2 are the flexural strain values, calculated from equation 24 and measured at the predetermined points on the stress strain curve.

The standard deviation, SD, is the measure that is used to quantify the dispersion of a set of values is calculated by equation 26:

$$SD = \left(\sqrt{(\Sigma X - n\bar{X})^2/(n-1)}\right)/\bar{X} \tag{26}$$

Where:

X is the value of single observation

n is the number of observations

$\bar{X}$ is the arithmetic mean of the set of observations

The procedure described above allowed to project specimens that guarantee valid results. The equations allowed to process the data collected by the Shimadzu AGS-X, to obtain the graphics required to understand the behavior of the sandwich structure when exposed to flexural stress, and to analyze those graphics to draw sustained conclusions about the mechanical behavior of this structure.

3.2.2.3 CFRP laminates

The CFRP sandwich skins were tested and mechanically characterized following ASTM D790 standard [83]. The specimens were cut from a plate using the Pronum, WaterJet cutting machine which followed a sketch made in CATIA® software. The standard states that the support span shall be at least 16 (tolerance ±1) times the depth of the beam. Specimens with 3.2 mm or less in depth shall be 12.7 mm in width. The specimen shall be long enough to allow for overhang on each end of at least 10 % of the support span but in no case less than 6.4 mm on each end.

CFRP short specimens were also produced by the same method described, but with dimensions equal to the sandwich short specimens' facings, 15mm depth and 70 mm length.

In Figure 3.17 is represented a CFRP laminate specimen and the different letters correspondent to each specimens measure according to ASTM D790 [83]:

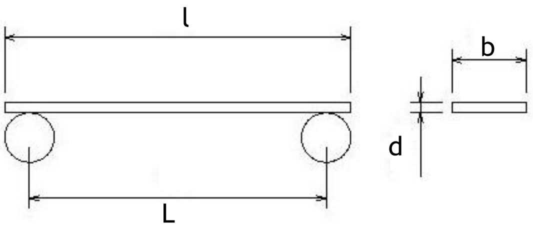

Figure 3.17- Representation of a CFRP laminate sample

For this structure the specimens must comply the following parameters:

$$L = 16d \pm 1 \tag{27}$$

$$b = 12.7 \tag{28}$$

$$l \geq L + 2 \times 0.1L \tag{29}$$

The rate of crosshead motion is calculated by equation 20.

Five specimens with geometries respecting these parameters were tested and all of those 5 failed to compression in the upper face. In section 7.5 from ASTM D790 [83] states that for high-strength reinforced composites, including highly orthotropic laminates an increase in the span-to-depth ratio up to 60:1 is recommended to eliminate shear effects when modulus data is required. Specimens with a span to depth ratio of 32:1 and 40:1 were tested and both failed to compression, thus, a span to depth ratio of 60:1 was adopted for the CFRP long specimens. The final measure of the CFRP specimens are listed in Figure 3.18:

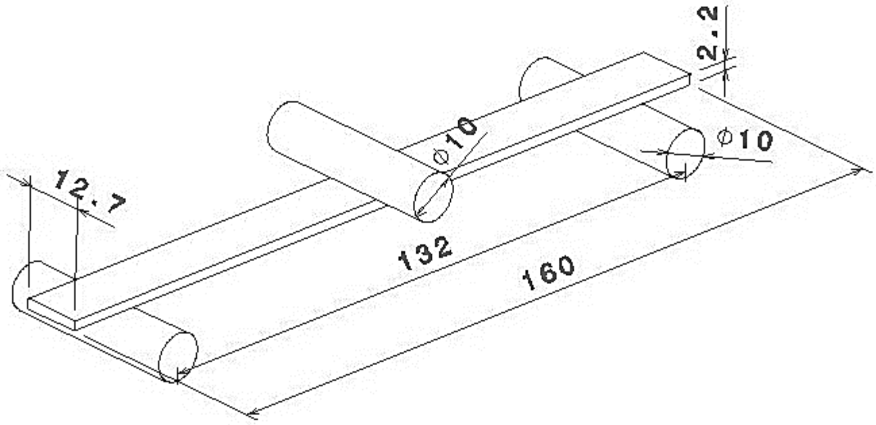

Figure 3.18- CFRP long specimen and three-point bending test measures

ASTM D790 [83] states that the maximum radius support should be is 1.6 times the specimen depth, thus the radius should be at most 3.52mm instead of 5mm. Unfortunately, the Shimadzu AGS-X only had those supports for three-point bending tests for such a wide span. Since the objective of the CFRP flexural tests was to study the skins of the sandwich beam, increase the depth of the beams by adding more layers of CFRP wasn't an option. The tests proceeded with these supports, despite the stress concentration on the supports is smaller, it is expected that the specimens would have the same behavior with smaller supports.

For this specimen geometry the rate of crosshead motion is:

$$r = \frac{0.01 * 132^2}{6 * 2.2} = 13.2 \approx 13\ mm/min \tag{30}$$

The flexural stress, σ, of a simple beam supported at two points and loaded at the midpoint is maximum at the midpoint of the lower face. Since the test had a large support span ($\geq 16d$), used such that deflection exceeds 10 % of the support span, the stress in the outer surface of for a simple beam can be reasonably approximated by equation 31.

$$\sigma = \left(\frac{3PL}{2bd^2}\right)\left[1 + \left(\frac{D}{L}\right)^2 - 4\left(\frac{d}{L}\right)\left(\frac{D}{L}\right)\right] \tag{31}$$

Where:

σ is the stress in the outer fibers at midpoint, [MPa]

D is the deflection at the middle of the support span, [mm] The flexural strain ε, the modulus of elasticity E, and the standard deviation DS, were calculated by means of equations, 24, 25 and 26 respectively.

The procedure described above allowed to project specimens that guarantee valid results for the mechanical characterization of the CFRP skins. The equations allowed to process the data collected by the Shimadzu AGS-X, to obtain the graphics required to understand the behavior of the CFRP skins when exposed to flexural stress, and to analyze those graphics to draw sustained conclusions about the structural role that this structure plays in the sandwich structure.

3.2.2.4 Foam

Before any sandwich beam was produced the foam was tested to understand the implications of the high temperature exposition. The foam manufacturer recommends a maximum operating temperature of 80°C, so to understand the consequences of a curing process at 90°C for 7 hours a set of 9 samples were exposed to different conditions: Foam sample 1 was exposed to the first cycle of temperature of 90°C during 24h and then was exposed to a temperature of 95°C during another 24h. Foam sample 2 and foam sample 3 were exposed to a temperature cycle of 95°C during 24h. Foam sample 4, 5 and 6 were exposed to a temperature cycle equal to the adhesive curing process, a temperature of 80°C for 7h. Finally, foam sample 7,8 and 9 are control samples and they were not exposed to any type of thermal treatment. Figure 3.19 shows the foam samples after the heat treatment.

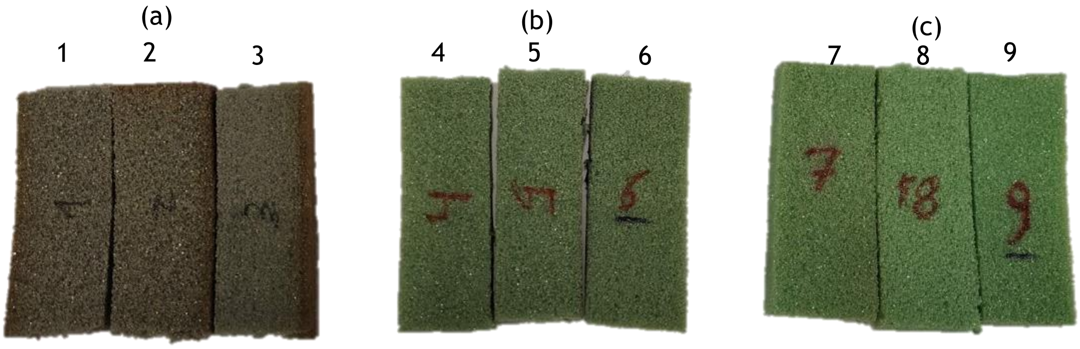

Figure 3.19- Foam samples subjected to different heat treatments, a-sample 1,2 and 3, b-sample 4, 5 and 6, c- sample 7, 8 and 9

It is obvious the difference in color of samples subjected to the heat treatment, sample 1,2 and 3 have a darker color which is a consequence of the long period of time exposed to high temperature and dry environment of the oven. The samples did not show any variations in mass or density.

Since there is no standard to guide three-point bending tests on foams and the objective of this mechanical tests was not to characterize the foam flexural proprieties, but to compare and understand the impact of the high temperature exposition on the foams behavior to flexural stress. Thus, three-point bending tests were performed on the 9 foam samples to understand if there was any change in the flexural proprieties of the specimens as a consequence of the thermal exposition. The sample's measures are presented in Figure 3.20:

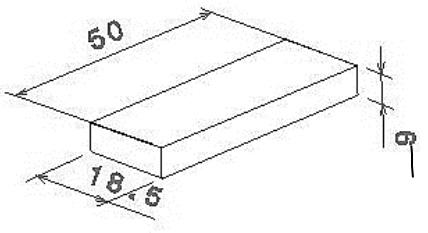

Figure 3.20- Foam specimen for flexural three-point bending test

The letters corresponding to the measures are shown in Figure 3.17.

The rate of crosshead motion was set to $r = 2\,mm/min$.

All the specimens broke due to flexion at the lower face, so it is secure to calculate the flexural stress as expressed in ASTM D790 [83] equation for the measures shown in Figure 3.20. The flexural stress, σ, was calculated by means of equation 9:

The flexural strain ε, the modulus of elasticity E, and the standard deviation s, were calculated by means of equations, 24, 25 and 26 respectively.

The process described above allowed to study the mechanical consequences of exposing the AIREX® C70 foam to the adhesive curing temperature of 90°C.

3.2.3 Piezoresistivity

Piezoresistivity is a phenomenon that occurs when the volume electrical resistivity of material changes with the strain in the material [7,71,84,85]. This phenomenon allows the use of the material as a strain sensor, as the variation in resistance relates to the strain.

The electrical resistance of a material is calculated throughout the relation between the applied voltage and the current passing through the material, this relation was first discovered by Georg Ohm in 1827 and was named after the physicist. Ohm's law states that the potential difference, V (voltage), across a conductive material is proportional to the current, I, where the resistance, R, is the constant of proportionality:

$$V = I \times R \leftrightarrow R = \frac{V}{I} \tag{32}$$

Where:

V is the potential difference, [V]

I is the current, [A]

R is the resistance, [Ω]

If the input voltage is controlled and the current is measured, it is possible to know the values of R. When a multimeter is set to make measures of resistance, it uses this principle to measure the materials resistance.

The accuracy of a piezoresistive material can be quantified for its gauge factor (GF), which is defined as the fractional variation of the resistance per unit of strain [84]. This parameter can be calculated as shown in equation 33 [86]:

$$GF = \frac{\Delta R/R_0}{\varepsilon} \tag{33}$$

Where:

ΔR is the resistance variation induced by the applied strain

R_0 is the material's resistance prior to the deformation

ε is the applied strain

When an elastic material is subjected to a force along its axis, it will also deform along the orthogonal axes. In other words, a tensile strain along the length will result in compressive strains in the orthogonal directions. Typically, the axial and transverse strains will defer and the ratios between the two is known as Poisson's ratio, v. The strains along the length, width, and thickness are denoted by ε_l, ε_b, and ε_d, respectively.

When the bulk resistivity (ρ_r) is known it is possible to calculate the volume resistance of a beam (equation 34):

$$R = \frac{\rho_r \times l}{A} \tag{34}$$

Where:

ρ_r is the bulk resistivity, $[\Omega * mm]$

l is the length of the specimen, $[mm]$,

A is the cross-section area, $[mm^2]$ (which is the product of the width, b, and the thickness d)

Hence,

$$R = \frac{\rho_r \times l}{b \times d} \tag{35}$$

Differentiating the equation 36 for resistance gives:

$$\mathrm{d}R = \frac{l}{b \times d}\mathrm{d}\rho_r + \frac{\rho_r}{b \times d}\mathrm{d}l - \frac{\rho_r l}{b^2 \times d}\mathrm{d}b - \frac{\rho_r l}{b \times d^2}\mathrm{d}d \tag{36}$$

From equation 37:

$$\frac{\mathrm{d}R}{R} = \frac{\mathrm{d}\rho_r}{\rho_r} + \frac{\mathrm{d}l}{l} - \frac{\mathrm{d}b}{b} - \frac{\mathrm{d}d}{d} \tag{37}$$

By definition, $\varepsilon = \frac{\mathrm{d}l}{l}$, the following equations apply on the assumption that these equations are dealing with small changes, hence $\mathrm{d}l = \Delta l$, $\mathrm{d}b = \Delta b$, and $\mathrm{d}d = \Delta d$:

$$\frac{\mathrm{d}b}{b} = \varepsilon_b = -\nu\varepsilon_l \text{ and } \frac{\mathrm{d}d}{d} = \varepsilon_d = -\nu\varepsilon_l \tag{38}$$

Where ν is the Poisson's ratio. It is worth noticing that the minus signs indicate that the width and the thickness are experiencing compression, thereby they shrink, and the above example illustrates a positive Poisson's ratio[3].

---

[3] Materials with negative Poisson's ratio as they are stretched their width and the thickness increase, such materials include special foams and polymers such as polytetrafluoroethylene (PTFE) [86]

Therefore, from equation 38, equation 39 can be written as:

$$\frac{\mathrm{d}R}{R} = \frac{\mathrm{d}\rho_r}{\rho_r} + \varepsilon_l + \nu\varepsilon_l + \nu\varepsilon_l \tag{39}$$

From equation 33 the gauge factor is therefore:

$$GF = \frac{\Delta R/R_0}{\varepsilon_l} = \frac{{}^{\mathrm{d}\rho_r}/_{\rho_r}}{\varepsilon_l} + (1 + 2\nu) \tag{40}$$

Equation 40 shows that there are two distinct effects that contribute to the gauge factor. The first term is the piezoresistive effect, and the second in the geometric effect, as the Poisson's ratio is usually between 0.2 and 0.3, the contribution to the gauge factor from the geometric is therefore between 1.4 and 1.6. Table 3.3shows the gauge factor of different materials.

Table 3.3- Gauge factor of different materials

Material	Gauge Factor
Metal foil strain gauge	2-5
Thin film metal	2
Single crystal silicon	-125 to 200
Polysilicon	±30
Thick film resistor	10

Piezoresistive materials can either show positive piezoresistivity (p-type) or negative piezoresistivity (n-type). In p-type materials, the resistance will increase with the applied strain, while in n-type the resistance decreases with the applied strain. In semiconductors, the piezoresistive effect is highly dependent on the orientation of the conductive substrate, if the geometric effect is neglected, then the fractional change in resistivity is given by:

$$\frac{\mathrm{d}\rho_r}{\rho_r} = \pi_l\sigma_l + \pi_t\sigma_t \tag{41}$$

Where:

π_l and π_t are the longitudinal and transverse piezoresistive coefficients,

σ_l and σ_t are the longitudinal and transverse stresses

The longitudinal direction is defined as the parallel to the current flow, while the transverse is the oronal to it. The two coefficients are dependent on the crystal orientation and doping (if the material show positive or negative piezoresistivity) and concentration.

So, to measure the resistance variation in the carbon skin while being flexed, a typical two-probe method [71] was set to the specimens, as it is shown in Figure 3.7 where the copper wires were glued with a conductive carbon paste to the specimen's tips. The two cables were connected to the multimeter terminals set to measure the resistance between the terminals, with a period of 0.5s (the smallest period it can measure).

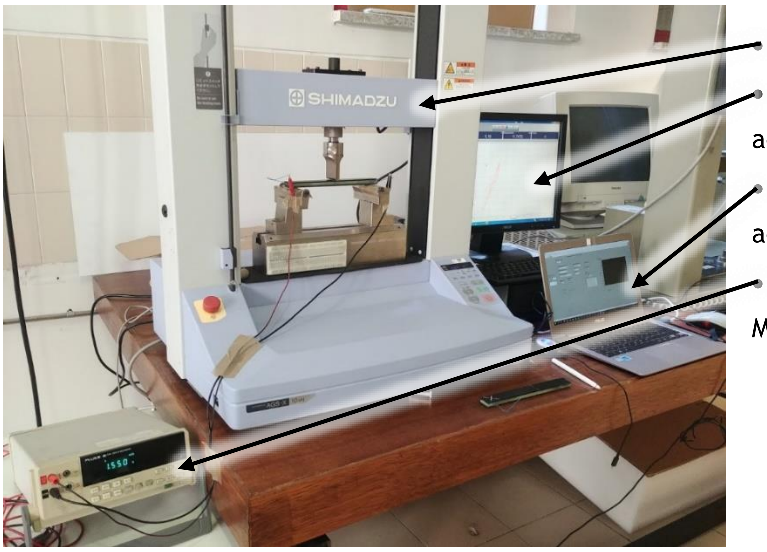

- *Shimadzu AGS-X*
- Flexural tests data acquisition system
- Electrical data acquisition system
- Fluke 45 Dual Display Multimeter

Figure 3.21- Experimental setup for the electromechanical bending tests

The electromechanical tests were performed at University of Beira Interior, Figure 3.21 shows the experimental setup assembled for this tests The electrical data acquisition system was set to acquire the electrical data from a Fluke 45 Dual Display Multimeter [87], at a rate of two measurements per second while the mechanical data was collected at the same rate but in a different computer. The electrical and mechanical data were then cross linked and treated in an excel worksheet.

4. Results and discussion

In the first subchapter, all the results are presented graphically and resumed in tables. The results are chronologically organized, to be more understandable the reasons that led to performing this variety of tests and specimens.

On the other hand, the discussion is subdivided into four different sections: Foam core, CFRP faces, Sandwich and Electromechanical response. A deep analysis of results is taken along this subchapter.

4.1 Results

To understand the impact of the adhesive curing temperature in the foam mechanical behavior, a set of nine samples were prepared and exposed to different thermal conditions . The first three samples were exposed to temperatures higher than eighty degrees Celsius, the adhesive curing temperature, for more than seven hours. The second set of three samples were exposed to exactly the same thermal conditions as the curing process. Finally, the last set of three specimens were control samples and they were not exposed to any type of thermal treatment.

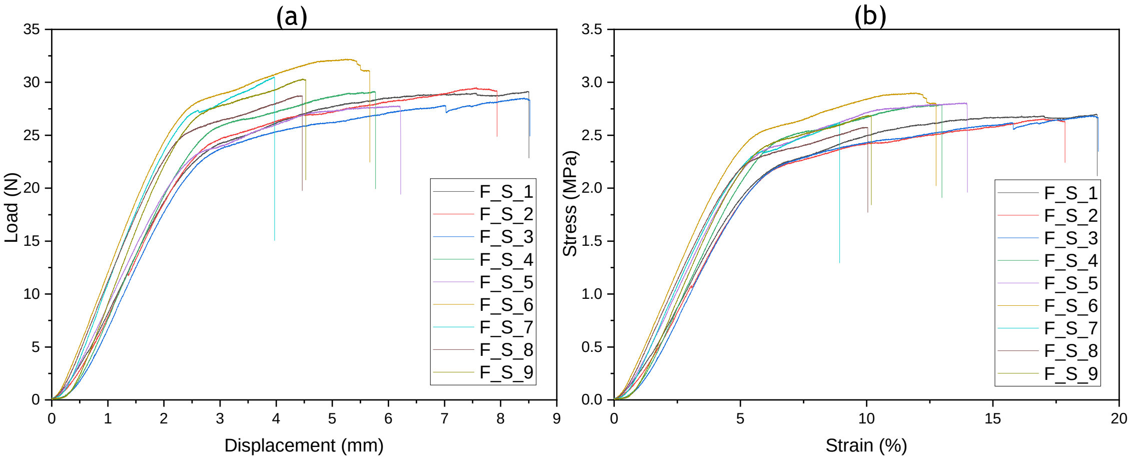

Figure 4.1-Foam samples flexural tests, a-Load versus displacement and b- stress versus strain experimental curves of the foam samples

From Figure 4.1, the increase of the plastic region between the three sets of samples is clear. The flexural proprieties calculated from the bending tests data are summed up in Table 4.1. Although the temperature shows a clear influence in the plastic region of the foam, the flexural strength and flexural modulus did not show relevant variations between sets of samples. So, from the tests performed the exposure to such high temperature only made the foam more ductile, this ductility isn't expected to affect the sandwich performance since the carbon faces are much more brittle than the foam.

Table 4.1- Flexural proprieties of the tested foam samples

	Temperature [C°]	Time [h]	Flexural strength [MPa]	Maximum strain [%]	Flexural Modulus [MPa]
F_S_1	80-90-95	1-24-24	2.70	19.14	45.68
F_S_2	80-90	1-24	2.66	17.86	49.55
F_S_3	90	24	2.69	19.18	48.45
Arithmetic mean			**2.68**	**18.73**	**47.90**
Standard deviation			0.79%	0.61%	4.16%
F_S_4	90	7	2.79	12.99	51.91
F_S_5	90	7	2.81	13.99	50.65
F_S_6	90	7	3.05	13.01	57.58
Arithmetic mean			**2.88**	**13.33**	**52.44**
Standard deviation			5.02%	0.468%	4.03%
F_S_7	-	-	2.62	8.94	53.97
F_S_8	-	-	2.58	10.05	52.04
F_S_9	-	-	2.62	10.19	55.63
Arithmetic mean			**2.61**	**9.72**	**53.88**
Standard deviation			0.98%	0.561%	3.33%

In Figure 4.2 are the load versus strain and stress versus strain curves of CFRP small samples.

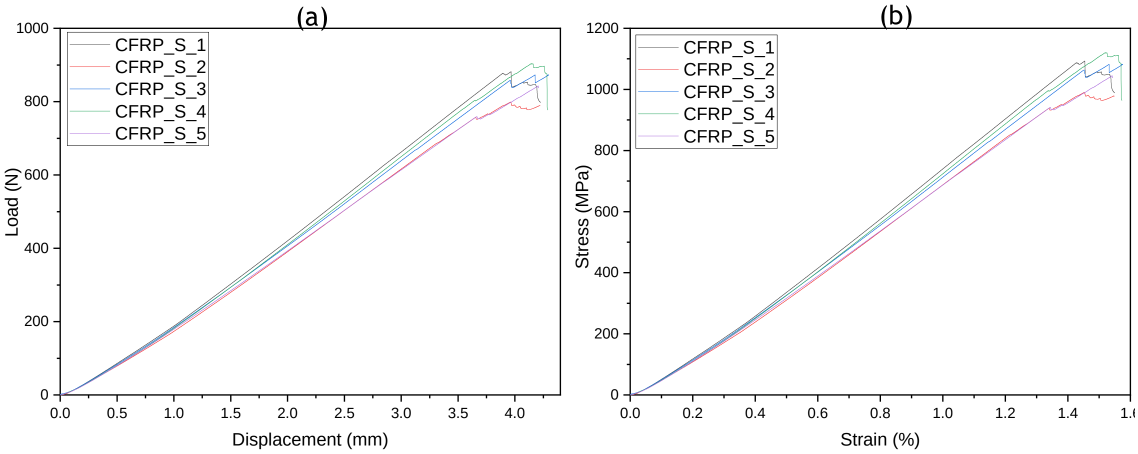

Figure 4.2- CFRP short laminates experimental curves, a Load versus Displacement and b Stress versus Strain curves

The charts show a linear-elastic behavior, followed by a little plastic deformation which leads to the rupture of the fibers. Carbon skins typically present a very small plastic regime when compared to the elastic one. Table 4.2 is a summary of the data collected from the flexural tests of this specimens. CFRP short laminates showed a consistent pattern between samples with little data spreading.

Table 4.2- Flexural proprieties of the CFRP small samples

	Flexural strength [MPa]	Maximum strain [%]	Flexural Modulus [GPa]
CFRP_S_1	1093.02	1.55	77.75
CFRP_S_2	990.44	1.45	72.46
CFRP_S_3	1082.00	1.53	74.04
CFRP_S_4	1120.58	1.57	76.64
CFRP_S_5	1045.02	1.54	72.14
Arithmetic mean	**1066.21**	**1.53**	**74.60**
Standard deviation	4.7%	3.0%	3.4%

The short sandwich samples, wich the skins have the same size as the CFRP_S samples, were divided into two series, R (reinforced) and U (unreinforced). As it was explained in section 3.1 the reinforcement was a glass fiber veil embedded between two layers of adhesive, which has the function of supporting and stabilizing the adhesive by avoiding its heterogeneous distribution over the surface.

The mechanical results of the sandwich short beams are illustrated in Figure 4.3.

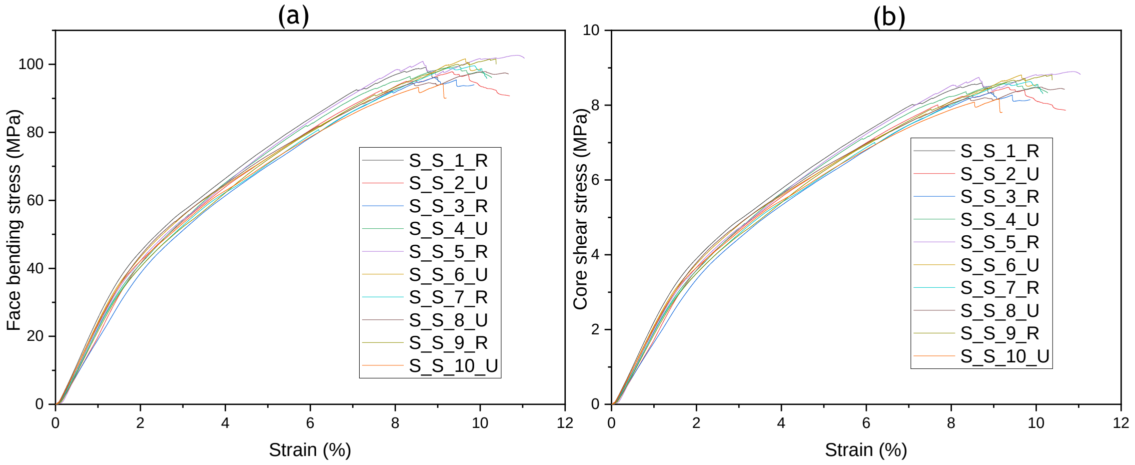

Figure 4.3- Sandwich short beams face bending stress versus strain (a) and core shear stress versus strain (b) charts

Along these charts, three different key features are clearly identified: the initial linear-elastic behavior, until proximally 2% in strain, followed by an elasto-plastic phase until the structure starts to collapse. Table 4.3 shows a summary of the data collected from the sandwich small samples' three-point bending tests.

Table 4.3- Flexural proprieties of the sandwich short samples

	Flexural strength	Maximum strain	Flexural Modulus
	[MPa]	[%]	[GPa]
S_S_1_R	99.17	9.03	2.76
S_S_2_U	97.87	10.70	2.25
S_S_3_R	96.21	8.55	2.11
S_S_4_U	99.44	8.56	2.59
S_S_5_R	102.68	11.03	2.73
S_S_6_U	101.64	10.16	2.67
S_S_7_R	99.60	10.00	2.47
S_S_8_U	97.90	10.67	2.63
S_S_9_R	101.63	10.38	2.49
S_S_10_U	94.19	9.20	2.60
Arithmetic mean unreinforced	**98.21**	**9.86**	**2.55**
Standard deviation unreinforced	2.8%	9.4%	8.1%
Arithmetic mean reinforced	**99.86**	**9.80**	**2.51**
Standard deviation reinforced	2.5%	10.3%	10.3%

Reinforced sandwich samples show slightly higher flexural strength yet slightly smaller modulus. The difference between maximum strains can't be considered since the standard deviation e is higher than the differences between arithmetic means.

All the sandwich and CFRP short laminates failed to compression, more specifically face sheet failure, mainly because of the small ratio between support spans and beam thickness. So, to explore other types of failure longer beams were projected as described in section 3.2.3.

CFRP long beams load versus displacement and stress versus displacement charts are shown in Figure 4.4.

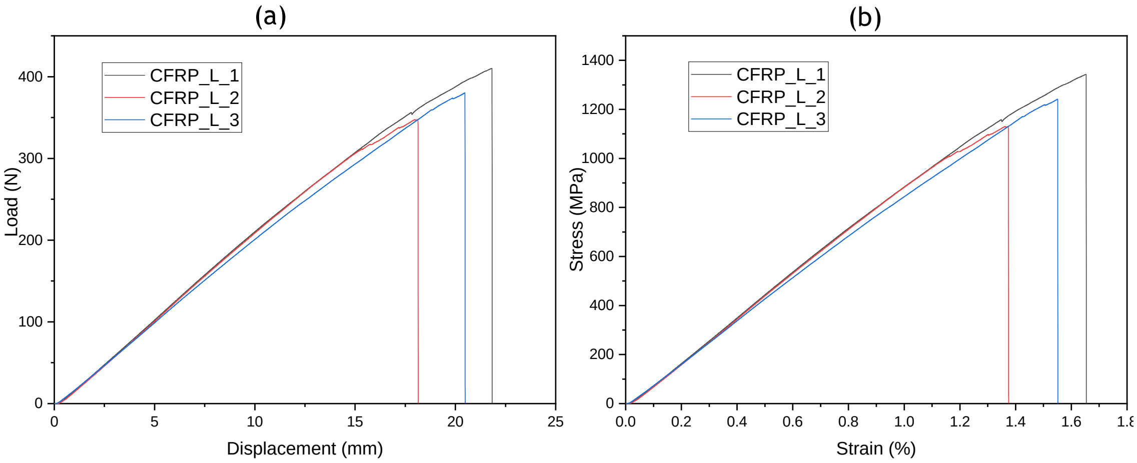

Figure 4.4-CFRP long beams (a) load versus displacement and (b) stress versus displacement charts

These laminates present a linear elastic behavior with no significant plastic deformation. Contrarily to the CFRP short samples, all the samples presented catastrophic failure with entire breakage of the beam. Table 4.4 shows the flexural proprieties of the CFRP long laminates.

Table 4.4- Flexural proprieties of the CFRP long samples

	Flexural strength	Maximum strain	Flexural Modulus
	[MPa]	[%]	[GPa]
CFRP_L_1	1343.01	1.65	91.52
CFRP_L_2	1130.54	1.37	90.28
CFRP_L_3	1241.93	1.55	86.71
Arithmetic mean	**1238.49**	**1.53**	**89.50**
Standard deviation	7.01%	0.32%	2.28%

Based on the sandwich short laminates results and in Cardoso [88] study about the effect of the application of the glass fiber veil in composite joints, the sandwich long beams were all reinforced with this veil to improve the joint quality. Sandwich long beams face bending stress versus strain and core shear stress versus strain charts are resented in Figure 4.5.

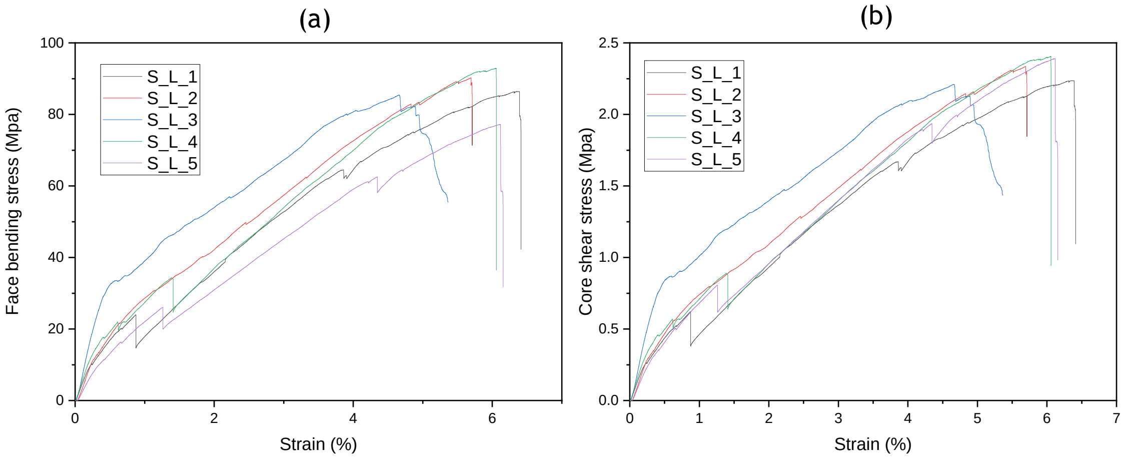

Figure 4.5- Sandwich long beams experimental curves, a- face bending stress versus strain and (b) core shear stress versus strain curves

Sandwich long beams have very short linear-elastic behavior presenting unstable distinct curves: Specimens S_L_1, S_L_4 and S_L_5 show initial failure due to core shear failure, while S_L_2 and S_L_3 although both did not fail prematurely, S_L_3 showed a significantly higher modulus than every other beam. Table 4.5 shows the sandwich long beams flexural proprieties measured from the three-point bending tests. Table 4.5 has two columns where is expressed the strain value of the first and second crack. A crack was considered only in load sudden decreases of at least 2.5% of the ultimate strength of the specimen

Table 4.5- Flexural proprieties of the sandwich long beams

	Flexural strength [MPa]	Core shear stress 1st crack [MPa]	Core shear stress 2nd crack [MPa]	Maximum strain %	Flexural Modulus GPa
S_L_1_R	86.39	0.62	1.67	6.41	5.24
S_L_2_U	90.23	-	-	5.71	5.35
S_L_3_R	85.41	-	-	5.36	8.51
S_L_4_U	92.91	0.88	-	6.06	6.11
S_L_5_R	77.20	1.26	4.35	6.16	3.71
Arithmetic mean	**86.43**	**-**	**-**	**5.94**	**5.78**
Standard deviation	6.91%	-	-	6.87%	30.31%

Sandwich long beams were exposed to a series of cyclic static loading to understand its behavior. Figure 4.6 shows two cyclic three-point bending tests, composed of five cycles each, with a loading rate of 13mm/s, maximum loading of 700N (~80% flexural strength). In test (a) without relaxation period and test (b) with 5 seconds interval between each loading cycle.

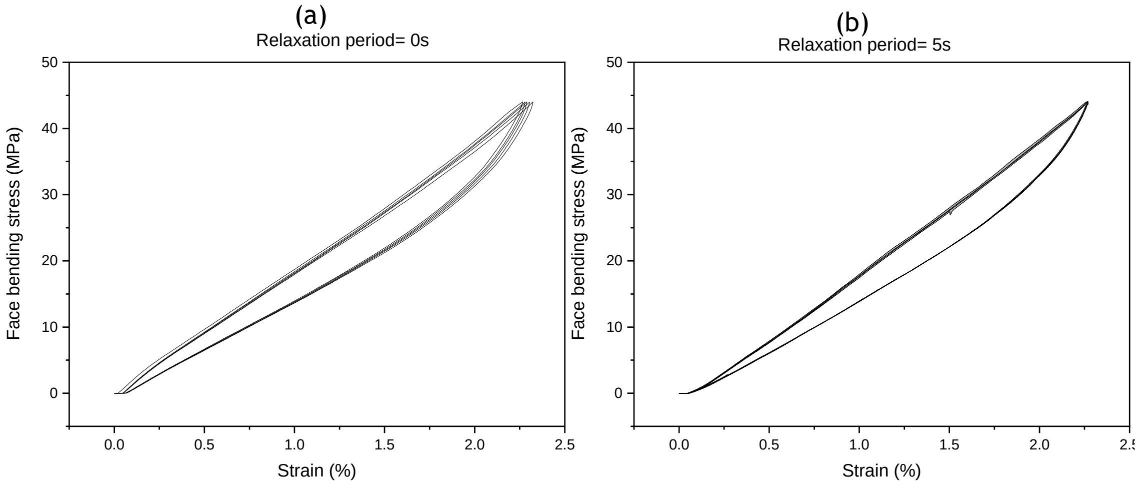

Figure 4.6- Sandwich long beam 700N cyclic loading tests (a) with no relaxation time (b) with 5 seconds of relaxation time

In both graphs of Figure 4.6, its clear a hysteresis phenomenon, where the material doesn't instantly follow the forces applied, instead it reacts slowly and absorbs some of the applied energy due to internal frictional forces [89]. In graph (a) both the loading and unloading curves vary from cycle to cycle, which represents a variation in the energy absorbed by the material. This means either the material is suffering internal damage and losing capabilities of storing the applied energy, or it did not have enough time to dissipate the stored energy during the discharge phase. A relaxation period of 5 seconds between cycles was added, in Figure 4.6- (b) are the cycle curves of this test, the loading and discharge curves are coincident from cycle to cycle, which means that the beam is recovering completely from the applied load without internal damage.

Finally, the electrochemical tests were set. First, a set of three CFRP long laminates was tested. Each test was composed of five cycles of 700N (~80% flexural strength) loading, with a relaxation period of five seconds between cycles and along the maximum load. The electrical resistance was measured and its variation during the tests is shown in the three graphs from Figure 4.7.

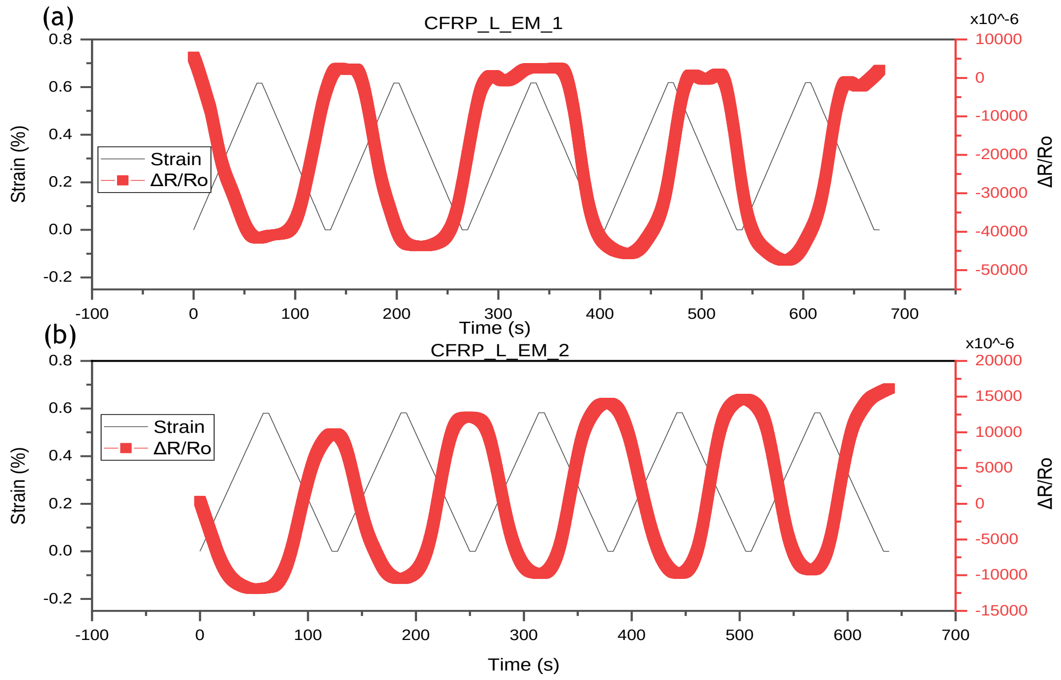

Figure 4.7- Electromechanical tests performed in CFRP laminates.

In graphic (a) from Figure 4.7, is possible to see a negative resistance variation trend, where the resistance tends to decrease when the applied load increases. In graphic (b) this trend is visible during the entire test, contrary to test (a), this showed a negative restistance variation trend always coordinated with the applied load. In test (b) is possible to see a slight increase in the maximum resistance from cycle to cycle. Figure 4.8 shows electromechanical rupture tests performed in CFRP laminates, in this tests the specimens were tested to rupture, with a crosshead motion rate fo 2mm/min.

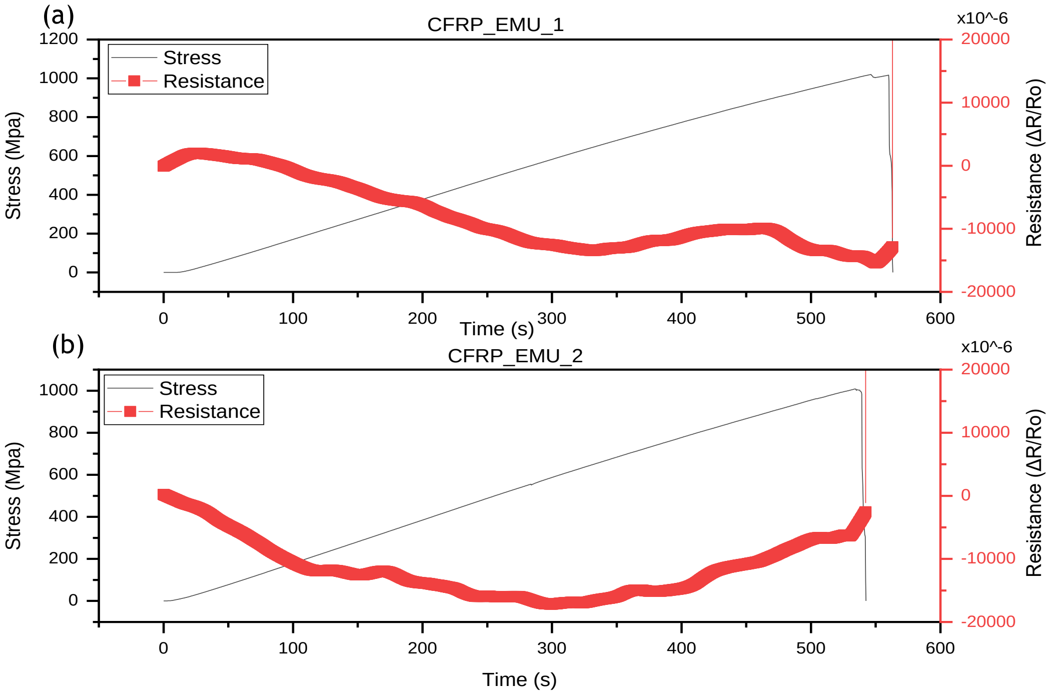

Figure 4.8- CFRP electromechanical rupture tests

In both tests, the specimens show negative resistance variation trend until approximately 600MPa of applied stress. After this, CFRP_EMU_1 presents a slight increase in resistance followed by a decrease until the structure starts to collapse. On the other hand, CFRP_EMU_2 increases resistance from this point until the specimen collapses.

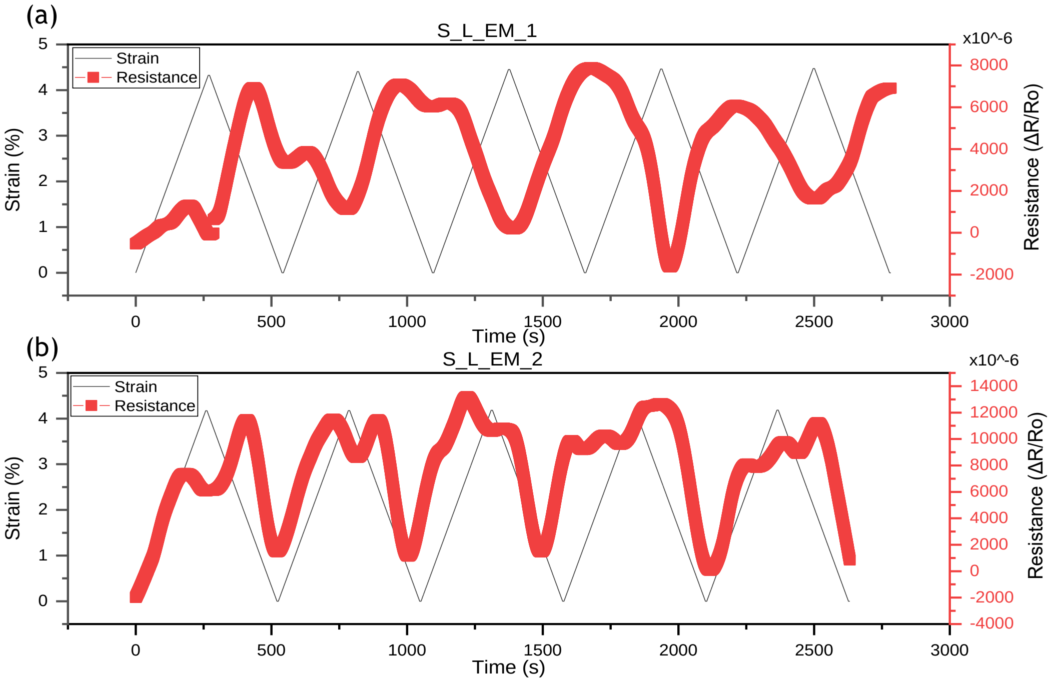

Figure 4.9- Sandwich electromechanical tests

Figure 4.9 shows the sandwich electromechanical tests, where the electrical resistance of the tensile face was measured. In the graphic (a) is possible to see the negative resistance variation trend, while in graphic (b) is possible to see a slight positive resistance variation. It is important to notice the instability of the measurements, this instability and lack of coherence between the different electromechanical tests will be analyzed and discussed in the next subchapter.

4.2 Discussion

4.2.1 Foam core

The nine foam core samples were exposed to different ranges of temperature through different periods of time. Table 4.6 resumes the temperatures and periods of exposition of the different specimens as well as the visual appearance of each set. These temperatures were chosen based on the curing process of the adhesive, despite the curing temperature is 90 C°, the autoclave can have peaks of temperature reaching a maximum of 95 C° for short periods of time.

Table 4.6- Temperature exposition of the foam samples

	Temperature [C°]	Time [h]	Visual appearance
F_S_1	80-90-95	1-24-24	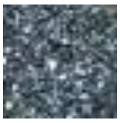
F_S_2	80-90	1-24	
F_S_3	95	24	
F_S_4	90	7	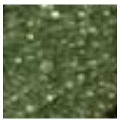
F_S_5	90	7	
F_S_6	90	7	
F_S_7	-	-	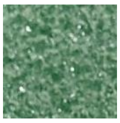
F_S_8	-	-	
F_S_9	-	-	

The first three samples had the propose of understanding the impact of temperatures higher than the maximum recommended from the supplier, as well as the influence of the exposition time. F_S_1 was placed in the oven for one hour at 80 C°, followed by a period of twenty-four hours at 90 C° and a final period of another twenty-four hours at 95 C°. F_S_2 was exposed to 80 C° for one hour and after to a temperature of 90 C° for twenty-four hours. F_S_3 was exposed to just one heat cycle of 95 C°. F_S_3, F_S_4 and F_S_5 were exposed to a temperature of 90C° for seven hours, exactly the same conditions of the adhesive curing cycle. Finally, F_S_7, F_S_8 and F_S_9 were control samples without any kind of high temperature exposition.

At the end of their cycles of temperature the first three samples had a similar visual appearance where the green color of foam was replaced for light grey. F_S_3, F_S_4 and F_S_5 had a slightly darker color than the control samples but preserved the green tone. Thus, the alterations in color are majorly influenced by the exposure time rather than the temperature.

Figure 4.1 and in Table 4.1. The strain reached before failure was consistent with the different sets of samples, Figure 4.10 shows this variation.

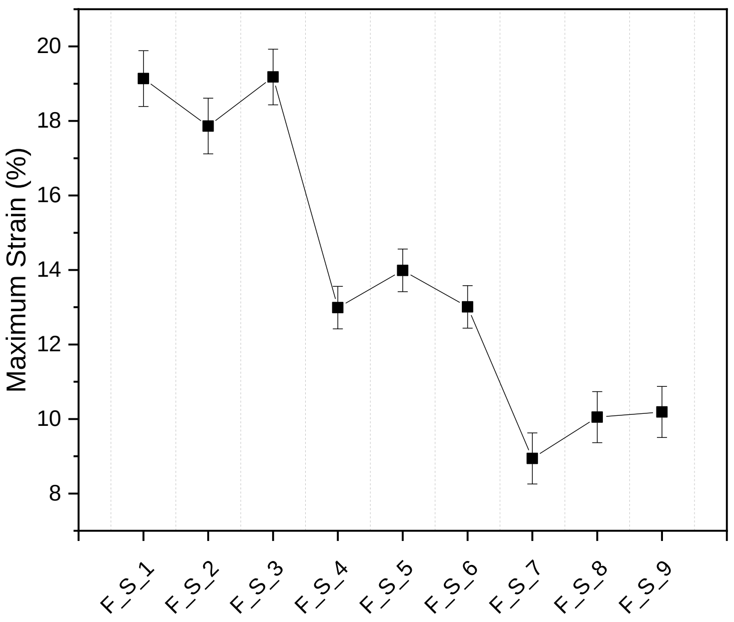

Figure 4.10- Foams specimens' maximum strain

In Figure 4.10, which represents the maximum strain reached by each foam specimen compared side by side, shows each set of samples distributed by three distinct regions of the graph. The first three specimens are the ones with the highest levels of maximum strain, followed by the foam samples exposed to adhesive curing process and the lowest are control specimens. The maximum strain reached by specimens F_S_4, F_S_5 and F_S_6 is on average 3.61% higher than the control samples and 5.4% lower than specimens F_S_5, F_S_6 and F_S_7. These results show an increase in foams ductility proportional to the time the samples were exposed to high temperatures. Since neither the modulus or the flexural strength were altered during the curing process, the exposure to a temperature of 80ºC provided more flexibility to the foam, which can be considered an improvement of the core mechanical proprieties.

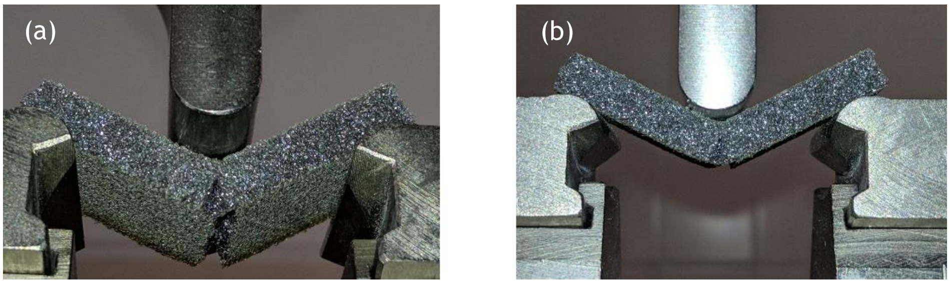

Figure 4.11- Foam three-point bending test (a)- crack view from below (b)- front crack view

Figure 4.11 shows the failure of a foam specimen after a bending test. It was observed that failure starts in the form of crack initiation on the tensile side of the specimen as the displacement increases and it tends to grow towards the compression side. All the samples showed a similar failure mode like the one in Figure 4.11. Despite the rate of crosshead motion was 2mm/min, all samples had a fast crack propagation through the specimen’s depth.

4.2.2 CFRP laminates

In Figure 4.2, shows the CFRP short laminates behavior under flexural stress. All the specimens showed a consistent pattern under these conditions, a linear elastic zone followed by small ruptures and finally the total failure of the structure. These specimens did not match ASTM D790 standard, their geometry was chosen based on sandwich short samples’ design, so the failure mode was quite different from the tension failure predicted by the standard. CFRP_S samples failed to the compression force between the crosshead and the top face of the sample. In Figure 4.12-(a), shows the crack propagation in the transverse direction, while the side view of the crack is shown in Figure 4.12-(b), where the crack reached only half of the specimens depth.

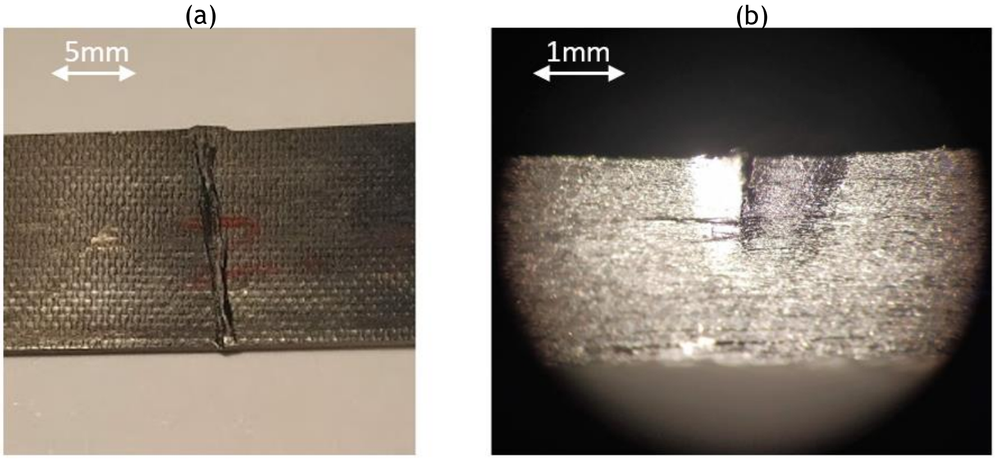

Figure 4.12- CFRP_S failure mode, (a)-top view, (b)- magnification of side view (x4)

From these figures, it is obvious that the crack only affected the top sheets of the specimen, so the failure was due to the local stress concentration in the top face, induced by the stress in the point of contact between the crosshead and the specimen, where the matrix was unable to disperse the load uniformly throughout all depth of the sample. This resulted in premature failure due to matrix cracking, followed by the fibers rupture due to the local compressive loads without matrix support. This test did not reflect CFRP behavior under flexural stress, instead, it showed the maximum compressive force under flexure that this specimen can handle.

Figure 4.4 represents the curves obtained for the CFRP long laminates, they were projected with a span to depth ratio of 60:1 to avoid premature compression failure. These curves present a linear elastic phase coherent between each sample. Contrary to the CFRP short samples, these specimens had a rupture much more spontaneous with almost none plastic regime. Figure 4.13 shows the three views of a CFRP_L sample after a three-point bending test.

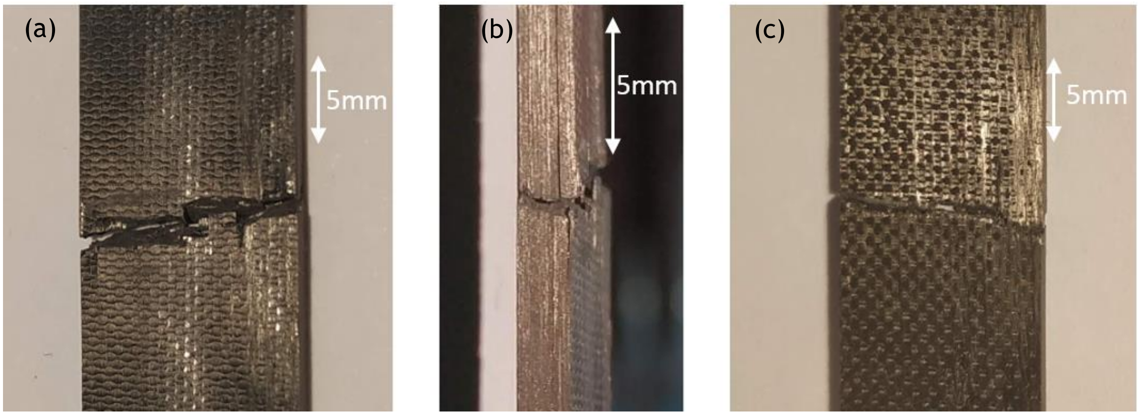

Figure 4.13- CFRP long samples failure mode, (a)-compression side view, (b)- side view, (c)- tensile side view

In Figure 4.13, is shown that the crack propagated throughout all the specimen’s depth. From a close analysis, despite the fracture is the same, it shows a very distinct appearance between the compression and the tension side, Figure 4.13- (a) and (b) respectively. In this case, the samples failed to tension, the crack propagated from the tensile side in the direction of the compression side. The propagation of the crack is irregular and grew in width from the tensile to the compression side. This growth and irregularity are a consequence of the energy dissipated along the cracking process, the structure is progressively less capable of storing the energy absorbed during the deformation and it dissipates it mainly by cracking. The rate of dissipated of energy grows from the start to the end of the crack, that is why the compressed side has a rift wider than the tensile side. In Figure 4.13-(b) it is possible to see delamination close to the compression side, which is common in this failure modes, it’s another consequence of the energy abrupt dissipation.

Y. Ma et. al. [90] investigated the flexural proprieties and failure behavior of two kinds of unidirectional CFRP laminates, using the same carbon fiber (T700SC 12K, Toray, Tokyo, Japan) but two different types of matrix systems. One matrix system was fabricated with Nylon 6 (MXD-PA, Mitsubishi Gas Chemical, Tokyo, Japan) film while the second was fabricated with epoxy (MCP939, Maruhachi Corporation, Fukui, Japan) film. The results obtained by Y. Ma et. al. [90] are shown in Table 4.7 as well as the results obtained in the three-point bending tests of the CFRP_S AND CFRP_L laminates.

Table 4.7- Experimental flexural proprieties CFRP_S AND CFRP_L and Y. Ma et. Al. [90] results

	Flexural strength [MPa]	Flexural Modulus [GPa]
CFRP_S	1066.21 ± 4.7%	74.60 ± 3.4%
CFRP_L	1238.49 ± 7%	89.50 ± 2.3%
CF/Nylon 6 [90]	1154.24 ± 6.4%	85.4 ± 4.1%
CF/Epoxy [90]	1512.2 ± 10.7%	89.45 ± 8.9%

CFRP_L laminates have a flexural strength and flexural modulus higher than CFRP_S, this can be justified by the different failure modes present in this two samples. CFRP_S failed to compression while CFRP_L failed to tension which is expected to occur at higher values of tension. The results confirm that CFRP_L failed in the tension face and CFRP_S to compression. Comparing to Y. Ma et. Al. [90] results, the flexural strength and modulus of CFRP_S are lower than the ones obtained by Y. Ma et. Al. [90] due to the premature failure mode. On the other hand, CFRP_L has a flexural strength higher than CF/Nylon 6 laminates and lower than CF/Epoxy, which can be justified by the different carbon fiber and matrix used by these authors. The modulus of CFRP_L is very similar to CF/Epoxy laminates, this means that these two types of laminates have a similar behavior when exposed to flexure. The CFRP laminates flexural results are by these means confirmed and sustained by the results obtained by Y. Ma et. Al. [90].

4.2.3 Sandwich specimens

Sandwich bending tests show a particular behavior under flexure, curves from Figure 4.3 and Figure 4.5 show three distinct areas: an initial linear elastic portion, followed by a slight deviation from linearity where the material enters in an elasto-plastic phase followed by failure.

Despite sandwich short beams have different bondings, it was not reflected in the curves, both reinforced and unreinforced bonds have similar elastic, elasto-plastic and failure phases. The samples showed elastic behavior until a strain of approximately 1.1%, after that it shows a deviation from the initial linearity, which rapidly takes over an almost linear behavior with a less accentuated slope. In Figure 4.14 it is possible to distinguish clearly the elastic from the elasto-plastic zones of this specimens, when the mean line starts to divert from its tangent (red line in Figure 4.14) the specimen enters in the elasto-plastic region.

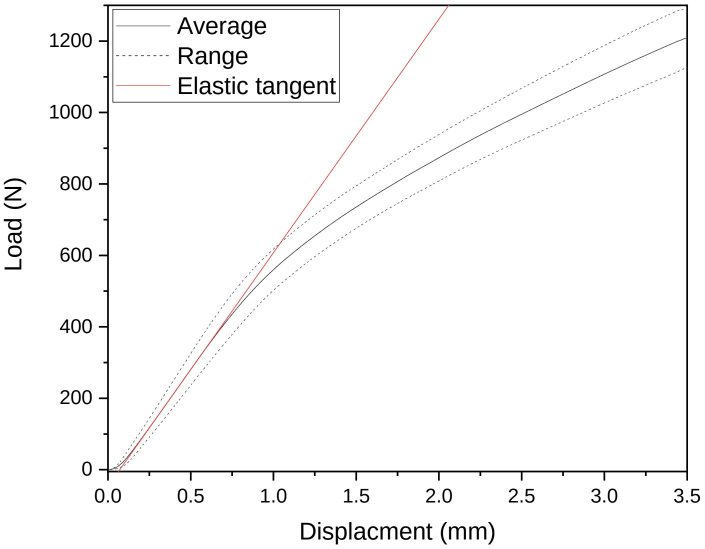

Figure 4.14- Sandwich short samples Load versus Displacement mean curve with respective error and tangent of the elastic phase

This deviation is due to a core adaptation to the applied compressive forces, from this point the material will not recover totally to the initial state. The decrease on the slope means that the material is deforming more with lower load rate. Carbon short samples just showed plastic deformation from a minimum load of ~750N (Figure 4.2), this means that the beginning plastic deformation of the sandwich short samples is due to yield of the core as the load is applied. Figure 4.14 shows that the elasto-plastic phase is not linear, in this phase, there is a progressive plastic deformation with progressive foam core yielding until the structure fails to compression due to facing compressive failure. For these specimens the facing bending strength was:

$$\sigma = 99.03\ MPa \pm 2.6\%$$

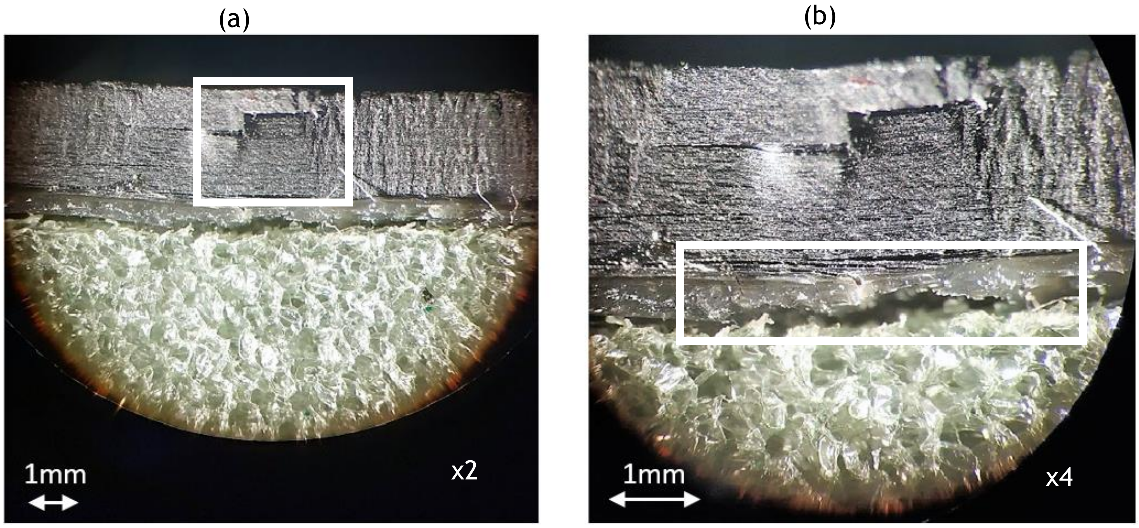

Figure 4.15-Fracture surface of sandwich short samples, a- magnification of x2, b- magnification of 4x

The ultimate strength is lower than expected because the shear loading component is significant and core failure precedes facing compressive failure. Core failure takes the form of core yielding, which results in reduced Young modulus, which reduces the core support of the facing and precipitates facing compressive failure at a lower stress. In Figure 4.15, it is possible to see the facing compressive failure crack, pointed out by the white rectangle in Figure 4.15-a, as well as the adhesive failure directly below the crack, pointed out by the white rectangle in Figure 4.15-b. The adhesive failure occurs as a consequence of the core yield, finally the facing fails due to the lack of support from the core which allows an ununiform distribution of strain, peaking at the center.

It is known that sandwich failure modes depend on material proprieties of the constituents, (facings, adhesive, core), geometric dimensions and type of loading [60]-62]. Sandwich long beams showed inconsistent behavior between samples, with a large dispersion of data, the flexural modulus presented an error of 30%. Figure 4.16 illustrates the four different failure modes obtained by sandwich specimens.

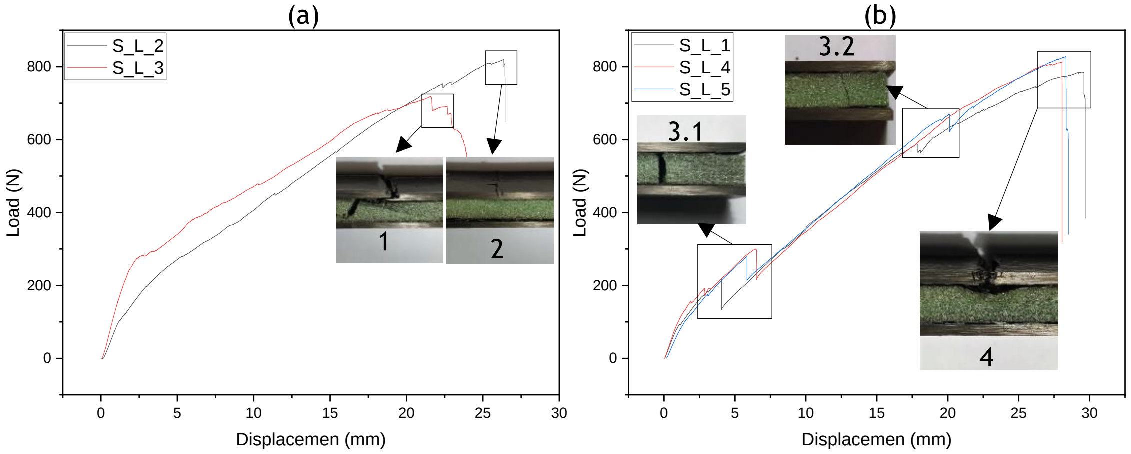

Figure 4.16- Sandwich long samples failure modes

In sandwich composites, the bending moment is taken mainly by the faces, this results in high normal stresses with low normal strains due to the high modulus of the facings. On the other hand, the shearing force is taken mainly by the core, resulting in high core strains due to the low shear modulus of the core. Thus, along the elastic region, the core is under nearly uniform shear stress, but when the material enters in the plastic region, the core begins to yield, and the shear strain becomes highly nonuniform peaking at the center [62]. In Figure 4.16- (a), the failure mode 1, was due to core shear failure in the center of the beam followed by face sheet failure. This specimen was the only one that failed as Gdoutos et al.[62] described, S_L_3 is the specimen with the highest flexural modulus and the one that tolerated the highest load before being plastically deformed. It is important to notice that this specimen was the one that showed the latest adhesive debonding and the only one where the partial debonding occurred from the center to the tip of the beam.

In Figure 4.16- (a), failure mode 2 in S_L_2 was face sheet wrinkling failure. This specimen showed a partial debonding between the tensile face and the core deployed by the shear stress between core and face. This means that in this test there was no physical bonding to bear the shear stress between the two faces, for this lack of adhesion they could move almost freely between each other. This premature adhesive failure explains the lower flexural modulus and the higher flexural strength compared to S_L_3 since this failure was not induced by the core shear strength but by the CFRP face compression strength.

Figure 4.16- (b) shows the specimens where the adhesive failure close to the tip is perfectly reflected in the load versus displacement graph. S_L_2, S_L_4 and S_L_5 failed almost simultaneously and coincided with their entrance into the plastic regime. Which suggests that the premature plasticity was induced by small failures triggered by the shear tensions in the core-facing interface, next to the tip, which led to partial debonding in this zone and the subsequent core breakage, which is shown in failure modes 3.1 and 3.2. In failure mode 4, is shown the catastrophic failure of this specimens, the core indentation is perfectly visible, Gdoutos and Daniel [61] state that the yield of the core under the load occurs when the interfacial stress, reaches the yield strength of the foam core. The interfacial stress is proportional to the local deflection [61], in the case of this specimens, the local deflection in the center of the beam increased to levels beyond core yield strength. Because the top face was detached from the core, it did not transfer shear tensions to the rest of the structure, instead, it deformed almost independently, which led to a larger deflection of the top face compared to the rest of the structure. This caused a high concentration of tensions in the center of the beam that led to core yielding and a subsequent compression face sheet failure, consequence of the high concentration of tensions in this area.

Sandwich long specimens with reinforcement showed a poor adhesive bounding, all had a premature failure due to lack of adhesion between core and face sheets. Figure 4.17 shows the visual appearance of an adhesive interface that failed completely (S_L_1, S_L_4, S_L_5):

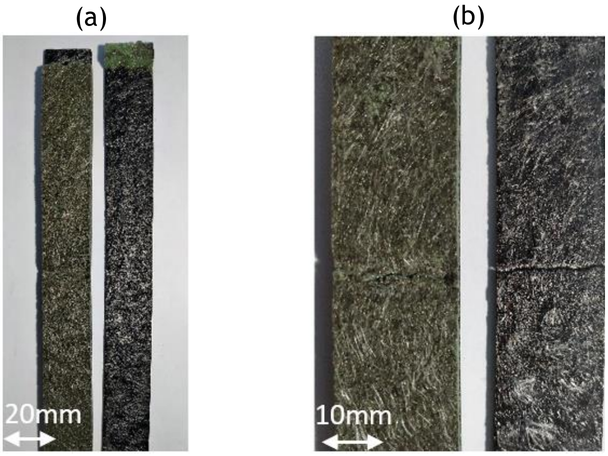

Figure 4.17- Visual appearance of an adhesive joint, a-Low magnification of the adhesive failed joint and (b)- High magnification of the adhesive failed joint

In Figure 4.17 is possible to distinct clearly the glass fiber veil on the faces of the core and the carbon skin, the interfaces do not show remains either from the carbon skin nor the core foam, according to ASTM D5573 [59], this is called an adhesive cohesive failure This suggests that the glass fiber vail, that was expected to act as a reinforcement of the bond, was indeed what weakened it.

Table 4.8- Experimental flexural strength of different studies and the sandwich samples

Face	Core	L [mm]	t [mm]	b [mm]	d [mm]	Flexural strength [MPa]	Ref.
W-CFRP	Re-entrant honeycomb	60	2.3	10	21.3	3.76	[91]
U-CFRP	Conventional honeycomb	60	1.5	10	20.5	8.39	[91]
GFRP	Polyurethane ρ=40 kg/m^3	70	1.5	51.3	22	1.96	[92]
GFRP	Polyurethane ρ=200 kg/m^3	70	2	33.2	15.6	40.18	[92]
CFRP_S_U	Airex C70 ρ=92.33±0.57% kg/m^3	60	2.2	15	10.4	98.21±2.8%	
CFRP_S_R		60	2.2	15	10.4	99.86±2.5%	
CFRP_L		170	2.2	21.4	10.4	86.43±6.9%	

Sandwich structures widely different from each other, the skin and core materials can vary a lot as well as the core geometry, so it is difficult to compare mechanical proprieties of different sandwich structures. As an example, Table 4.8 shows different experimental values of flexural strength. The sandwich samples manufactured in this work have a substantially higher flexural strength due to the carbon faces thickness ally to the core compressive strength. In the work developed by Li et.al. [91] both honeycomb cores failed to sustain the applied load while in the work developed by Costa [92] the specimens failed to compression. Each sandwich structure will fail from its weakest point, sandwich long samples proved that the weakest point in this structure was the adhesive bond.

The mechanical behavior of the sandwich and CFRP samples used in electromechanical tests are expressed in Figure 4.18. The sandwich and CFRP tests were conducted with loading cycles of a maximum load of 700N. None of the CFRP specimens showed any type of permanent damage, Figure 4.18-a shows straight lines along the charging portion of the cycles followed by typical unloading curves. On the other hand, S_EM_1 showed a premature core shear failure, like the failure mode shown in Figure 4.16- b- mode 3.1.

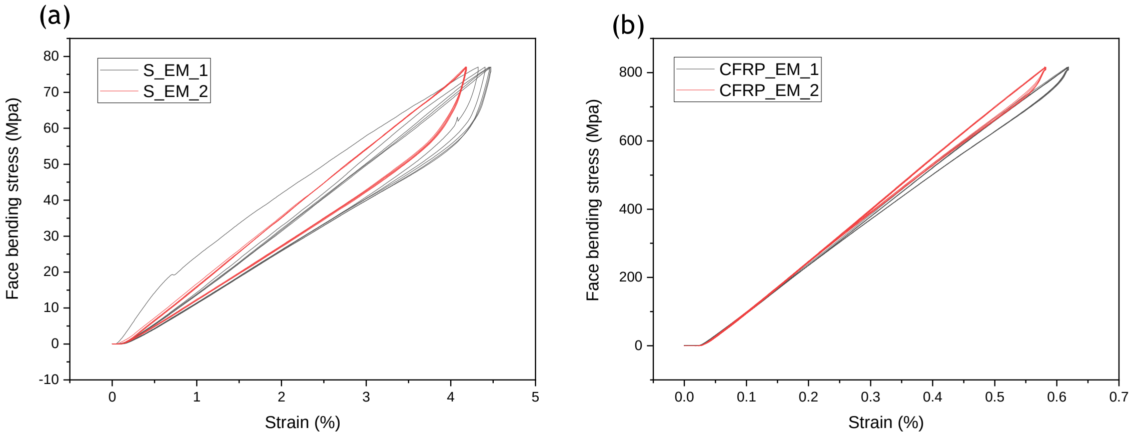

Figure 4.18-Cyclic mechanical tests. a- CFRP_EM face bending stress versus strain and b- S_EM stress versus strain

Sandwich specimen S_EM_2 showed a consistent mechanical response between the five cycles and did not show any type of visible damage. In Figure 4.18-b, S_EM_2 loading and unloading portions of the lines are consistent between cycles, these means that there was no hysteresis, leading to the conclusion that no permanent damage was induced along this test. S_EM_1, showed significant deviation between cycles, this can be interpreted as a consequence of the dynamic behavior of the core shear failure. In the first two cycles, the crack tended to grow, after those two cycles, the crack stabilized, and the last three cycles showed a consistent behavior between them.

4.2.4 Electromechanical tests

Electromechanical tests were intended to make a proof of concept. With the available resources demonstrate that carbon laminates with unidirectional fibers can be used as self-sensors.

Despite gauge factor (equation 40) being the most used parameter to define a material piezoresistivity, in some cases it can lead to miss understood, a material with a negative gauge factor must show negative piezoresistivity, but a material with positive gauge factor can also show negative piezoresistivity, if the geometric factor exceeds the modulus of piezoresistive factor [93]. Since this work has the objective of studying this concepts viability and the possibility of application to realtime monitorization of structures, the results are expressed in terms of the piezoresistive effect, $\frac{\mathrm{d}\rho_r}{\rho_r}/\varepsilon_l$, so no miss understood is induced by a possible low (~0) negative piezoresistive factor.

Looking at Figure 4.19 the inconsistent pattern between tests is obvious, from the two CFRP samples, only CFRP_EM_2 (Figure 4.7-b) showed an electromechanical behavior consistent throughout the all test, but inconsistent with the other tested sample. Both sandwich specimens show an inconsistent behavior between each other too. The piezoresistive effect of each cycle[4] from the four tests is shown in Figure 4.19:

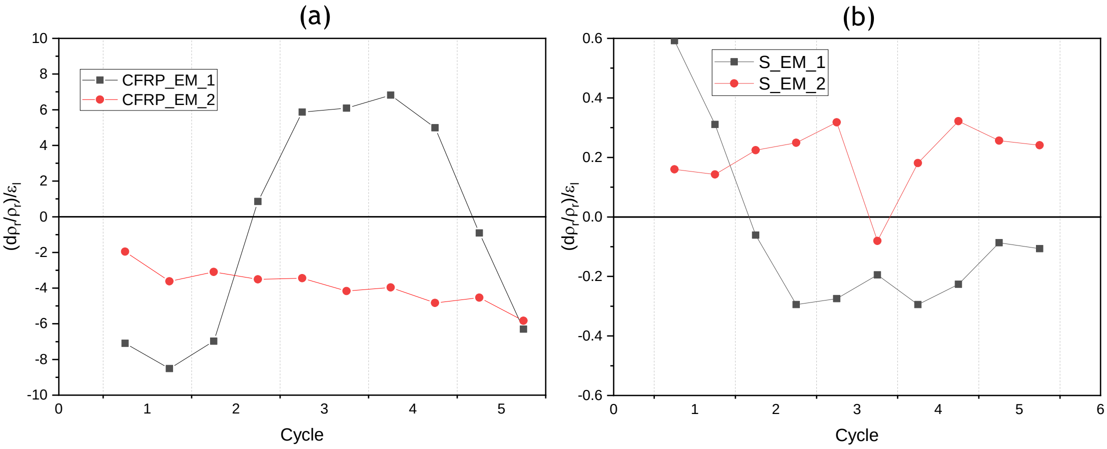

Figure 4.19- Piezoresistive effect for each cycle of the CFRP samples (a) and sandwich samples (b)

In Figure 4.19-b, CFRP_EM_1 has a notable piezoresistivity inversion, during the second cycle the piezoresistive effect passed from –6.98 to 0.86, showing positive piezoresistive effect along the third and fourth cycles. This test showed another inversion from the fourth to the fifth cycle. CFRP_EM_2 showed negative piezoresistive response along the entire test, the piezoresistive effect was allways lower during the unloading phase compared to the the loading phase.

Figure 4.19-b shows the sandwich piezoresistive effect for each cycle, S_EM_1 starts the first cycle with positive factor followed by four negative ones. On the other hand, S_L_EM_2 shows positive piezoresistivity along almost the complete test. Along the third cycle, the piezoresistive effect of the loading and unloading portions differed significantly, during the unloading phase it reached a negative value of -0.081 while in the loading period it reached the piezoresistive effect of a magnitude of 0.32.

Comparing the two graphs from Figure 4.19, the piezoresistive effect of the sandwich tensile faces is lower than the CFRP samples, this can be justified by the sandwiches higher strain magnitude which depends on the specimens' thickness. Thus, the sandwich thickness is much higher than the CFRP thickness, which reaches higher values of strain in the outer surface, and if ${}^{\Delta R}/_{R_0}$ of the sandwich is not proportionally higher, the piezoresistive effect will be lower. That is what happen in sandwich samples, the resistance variations did not increase proportionally to the strain compared to the CFRP samples.

---

[4] The piezoresistive effects of each cycle is devided in two points, the first of each cycle corresponds to for the loading phase and the second corresponds to the unloading phase.

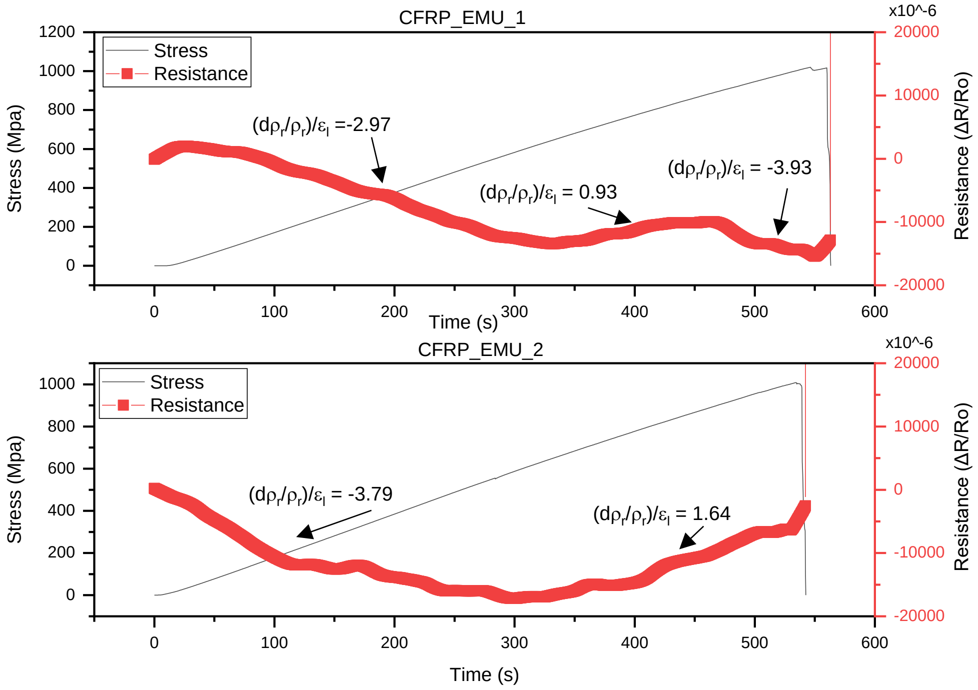

Figure 4.20- CFRP electromechanical rupture tests and corresponding piezoresistive effects along the bending tests

Figure 4.8 shows the resistance response of two CFRP samples that were flexed until rupture. Both showed negative piezoresistivity, until approximately a strain amplitude of 0.456%, then CFRP_EMU_1 showed a slight deviation from this trend but recovered the negative piezoresistive response after a strain amplitude of 0.71%. On the other hand, CFRP_EMU_2 did not recovered the negative piezoresistivity and showed a piezoresistive effect of 0.83 throughout the rest of the test.

Wang and Chung [85] have reported that the longitudinal piezoresistivity of a carbon fiber beam, under flexure, is negative along the compression surface and positive along the tensile surface. This is because of the decrease in the current penetration at the tension surface and the increase in the current penetration at the compression surface. The test setup did not allow to distinguish between the tensile and compressive piezoresistivity, instead, it gives the general longitudinal piezoresistivity of the beam. By these means, the specimens with positive piezoresistive effect can indicate a higher contribution of the tensile fibers, while the negative trends can represent a higher contribution of the compressed fibers to the material's piezoresistivity. The results were not consistent between samples to take conclusions about this matter. This inconsistency can be explained by several factors:

> Wang and Chung [93] claim that the two-probe method used to measure the resistance of the specimens is not the most accurate method. They defend that in this method, the measured resistance is the specimen resistance plus the contacts resistances, which sometimes can exceed the CFRP resistance. In the two-probe method, the measures of resistance depending on the quality of the electrical contacts, which represent a source of error.
>
> Angelidis et.al.[94] reported that, using the four-probe method, opposite piezoresistance values were obtained in the same specimen using carbon paste and silver paste. They reported that carbon paste can leave gaps in the interface contact, which leads to inhomogeneous current distribution.

Along the tests conducted during this work, a wide range of resistances (R_0) were measured in identical specimens, this can be explained by the unreliable contact interface. Since the use of silver paste was not possible, it is impossible to know the impact of the carbon paste in the results.

Further work on this matter must be conducted, to understand the discrepancies found along the electromechanical tests and to sustain the obtained results. The used Fluke 45 Dual Digital Multimeter must be updated for a more accurate one. Silver paste must be used to decrease the contact resistance, and by these means, understand if the results obtained by Angelidis et.al.[94], regarding the opposite piezoresistivity measured by silver paste and carbon paste contacts, are applicable to the two-probe method. Finally, the four-probe method must be implemented to minimize contact resistance and understand the impact of these two different methods (two and four-probe method). The collocation of the electrodes covering just the tensile or the compressed fibers should be tried to understand the contribution of each (compression and tension) to the material's piezoresistivity. With these improvements, it is expected to achieve cleaner and more reliable results and to sustain or refute the results obtained in this work.

5. Conclusion

In this chapter is given an overview of the principal conclusions taken from the study developed along this work, as well as the suggestions for future work.

5.1 Overview

Along this work a sandwich structure was developed and constructed, its different components were exposed to different flexure tests, and the piezoresistivity of the facings was studied as well.

This work allowed to contact with different materials and manufacture technics, as well as to develop skills and methodologies on three-point bending tests and electromechanical tests.

Different foam core specimens were exposed to a temperature above the ones recommended by the supplier, for different periods of time, to understand the impact of these variables on the flexure proprieties of this material. The tests showed an increase in material ductility proportional to the time of exposition, but the flexural strength was not affected.

Several CFRP laminates were bent to rupture to understand the different failure modes present in this material as well as the influence that the support span had in these failure modes. These tests led to the conclusion that the specimens had to have a ratio of at least 60:1 to offer solid conclusions about the CFRP flexural proprieties.

Table 5.1- Experimental flexural proprieties of the tested specimens

	Flexural strength [MPa]	Flexural Modulus [GPa]
CFRP_S	1066.21 ± 4.7%	74.60 ± 3.35%
CFRP_L	1238.49 ± 2.0%	89.50 ± 2.28%
S_S_U	98.21 ± 2.8%	2.55 ± 8.13%
S_S_R	99.86 ± 2.5%	2.51 ± 10.26%
S_L	86.43 ± 6.91%	5.78 ± 30.31%

Table 5.1 shows the experimental flexural strength and flexural modulus obtained to the different materials and specimens tested in this work.

Sandwich short samples failed to compression which led to the construction of longer ones to explore different failure modes of this structure. All the sandwich long specimens prematurely failed to weak bound between the core and facing.

A new experimental setup for piezoresistive measurements was assembled with the available resources. The results obtained from the electromechanical tests allowed to confirm that there is a variation in the electrical resistance of the material dependent on its deformation.

Successful measurements of the sandwich piezoresistive proprieties were taken. Although the results were accomplished, its reliability was not satisfactory, practical factors such as the contact resistance, the use of carbon paste and the adoption of the two-probe method can have induced errors that are impossible to confirm or refute with the available resources.

5.2 Future work

After an analysis on the state of the art, the experimental work and the results discussion, several suggestions of work with potential arise, and constitute a good complement for this study and generate new lines of research, namely:

- A study on the adhesive interface between the core and the facings should be conducted to access the impact of the glass fiber vail in this interface;
- The sandwich long specimens should be submitted to a significant number of cycles to study the fatigue response of this material.
- A study on the core mechanical response when exposed to hostile fluids, or temperature cycles covering the entire range of aviation working temperatures, by these means understand the impact that possible applicable environments might have in the mechanical response of this material.

In order to improve the electrical data acquisition method and obtain more reliable results:

- Other contact interfaces shall be tested and the four-probe method shall be applied;
- Different contacts just covering the tensile or the compressed fibers should be tried;
- Other variables, such as different ranges of temperature exposition, or different loading cycles can be introduced to verify by what means these new variables can affect the piezoresistive response of the material.
- The implementation of reinforcement conductive material such as graphite nano-tubes should be studied to access if this material increases the piezoresistive response and the mechanical proprieties simultaneously.

These work suggestions have the potential to improve the reliability of the electromechanical tests, improve the material’s mechanical proprieties and approach the tests conditions to situations this material can be exposed when applied to aircraft structures.

6. References

[1] W. Callister and D. Rethwisch, *Materials science and engineering: an introduction*, 7th ed., vol. 94. United states, 2007.

[2] M. Dekker, *Compsites Engineering Handbook*, 11th ed. New York, 1997.

[3] W. G. Roeseler, B. Sarh, and M. U. Kismarton, “Composite Structures: The First 100 Years,” *16th Int. Conf. Compos. Mater.*, pp. 1–10, 2007.

[4] A. P. Mouritz, “2 - Aerospace materials: past, present and future A2 - Introduction to Aerospace Materials,” Woodhead Publishing, 2012, pp. 15–38.

[5] The Boeing Company, “Boeing, ANA Celebrate First 787 Dreamliner Delievery,” *Boeing Media Releases*, 2011. [Online]. Available: http://boeing.mediaroom.com/2011-09-26-Boeing-ANA-Celebrate-First-787-Dreamliner-Delivery.

[6] O. T. Thomsen, E. Bozhevolnaya, and A. Lyckegaard, *Sandwich Structures 7: Advancing with Sandwich Structures and Materials: Proceedings of the 7th International Conference on Sandwich Structures, Aalborg University, Aalborg, Denmark, 29-31 August 2005*, 1st ed. Dordrecht: Springer, 2005.

[7] A. D. B. L. Ferreira, P. R. O. Nóvoa, and A. T. Marques, “Multifunctional Material Systems: A state-of-the-art review,” *Compos. Struct.*, vol. 151, pp. 3–35, 2016.

[8] W. H. Prosser, M. C. Wu, S. G. Allison, S. L. Dehaven, and A. Ghoshal, “Structural Health Monitoring Sensor Development at NASA Langley Research Center,” *Proceedings, Int. Conf. Comput. Exp. Eng. Sci. (Corfu, Greece)*, 2003.

[9] D. Gay, S. V Hoa, and S. W. Tsai, *Composite materials and applications*, 1st ed. New York: CRC Press, 2003.

[10] V. Birman and G. A. Kardomateas, “Review of current trends in research and applications of sandwich structures,” *Compos. Part B Eng.*, vol. 142, no. January, pp. 221–240, 2018.

[11] P. M. G. Belbute, “Estudo do Comportamento em Flexão de Vigas Compósitas Sandwich,” *Mestr. em Eng. Aeroesp. Univ. Técnica Lisboa, Lisboa*, 2010.

[12] K. Marguerre, “The optimum buckling load of a flexibly supported plate composed of two sheets joined by a light weight filler when under longitudinal compression,” *Dtsch.*

Viertaljahrsschrift fur Lit. und Giests Geschichte. DVL (ZWB UM1360/2), 1944.

[13] C. Libove and S. B. Batdorf, "A general small-deflection theory for flat sandwich plates," National Aaeronautics and Space Aadministration, Washington DC, 1948.

[14] W. Flugge, "Determination of optimum dimensions of sandwich panels," *La Rech. Aeronaut.*, vol. 7, 1949.

[15] O. T. Thomsen, E. Bozhevolnaya, and A. Lyckegaard, *Sandwich Structures 7: Advancing with Sandwich Structures and Materials: Proceedings of the 7th International Conference on Sandwich Structures, Aalborg University, Aalborg, Denmark, 29-31 August 2005*. Springer Netherlands, 2006.

[16] P. P. Bijlaard, "Analysis of the elastic and plastic stability of sandwich plates by the method of split rigidities-I," *J. Aeronaut. Sci.*, vol. 18, no. 5, pp. 339–349, 1951.

[17] G. Gerard, *Minimum weight analysis of compression structures*. New York University Press, 1956.

[18] L. E. Kaechele, "Minimum-Weight Design of Sandwich Panels," 1957.

[19] L. E. Kaechele, "Design Procedures and Data for Sandwich Panel Tests," 1957.

[20] F. J. Plantema, *Sandwich construction: the bending and buckling of sandwich beams, plates, and shells*. Wiley, 1966.

[21] H. G. Allen and B. G. Neal, *Analysis and Design of Structural Sandwich Panels: The Commonwealth and International Library: Structures and Solid Body Mechanics Division*. Elsevier Science, 2013.

[22] K.-A. Olsson, "Summary of some composites applications and Research in Sweden," in *Mechanics of Composite Materials*, 1, Ed. Pergamon, 1970, pp. 859–865.

[23] A. K. Noor, W. S. Burton, and C. W. Bert, "Computational Models for Sandwich Panels and Shells," *Appl. Mech. Rev.*, vol. 49, no. 3, pp. 155–199, Mar. 1996.

[24] R. Kuhbander, D. Mikelson, and T. Bitzer, "Long-term tropic environmental exposure of rigid wall honeycomb sandwich panels," in *National SAMPE Symposium and Exhibition (Proceedings)*, 1990, vol. 35, no. pt 2, pp. 2112–2126.

[25] H. G. Chae *et al.*, "High strength and high modulus carbon fibers," *Carbon N. Y.*, vol. 93, pp. 81–87, 2015.

[26] D. D. L. Chung and D. Chung, *Carbon Fiber Composites*. Elsevier Science, 2012.

[27] R. L. King, *Fibre-reinforced composites materials, manufacturing and design*, vol. 20, no. 2. 1989.

[28] A. Lefeuvre, S. Garnier, L. Jacquemin, B. Pillain, and G. Sonnemann, “Anticipating in-use stocks of carbon fiber reinforced polymers and related waste flows generated by the commercial aeronautical sector until 2050,” *Resour. Conserv. Recycl.*, vol. 125, no. April, pp. 264–272, 2017.

[29] DIAB, “DIAB Guide to Core and Sandwich,” p. 48, 2012.

[30] 3A Composites AG, “AIREX® C70 PVC foam - 3A Composites AirexBaltekBanova.” [Online]. Available: http://www.airexbaltekbanova.com/products/airex/airexreg-c70.html. [Accessed: 09-Jul-2018].

[31] C. Composites, “Nomex Honeycomb_ Core Composites.” [Online]. Available: http://www.corecomposites.com/products/honeycomb/nomex-honeycomb.html. [Accessed: 09-Jul-2018].

[32] S. K. Mazumdar, *Composites Manufacturing Materials, Product,and Process Engineering*, 1st ed. Boca Raton: CRC Press, 2002.

[33] L. K. English, “Honeycomb: million-year-old material of the future,” *Mater. Eng.(Cleveland)*, vol. 101, no. 1, pp. 29–33, 1985.

[34] W. Yuan, H. Song, and C. Huang, “Failure maps and optimal design of metallic sandwich panels with truss cores subjected to thermal loading,” *Int. J. Mech. Sci.*, vol. 115–116, pp. 56–67, 2016.

[35] A. Ingrole, A. Hao, and R. Liang, “Design and modeling of auxetic and hybrid honeycomb structures for in-plane property enhancement,” *Mater. Des.*, vol. 117, pp. 72–83, 2017.

[36] M. D. Banea and L. F. M. da Silva, “Adhesively bonded joints in composite materials: An overview,” *Proc. Inst. Mech. Eng. Part L J. Mater. Des. Appl.*, vol. 223, no. 1, pp. 1–18, 2009.

[37] J. A. Bishopp, “The history of Redux® and the Redux bonding process,” *Int. J. Adhes. Adhes.*, vol. 4, no. 17, pp. 287–301, 1997.

[38] R. Hollingham, “BBC - Future - The British airliner that changed the world,” *BBC*, 2017.

[39] C. M. (Italy) S.r.l., “EA451 Adhesive Film.” datasheet, Legnano, 2015.

[40] L. F. M. da Silva and R. D. Adams, “Measurement of the mechanical properties of structural adhesives in tension and shear over a wide range of temperatures,” *J. Adhes. Sci. Technol.*, vol. 19, no. 2, pp. 109–141, 2005.

[41] D. M. Brewis, *Handbook of adhesive technology*, vol. 15, no. 4. 1995.

[42] A. Baldan, “Adhesively-bonded joints and repairs in metallic alloys, polymers and composite materials: Adhesives, adhesion theories and surface pretreatment,” *Journal of Materials Science*, vol. 39, no. 1. pp. 1–49, 2004.

[43] A. Kinloch, *Adhesion And Adhesives: Science And Technology*. 1987.

[44] P. Molitor, V. Barron, and T. Young, “Surface treatment of titanium for adhesive bonding to polymer composites: a review,” *Int. J. Adhes. Adhes.*, vol. 21, pp. 129–136, 2001.

[45] B. R. K. Blackman, A. J. Kinloch, and J. F. Watts, “The plasma treatment of thermoplastic fibre composites for adhesive bonding,” *Composites*, vol. 25, no. 5, pp. 332–341, 1994.

[46] J. R. J. Wingfield, “Treatment of composite surfaces for adhesive bonding,” *Int. J. Adhes. Adhes.*, vol. 13, no. 3, pp. 151–156, 1993.

[47] G. Kempe and H. Krauss, “Adhesion bonding techniques for highly loaded parts of continuous carbon-fiber reinforced polyetheretherketone (CF-PEEK/APC2),” in *ICAS, 18th Congress*, 1992, vol. 2, pp. 1892–1900.

[48] J. Comyn, L. Mascia, G. Xiao, and B. M. Parker, “Plasma-treatment of polyetheretherketone (PEEK) for adhesive bonding,” *Int. J. Adhes. Adhes.*, vol. 16, no. 2, pp. 97–104, 1996.

[49] G. W. Critchlow and D. M. Brewis, “Review of surface pretreatments for aluminium alloys,” *Int. J. Adhes. Adhes.*, vol. 15, no. 3, p. 161, 1995.

[50] J. M. G. K. A. KODOKIAN and A. J . KINLOCH, “Lett. 7.” p. 627, 1998.

[51] A. J. Kinloch, “Adhesion and Adhesives Chapman and Hall,” *New York*, 1987.

[52] J. R. Arnold, C. D. Sanders, D. L. Bellevou, and A. Martinelli, “A study of titanium surface pretreatments for bonding with polyimide and epoxy adhesives,” *Compos. Real World*, pp. 345–353, 1997.

[53] M. Davis and D. Bond, “Principles and practices of adhesive bonded structural joints and repairs,” *Int. J. Adhes. Adhes.*, vol. 19, no. 2, pp. 91–105, 1999.

[54] A. S. Wang, “Fracture analysis of matrix cracking in laminated composites.,” 1985.

[55] S. T. Pinho, C. G. Dávila, P. P. Camanho, L. Iannucci, and P. Robinson, “Failure Models and Criteria for FRP Under In-Plane or Three-Dimensional Stress States Including Shear Non-linearity,” *Nasa/Tm-2005-213530*, no. February, p. 68, 2005.

[56] N. J. Pagano and S. R. Soni, “Chapter 1 - Models for Studying Free-edge Effects,” in *Interlaminar Response of Composite Materials*, vol. 5, N. J. B. T.-C. M. S. Pagano, Ed. Elsevier, 1989, pp. 1–68.

[57] A. M. Waas, B. V Sankar, and M. W. Hyer, *Failure in Composites*. Destech Publications Incorporated, 2013.

[58] A. Todoroki, M. Tanaka, and Y. Shimamura, “Measurement of orthotropic electric conductance of CFRP laminates and analysis of the effect on delamination monitoring with an electric resistance change method,” *Compos. Sci. Technol.*, vol. 62, no. 5, pp. 619–628, 2002.

[59] ASTM Standard D5573-99, . “Standard practice for classifying failure modes in fibre-reinforced-plastic (FRP) joints.” ASTM International, West Conshohocken, PA, pp. 3–5, 1999.

[60] A. Russo and B. Zuccarello, “Experimental and numerical evaluation of the mechanical behaviour of GFRP sandwich panels,” *Compos. Struct.*, vol. 81, no. 4, pp. 575–586, 2007.

[61] E. E. Gdoutos and I. M. Daniel, “Failure modes of composite sandwich beams,” *Theor. Appl. Mech*, vol. 35, no. 3, pp. 105–118, 2008.

[62] I. M. Daniel, E. E. Gdoutos, J. L. Abot, and K. Wang, “Deformation and Failure of Composite Sandwich Structures,” *J. Thermoplast. Compos. Mater.*, vol. 16, no. 2, pp. 345–55, 2003.

[63] M. A. Douville and P. Le Grognec, “Exact analytical solutions for the local and global buckling of sandwich beam-columns under various loadings,” *Int. J. Solids Struct.*, vol. 50, no. 16–17, pp. 2597–2609, 2013.

[64] P. Jasion and K. Magnucki, “Face wrinkling of sandwich beams under pure bending,” *J. Theor. Appl. …*, no. 2001, pp. 933–941, 2012.

[65] E. E. Gdoutos, I. M. Daniel, and K. A. Wang, “Indentation failure in composite sandwich structures,” *Exp. Mech.*, vol. 42, no. 4, pp. 426–431, 2002.

[66] R. F. Gibson, “A review of recent research on mechanics of multifunctional composite materials and structures,” *Compos. Struct.*, vol. 92, no. 12, pp. 2793–2810, 2010.

[67] A. V Srinivasan and D. M. McFarland, *Smart Structures: Analysis and Design*. Cambridge University Press, 2001.

[68] P. Foote, “New Guidelines for Implementation of Structural Health Monitoring in Aerospace Applications,” *SAE Int. J. Aerosp*, p. 6(2):525-533, 2013.

[69] R. W. Ross, “1 - Integrated vehicle health management in aerospace structures A2 - Yuan, Fuh-Gwo BT - Structural Health Monitoring (SHM) in Aerospace Structures,” Woodhead Publishing, 2016, pp. 3–31.

[70] J. M. M. L. da Saúde, *Aircraft Maintenance*, 1st ed. Covilhã: Universidade da Beira Interior, 2015.

[71] A. Todoroki, M. Ueda, and Y. Hirano, “Strain and Damage Monitoring of CFRP Laminates by Means of Electrical Resistance Measurement,” *J. Solid Mech. Mater. Eng.*, vol. 1, no. 8, pp. 947–974, 2007.

[72] P. C. CONOR and C. N. OWSTON, “Electrical Resistance of Single Carbon Fibres,” *Nature*, vol. 223, p. 1146, Sep. 1969.

[73] C. M. (Italy) S.r.l., “CIT HS160 T700 REM UD tape 36%.” datasheet, Legnado, 2015.

[74] A. Ag, “Material Safety data sheet for AIREX ® R63 Material Safety data sheet for AIREX ® R63,” no. 1907, pp. 2009–2011, 2009.

[75] C. M. (Italy) S.r.l., “REM Epoxy matrix.” datasheet, Legnano, 2015.

[76] Composite Materials (Italy) s.r.l., “EA451 Adhesive Film.” datasheet, Legnano, 2015.

[77] M. to Nano, “EM-Tec C39 conductive carbon cement.” datasheet, Wateringweg, 2015.

[78] ASTM Standard C20-00, “Standard Test Methods for Apparent Porosity, Water Absorption, Apparent Specific Gravity, and Bulk Density of Burned Refractory Brick and Shapes by Boiling Water.” ASTM International, West Conshohocken, PA, 2015.

[79] G. Morada, A. Vadean, and R. Boukhili, “Failure mechanisms of a sandwich beam with an ATH/epoxy core under static and dynamic three-point bending,” *Compos. Struct.*,

vol. 176, pp. 281–293, 2017.

[80] V. Crupi and R. Montanini, “Aluminium foam sandwiches collapse modes under static and dynamic three-point bending,” *Int. J. Impact Eng.*, vol. 34, no. 3, pp. 509–521, 2007.

[81] E. Linul and L. Marsavina, “Assesment of Sandwich Beams with Rigid Polyurethane Foam Core Using Failure-Mode Maps,” *Proc. Rom. Acad.*, vol. 16, no. 4, pp. 522–530, 2015.

[82] ASTM Standard C393-00, “Standard Test Method for Flexural Properties of Sandwich Constructions.” ASTM International, West Conshohocken, PA, pp. 1–4, 2000.

[83] ASTM Standard D790-03, “Standard Test Method for Flexural Properties of Unreinforced and Reinforced Plastics and Electrical Insulation Materials.” ASTM International, West Conshohocken, PA, 2003.

[84] S. Wen, S. Wang, and D. D. L. Chung, “Piezoresistivity in continuous carbon fiber polymer-matrix and cement-matrix composites,” *J. Mater. Sci.*, vol. 35, no. 14, pp. 3669–3675, 2000.

[85] S. Wang and D. D. L. Chung, “Self-sensing of flexural strain and damage in carbon fiber polymer-matrix composite by electrical resistance measurement,” *Carbon N. Y.*, vol. 44, no. 13, pp. 2739–2751, 2006.

[86] B. Stephen, E. Graham, K. Michael, and W. Neil, “Mechanical Transduction Techniques,” *MEMS Mech. Sensors*, pp. 85–112, 2004.

[87] C. P. Communications, “Fluke 45 Multimeter,” vol. 35. datasheet, 1989.

[88] J. Cardoso, “Design and Analysis of the Mechanical Behaviour of Adhesively-Bonded CFRP T-Joints,” Universidade da Beira Interior, 2018.

[89] C. Foreman, “Nondestructive detection and characterization of damages in honeycomb composite structures,” *Retrosp. Theses Diss.*, 2008.

[90] Y. Ma, M. Ueda, T. Yokozeki, T. Sugahara, and Y. Yang, “Investigation of the Flexural Properties and Failure Behavior of Unidirectional CF / Nylon 6 and CF / Epoxy Composites,” pp. 227–249, 2017.

[91] T. Li and L. Wang, “Bending behavior of sandwich composite structures with tunable 3D-printed core materials,” *Compos. Struct.*, vol. 175, pp. 46-57, 2017.

[92] J. Costa, “Análise de vigas laminadas compósitas à flexão,” 2017.

[93] S. Wang and D. D. L. Chung, “Negative piezoresistivity in continuous carbon fiber epoxy-matrix composite,” *J. Mater. Sci.*, vol. 42, no. 13, pp. 4987–4995, 2007.

[94] N. Angelidis, C. Y. Wei, and P. E. Irving, “The electrical resistance response of continuous carbon fibre composite laminates to mechanical strain,” *Compos. Part A Appl. Sci. Manuf.*, vol. 35, no. 10, pp. 1135–1147, 2004.